THE X3 100-KW CLASS NESTED-CHANNEL HALL THRUSTER: MOTIVATION, IMPLEMENTATION AND INITIAL PERFORMANCE

by

Roland Edward Florenz

A dissertation submitted in partial fulfillment
of the requirements for the degree of
Doctor of Philosophy
(Aerospace Engineering)
in The University of Michigan
2014

Doctoral Committee:

       Professor Alec. D. Gallimore, Chair
       Daniel L. Brown, United States Air Force Research Laboratory
       Associate Professor John E. Foster
       Hani Kamhawi, NASA Glenn Research Center
       Assistant Professor Benjamin W. Longmier

To my parents, who gave me more opportunities than I deserved.

A memoria di Ziu Luigi, Cuginu Michele, Nannu H., e Ziu Ed. A tutti : non mai

scordat'.

ACKNOWLEDGEMENTS

The pursuit of a PhD is a singular journey which I believe to be centered on the improvement of the individual. In truth, the actual subject of the dissertation does not matter so much as the candidate's ability to confront a problem about which he or she knows little to nothing about, which has not been previously solved, and work independently towards finding a solution. However, the paradox of this statement is that in order to cultivate this ability one must receive a certain amount of aid and assistance from persons who are not oneself. In my personal experience, I have been beyond fortunate to receive the support (mental, physical and emotional) of a number of outstanding individuals. Reader be warned, this is a longer than average acknowledgements section. A project such as this (and a person such as myself) can not succeed without the help of so many hands. I shall do my best herein to thank them.

Alec D. Gallimore, PhD., professor of aerospace engineering, applied physics, director of the Plasmadynamics and Electric Propulsion Laboratory, super-dean, and dissertation committee chair, I owe you a debt of gratitude which my weak and pittily words here can not begin to repay. Alec, to this day, I have exactly no idea why you chose to take a chance and accepted me into your lab over five years ago. I am, to the surprise at many, a very difficult person and I have appreciated your unflinching support all throughout my journey. There have certainly been some challenging times getting this thruster off the ground, and with out your insightful wise words—measured when calm

was required, and heated when cooler heads clearly would not prevail—we have managed to come out the other side with a spectacular piece of hardware. While this does border on the edge of gushy, I hope you know how heartfelt and sincere my thanks are.

To the rest of my committee, I also offer my sincerest thanks and will do my best to keep said thanks succinct so as not to make you all blush.

Professor Ben Longmier: Ben, while you and I have only worked together for a short time, I greatly appreciate the fresh outside perspective you have brought to my work. For me, I have found the vantage point that you are able to provide with your experience in private industry very helpful in my attempt to place this work in greater context.

Professor John E. Foster: John, you have served as amazing a cognate as one could hope for. I know that we did not get a chance to explore all the diagnostics that we discussed, but I have found your counsel to be exceptionally valuable nonetheless. You have helped me out in both technical and personal ways, helping me to see the path forward through the haze of the terminal final months of graduate school. For this, I will be forever grateful.

Dr. Hani Kamhawi: Hani, without your sustained support, the X3 would have not come into existence in the excellent shape that it has. I have learned a great deal from working with you and the colleagues of yours that you made available to me. I am stubborn and have certainly stumbled along the way, but you never wrote me off as a foolish graduate student though it would certainly have been within your rights at times to do so. I have very much enjoyed working with you.

Dr. Daniel L. Brown: Dan, simply put, without you championing this project my dissertation would not have happened. Your contribution to my graduate school career

through years of contributing your technical expertise, as well as your cool head, is certainly immeasurable. Not to mention, we have managed to have some fun along the way. Thank you.

I would be remiss if I did not thank Dr. Mitat Birkan of the AFOSR for his financial support throughout the length of this project.

To the rest of the 'X3 Team' your contributions are far too numerous to list in completion here, but I would like to thank each of you nonetheless. To Dr. Daniel Goebel of NASA JPL, I would like to sincerely thank you for the use of your cathode and for your trust in a student that you didn't know from Adam. Dan you have answered every single one of my questions quickly and in detail, never once giving me a hard time; in fact, quite the opposite. Dr. Peter Peterson, without your Hall thruster expertise, this thruster would not have come to be as it did. Despite some challenging moments, I am sincerely appreciative of all the instruction you gave me along the way. Dr. James E. Polk, thermocouples being the bane of my existence notwithstanding, your contributions to the X3 helped us avoid some nasty outcomes (if I said exactly what, someone will likely get mad at me ☺). Dr. Richard R. Hofer, you have always been consistent in your support. Rich, while it may not always seem this way, I respect and appreciate your incredible attention to detail and your ability to ask me very difficult questions—not to mention, your invaluable guidance at the very early stages of this project. I would like to thank Dr. James "Boss" Haas for being the strong silent support that this project needed. James, lest I confuse the reader, I would like to point out that what I mean by silent is not absent: your opinions and insights have always been well timed and appropriately vocal. Rather, I should like to say that you have been the best chief/manager one could hope for: not

detail, and willingness to entertain my crazy ideas and take chances have been invaluable to me. Your willingness to not only tell me when I was wrong, but how to fix my incorrectness, has been priceless.

components to exceptional tolerances, and so much more. Your willingness to explain to me how things out to be done when I clearly did not know my ass from my elbow definitely saved me on numerous occasions.

To the gang over at EDA: Doctah Dean, Eric, Chris and Jonathan. You all have offered up equipment and technical expertise and endured my tempestas as they came through. Dean, thank you for teaching me to challenge established processes that are justified only with "because." Eric, thank you for teaching me (and continually re-teaching me) how to use the XRS.

The heart of PEPL has always been the outstanding people that Alec brings together to work on some very fancy toys. To the previous generation that I have had the pleasure of working with, I would say the following. Dr. Bryan Reid, you searched back through dusty notebooks that had been untouched for years to help me in my time of need, thank you. Dr. Timothy Smith, your encyclopedic knowledge of the history of the lab has aided me on numerous occasions "so and so said this was there, do you know what in God's name they are talking about?" Your counsel on all things mechanical as well as general lab procedure has been critical. To Dr. LT: You were a calm voice amidst madness, the first person to teach me how to build a probe (we had to stay until 2 AM, but dammit did I learn to do something right!), as well as my first source of practical electronics information—I always enjoy our conversations. Dr. Spec Four: "Is it working?" "No, it melted again!! How about you?" "What do you think, it just crashed for the fourth dang time this hour!". Dr. Rohit Shastry: you let me hang around while you tested and provided me with my first experiences observing the firing of a hall thruster. Also, who can forget, "No Rohit! NOT LIKE THAT!" I have never not laughed at that, truly a gift.

Dr. Wensheng Huang: you introduced me to PEPL, gave me access, helped me pick out my classes, and have given me input and help ever since. Your ability to ask me hard yet useful questions is incredibly valuable—please don't stop doing that. Dr. RoSheng: thank you for the use of your floor on multiple occasions. Those neighbors were only creepy that one time. Dr. Mícheál: among the many lessons you taught me, two stand out. The first is "what if there was a device that could tell if the electrical current was continuous, a continuity if you will?". The second is that I am likely not the first person to have had this problem, and it is likely that someone smarter already found a solution. Who will buy me nuggets and McDoubles now? Doctah Tom!! You and I went through a long, dark, tunnel together and at the end fought "the Gambitron." Your steady brand of madness complimented my own quite nicely, if I do say so myself.

While still "the previous generation", the next grouping of individuals are more like the older siblings that were ahead of me a grade in school. Doctah Laura: holy cow, nested cupcakes. Janitor Laura inspired me in my final months of graduate school to forge on "for the sake of science" (ok, the real quote isn't exactly repeatable…). Doctah Shab: There is no such a thing as a stupid question, only stupid people. I miss the constant challenges that kept me on my toes. Your foray into the dark arts taught me much about perseverance—thank you for setting a good example. Doctah Ray! Without your baby, mine would never have been born. You quite literally taught me everything I know about how to run an NHT, how it is important to do things "the right way", that attention to detail should no be sacrificed for anything. You have selflessly supported the development of my own project and my continued learnings even after you left. I count

all three of you as my friends, can not thank you enough in this teeny paragraph, and hope we can continue to cause trouble together for years to come.

To my contemporaries: Bruce and Lady Josephine, I have always been suspicious of your collusion regarding all things physics. That said, we have all endured years of the siren song of the cryos together, and that bond will never go away. Bruce, you keep me on my toes and when push comes to shove, know how to get things done. Lady Josephine, you have always helped when asked without any request for recompense; some of the tasks were certainly not pleasant, and it was certainly within your rights to ask (I'm still waiting). Through many late night madness hours, you have certainly helped to calm me down and help me actually get something done.

To my PEPL Cousin: Penny, you are the best Vice-Mayor anyone could ever ask for. Keep the faith.

To PEPL the next generation, Mike, Scott, Doctah JP, Ingrid, Franz, Ethan and Tim: Do not screw it up. The incredible individuals that came before us have gifted us with stellar legacy, and thought it may not seem like it at times, it is truly a gift to be able to work at this lab. Doctah JP, thank you for the help and whimsy. Mike, I respect and am impressed with your ability to be an astute physics nerd as well as mechanically inclined. As always, I will forever be thankful for your service to this country. Scott, let's not kid ourselves; I put you through the ringer. You helped me through some long difficult hours, and I hope you got out of it as much as I did. I am giving you my baby, treat her well.

To my friends that suffered through quals with me: Paulie G. and Cyril. Your friendship has been invaluable to me, and as much as I love the people I work with, it has been a blessing to enjoy the company of individuals outside my close-knit PEPL family.

Paesa, I miss our early morning gym time and the nonsense of our two talkative buddies. Cyril, who will allow me to participate in taste tests of the most incredible homemade ice cream I have ever encountered now?

As is PEPL tradition, I have saved my family and closest friends for last. I have been blessed with three spectacular best friends, who in characteristic fashion, shall not here be named. I have known you all a long time, and, to this day, it amazes me that you all even still talk to me much less remain close and trusted friends.

Ai miei nanni, tutti I quattri. Se unu vi disse a primu che dopo ottanta anni venutu unu niputu comu iu, che potsa guadagna na dotto', paga nente, si potsa di « mangu pe suonnu> U sacciu tuttu che fatsa voi, la vida molto pesante, molto duro. Tuttu chillu che ti dicu, mi fa na insparazzione. Non potsu scordat' mai.

To my parents and sister: you all have supported my nonsense for nearly three decades. I've tried to right this section several times and come up with nothing. My parents, you have provided me with so many opportunities I simply do not deserve. Sister, your hard work continuously puts me to shame and I do my best to not let you down. I love you all.

And finally, a short little saying, a story if you will, that should serve as a reminder. No, I will not translate it. You do that yourself.

Ue, spacone, ti dicu na cosa.
Saranno grandi i papi,
Saranno potenti rei,
Ma quando qui siedono, soni tutti come me.
Non scordo mai tuttu che fatsa du. U consucu veru du.

-Bahtman
Rahm
B.O.C.
"The Mayor"
December 2013

TABLE OF CONTENTS

LIST OF FIGURES

LIST OF TABLES

LIST OF APPENDICES

ABSTRACT

The X3 100-kW Class Nested-Channel Hall Thruster: Motivation, Implementation

and Initial Performance

By

Roland Edward Florenz

Chair: Alec D. Gallimore

There is a demonstrated need within the aerospace community for propulsion units that can accomplish an ever increasing broad range of missions. One such mission, which has the prospect of coming to fruition within two decades, is to send people to Mars. In order to accomplish such a mission in a manner that minimizes cost and trip time, high-power electric propulsion systems on the order of hundreds of kilowatts have been deemed the best avenue of approach for propelling piloted spacecraft bound for Mars.

Two key elements of the technology pipeline as they apply to propulsion are the availability of in-space power and a propulsion unit that can effectively process that power to reach the destination. With the power available on spacecraft doubling every four years, one could fly a spacecraft with the desired power level in the time that it will take to fully develop the components to process several hundreds of kilowatts. Nested channel Hall-effect thrusters (NHTs), with their scalability to high power without sacrificing footprint or mass and their exceptional throttleability, have been identified as the EP technology most scalable to this power level.

It is the contribution of this work to develop the world's first 100-kW-class, three-channel NHT capable of propelling humans to Mars. The dissertation work demonstrates the need for, the implementation of, and the preliminary performance of the high-power three-channel NHT, designated the X3 NHT. In this work, the goals that organizations outside of academia have for high-power EP are outlined. The substantial facility modifications necessary to test such a thruster are presented in detail. These include but are not limited to: facility power modifications, upgrade of propellant delivery, and modification of a key performance measurement diagnostic (thrust stand). Preliminary operational characteristics of the X3 on krypton and xenon propellant gas are presented. It is the conclusion of this work that the initial characterization of the X3 NHT supports the viability of this kind of thruster as an option for high-power operation.

CHAPTER I

Introduction

"Sullu sullu posciu le vacche, sullu sullu mengu la vatte, sullu sullu fatsa ricotta, sullu sullu mi lu mangiu!"

1.1. General Commentary

"Roland, what exactly is it that you do?" This is a question that is probably familiar to many pursuing PhD's in the sciences. In my own case, it is a question I heard most often from a particular member of my family as well as a close friend of mine. This document is an attempt to outline what it was that constituted my five year career at the top academic electric propulsion laboratory in the country. To round-out the story, it will not only be the what, but the why and some of the how.

Improving the human condition is the underlying motivation that lies at the heart of this work. This is a lofty and somewhat over-used statement to be sure, but true nonetheless. The beauty of engineering is that it seeks not only to understand the world through math and science, but to then use that understanding of nature to bend it to the purpose of advancing human society. At a time when there are many problems facing this country, both at home and abroad, some have questioned the worthiness of investing resources, both in the form of monetary and talent-based capital, in developing technologies that will further enable our exploration and understanding of the cosmos. My rejoinder begins with the fact that that there will always be a health-care crisis, a war, a jobs problem. The human animal is a flawed one and always will be one, and even if

one were to throw 100% of the nation's resources at a single problem, that does not guarantee success. Take the research on the cure for cancer as an example: billions upon billions of dollars have been poured into finding a cure to this scourge, and generations of capable and dedicated researchers, physicians, and patients have put themselves towards this single end. While successes have been made, the disease still takes innumerably large numbers of good people before their time.[1]

I would argue that pursuing a problem from many directions is sometimes the best way to find a solution. In this case, putting money into a field where developed technology must meet an extreme threshold of what is considered satisfactory is an excellent way to push society forward. There are many inventions that came out of the space programs of this country that have found their way to the population at large. From advanced fire-retardant systems and computer systems, to better weather prediction and advanced medical science, advancements in space have touched 'the common man' at every step of life.[2,3] The reality is, if we wait for the time when we need extraordinary technologies to start developing them, it will be too late. Reality is not Bruce Willis flying up in a spacecraft at the last minute with a nuke to avoid the asteroid (reference to 1998 film "Armageddon" directed by Michael Bay). It takes years to make the craft that would reliably get him there.

1.2. Overview of the project

The development and characterization of a 100 kW class Nested-channel Hall-effect thruster (NHT), the X3, has been the single pursuit of my graduate career. This has included substantial design work which will not appear in this document. Beyond design, one encounters the other half of "development." Namely, that is preparing the facilities

necessary to test such a thruster. In Chapter IV we will examine in detail the extent to which the Plasmadynamics and Electric Propulsion Laboratory (PEPL) needed upgrading, as well as some general recommendations for testing other high power thrusters that cover all aspects from mechanical setup to electrical infrastructure.

The primary scope of this project as it relates to this dissertation is enabling of testing and the preliminary evaluation of the performance of the X3 to provide a starting point for establishing the viability of such a thruster as the "line in the sand" against which all others to follow will be measured. While not a flight model thruster, it is a significant step towards a propulsion unit capable of processing the hundreds of kilowatts necessary for the exploration missions to which it is suited.

1.3. Electric propulsion versus chemical propulsion

Electric propulsion (EP) devices have been flying in space since the mid 1960's (gridded ion thrusters)[4] with the first Hall-effect thrusters flying in the 1970's.[5] There are many advantages to using electric propulsion for in-space propulsion when compared to the more "traditional" chemical systems. EP devices are widely known to provide substantially higher specific impulses than chemical systems while drastically decreasing vehicle weight.[6] In other words, the return on investment for an EP system is substantially higher—the spacecraft can travel faster and/or carry more payload than would have been possible with a chemical system.

These advantages can be boiled down to the fact that a chemical propulsion system can not practically achieve anywhere near the required amount of ΔV necessary to move people to a target of interest, such as a Near Earth Object or the ever elusive Mars. One could get the necessary performance from a chemical system, but the cost would be that

3

the vehicle would have to carry an unfeasibly large amount of propellant, which would drive launch requirements, limiting the spacecraft. ΔV, as defined below in the famous Tsiolkovsky rocket equation[7]

$$\Delta v = v_e \ln\left(\frac{m_o}{m_f}\right) \qquad [1.1]$$

where v_e is the effective exhaust velocity ($v_e = Isp*g_o$), Isp is specific impulse as defined in Equation 1.3, m_o is the initial wet mass of the vehicle, and m_f is the final craft mass. It is a measure of the amount of change in velocity the craft must undergo to complete a certain mission, not accounting for any external forces. Several missions of interest are presented in the graphic below:

Table 1.1. Space exploration missions where electric propulsion would be appropriate.[8] ΔV values are approximate.

Mission	Required ΔV [km/s]
LEO-GEO	6
Mars, Sample Return	20
Mars, Manned	20
Europa Orbiter	30
Titan Explorer	30
Neptune Orbiter	40
Kuiper Belt Object (KBO)	40
Titan Sample Return	50

While chemical propulsion is the only choice for launching craft into space, it can be clearly shown that in order to achieve any of the missions in Table 1.1 EP is the best option current available. When written in terms of specific impulse (Isp), a performance metric commonly measured for propulsion devices, the rocket equation takes the following form:

$$\Delta v = v_e \ln\left(\frac{m_o}{m_f}\right) = Isp \cdot g_o \cdot \ln\left(\frac{m_o}{m_f}\right) \qquad [1.2]$$

$$Isp = \frac{T}{\dot{m} \cdot g_o} \qquad \textbf{[1.3]}$$

The chemical propulsion unit's deficiencies stem from its inability to produce Isp's of the magnitude and range of electric propulsion devices. The figure below, compiled by Liang[9], shows the differences between the two types of propulsion devices.
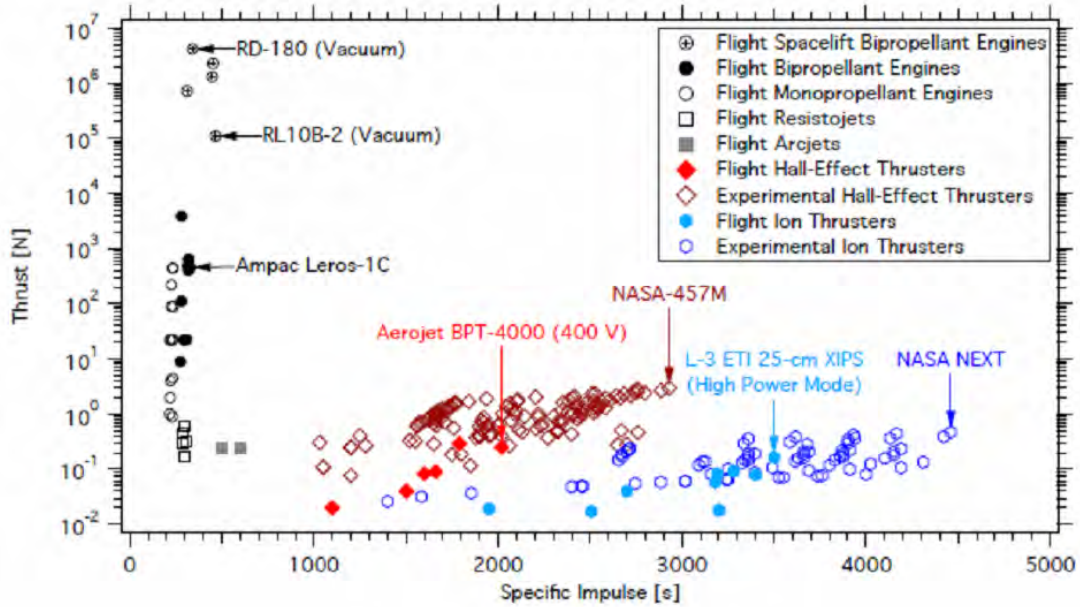
Figure 1.1. Figure illustrates thrust as a function of specific impulse for a variety of flight chemical (both monopropellant and bipropellant) units as well as flight and experimental EP devices. Here we see that the range of Isp's offered by electric propulsion units far outpaces those offered by chemical units, whereas chemical units produce far greater amounts of thrust.

Figure 1.2 below shows the missions a high power EP device could achieve as compared to a number of well known chemical rocket systems:
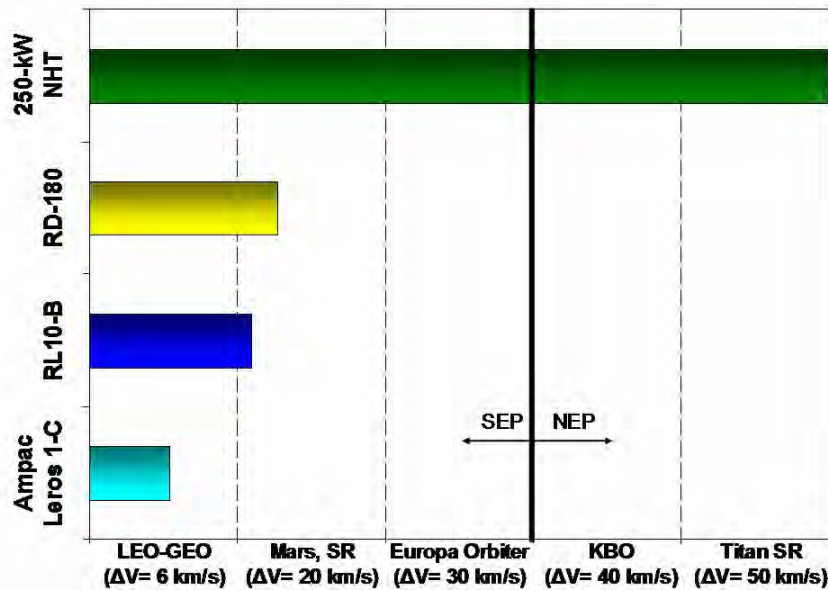
Figure 1.2. Propulsion units as a function of the missions (read ΔV's) they can achieve. SEP= Solar electric propulsion (for the NHT), NEP= Nuclear electric propulsion. To create this figure, vehicle dry masses were kept constant across propulsion units and throughputs used were stated maximums for each propulsion system. Data for Leros 1-C, RL10-B, and RD-180 obtained from Figure 1.1. Each mission uses the same spacecraft dry mass (not including propulsion system) and allows the propulsion to run for its expected lifetime/rated throughput. Assumed lifetime of 250-kw NHT for this figure is 11,000 hrs. Rated throughput of the RD-180 is 248,090 kg,[10] of the RL10B-2 is ~16,700 kg,[11] and of the Leros 1-C is ~4300 kg.[12]

EP requires a much lower propellant mass to be loaded onboard the spacecraft to complete the mission as a result of higher operating exhaust velocities, as is evidenced by Figure 1.1 and Equation 1.1. EP units do incur a power penalty, that is to say that the additional electrical processing infrastructure required to run an EP system adds mass to the spacecraft/launch vehicle that is not present for a chemical system. That said, the effects of this "power penalty" are outweighed by the benefits gained from reduced propellant mass requirements as compared to a chemical system. This means that for a given payload, the launch cost to put it into orbit is reduced because its initial wet mass is lower. Alternatively, extra space, weight capacity, and monetary resources created by the reduced propellant mass requirement can be utilized to include extra cargo, or for an extra suite of scientific equipment, increasing the overall value of the mission.

6

1.4. Picking an EP System

Now that the argument for electric propulsion has been made, yet another line of questioning is opened: what type of EP system will be chosen to propel us forward and how high a power level will it need to be.

In recent years, the variable specific impulse magnetoplasma rocket (VASIMR)[13] as a relatively high technology readiness level (TRL) engine has made many advances for high-powered electric propulsion devices and has done an excellent job of bringing more attention to the potential of the field. VASIMR's has the potential to operate in a regime of power of 1-10MW's or more, which fits the bill of heavy cargo and piloted missions to the outer solar system and possibly beyond. However, the space-board power required to make piloted travel to the outer solar system is still decades away. Thus, it is important to note that the VASIMR has demonstrated operation at 200-kW and below discharge powers.

What, then, can be utilized to truck the first explorers to the red planet? Studies suggest that solar electric propulsion (SEP) devices on the order of 100's of kW would be appropriate for such a mission.[14,15] Gridded ion thrusters, while highly efficient[16] and highly successful for long range missions,[17] are most suited to the smaller scale robotic missions which they have flown. They do not scale as well to high power nor produce the tens of newtons of thrust that would be ideal for long range manned missions.[15,18] It is worth noting here that one could conceivably produce a gridded ion thruster that has been scaled up to achieve higher thrusts, but it would be of impractical size and power levels due to the technology's limited thrust-to-power capabilities.

Many other types of thrusters, such as magnetoplasmadynamic thrusters (MPD's) and field-reversed configuration thrusters (FRC's) are neither mature/efficient enough to

make them a worthwhile candidate. MPD's have only once been flown successfully on-orbit.[19] As of this writing, only preliminary data has been produced for FRC thrusters such as MSNW's thruster ELF[20]. Such technologies are arguably still in developmental phases, with only sub-scale (<50kW) units being studied at this time.

1.5. Nested-channel versus single-channel Hall thrusters

This brings the community to the natural conclusion that the Hall effect thruster (HET), first flown by the Soviets in 1972[21] with hundreds of Stationary-Plasma Thrusters (SPTs) model thrusters having been successfully operated in the intervening years between that first launch and the writing of this document[22], is the technology to pursue for high-power missions. According to Aerojet Rocketdyne,[23] BPT-4000 (now the XR-5) 4-5 kW HET is currently the highest power flight-qualified Hall thruster. This means that a cluster of at minimum of 50 thrusters would have to be flown on a spacecraft in order fill the requirements of a 200-kW mission. This introduces a nightmare of logistics for the system integrator that would have to coordinate flow and power to 50 separate single propulsion strings. Further, the associated engine surface area of an array would be massive. This motivates the clear need to move to much higher power Hall thrusters. At the writing of this work, NASA had produced and tested several thrusters in the high-power range of >20 kW. The highest power is the 50-kW class NASA 457v1, with a total discharge power of 72 kW[24] (though tests in Russia have ran in excess of 100 kW[25]). While this reduces the necessary number of thrusters to four, this is still not the optimum approach (e.g. due to limitations in performance range of these thrusters at their highest power ratings). Comparison in terms of size between different single channel HET options and the use of NHTs for a 200-kW mission is presented in Figure 1.3.
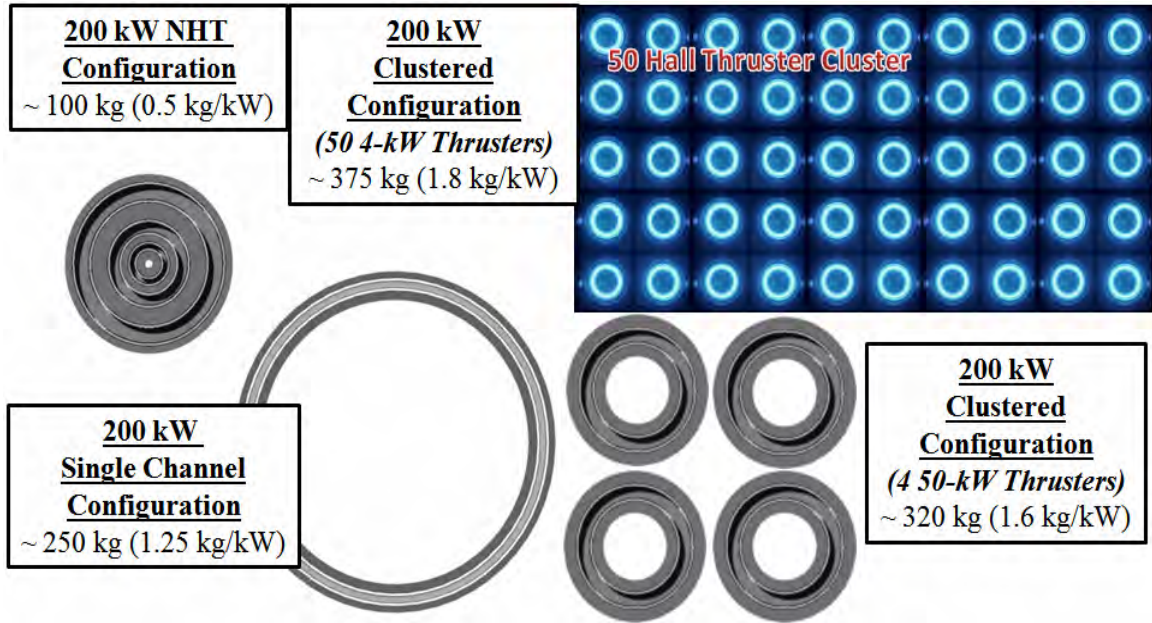
Figure 1.3. Comparison of a 200-kW NHT, a cluster of 50 4-kW SOA Hall thrusters, a cluster of 4 50-kW ASOA Hall thrusters, and monolithic 200 kW thrusters (thrusters in figure are for comparison purposes only).

Let us further extend this logic to the next step: what happens when instead of hundreds of kilowatts of power one is talking about onboard powers in the megawatts? In order to process 2 MW of propulsive power, one would need eight 250-kW NHTs, 40 50-kW HETs, or the absurd number of 500 4-kW flight qualified HETs. Figure 1.4 provides one with a rough concept of what each of these thrusters configurations would look like installed on a concept spacecraft likely to have that much power on board.
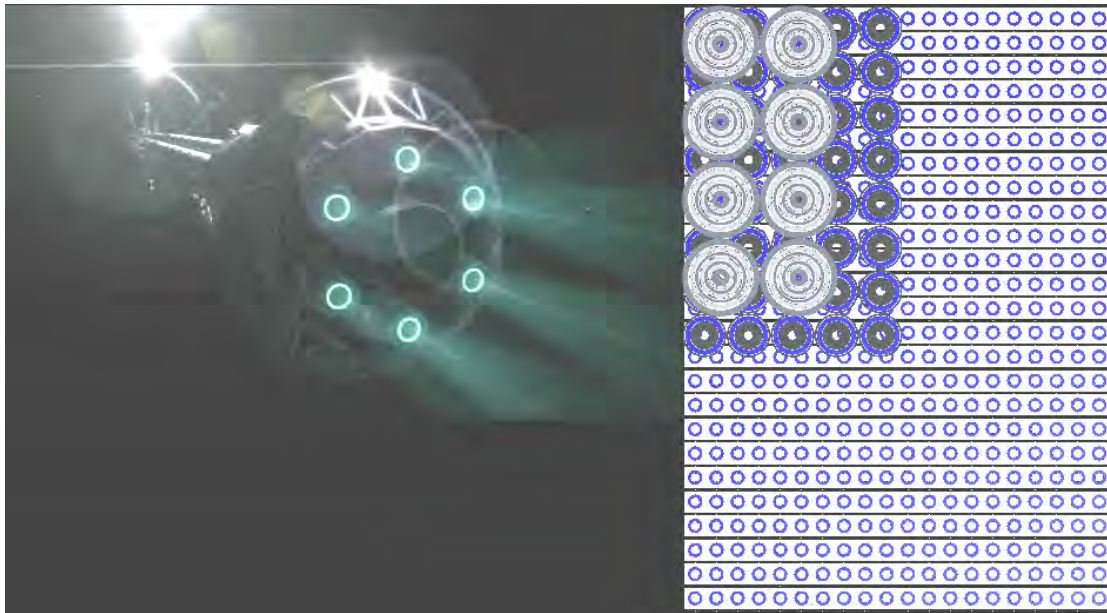
Figure 1.4. The Antares spacecraft from the television show Defying Gravity on the left, and the scaled versions of various thruster solutions for 2-MW of propulsion power: (8) 250-kW NHTs, (40) 50-kW HETs, (500) 4-kW HETs.[26]

Nesting channels is the most effective way to scale Hall thrusters to high power, period. They allow for a wide throttle range, both in Isp and power.[9,27-28] Before delving into the advantages of NHTs, however, at this point I would like to take a step back and put the amount of power that we are discussing into context here. In the average year, the average household in America uses 95 million BTU of electrical power.[29] This is equivalent to leaving a 200-kW thruster on for nearly six days straight. Another useful analogy is to that of an automobile. Car engine power is usually given in horsepower. Figure 1.5 gives a graphic showing how many horses would be required to pull a spacecraft to have the same "effective" power.
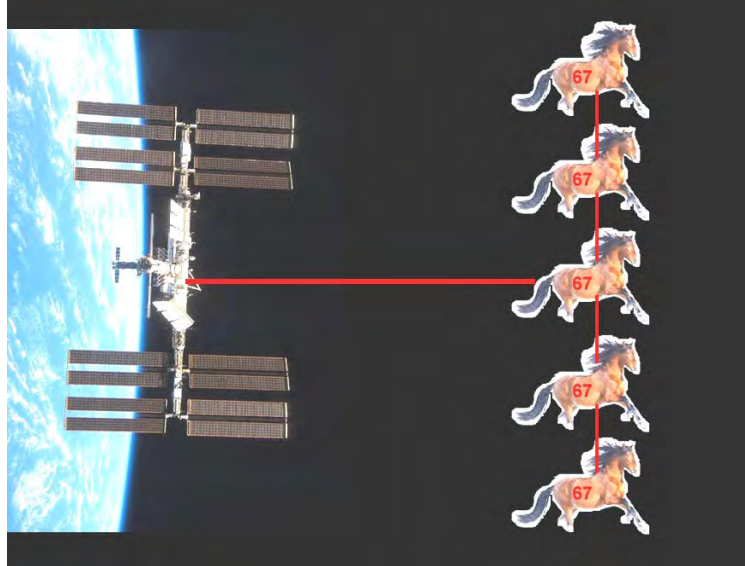
Figure 1.5 Picture of equivalent number of horses pulling the International Space Station. Each horse represents 67 horses, for a total of 268 horsepower (assuming the use of 250-kW propulsive power).

To further bring home the car analogy, Table 1.2 below gives propulsive power of a 200-kW NHT in horsepower and then lists several well known cars and the engine horsepowers that come with the standard engine for that car.

Table 1.2 NHT power as compared to the horsepower of well-known cars. 2014 model-year versions of each car were chosen, with the base model being selected. It should be noted that higher performance versions do exist, such as a version of the Camaro which has over 500 hp available.

Engine	Horsepower
250-kW NHT	335
Chevy Camaro Coupe[30]	323
Ford Mustang[31]	305
Audi A4[32]	220
Mini-Cooper[33]	121

The advantages of NHTs span a variety of attributes but can be boiled down to one word: flexibility. This is the flexibility to plan a mission that requires a wide range of power, thrust and Isp operating points within a given vehicle form factor. Not only can a 250-kW NHT operate efficiently over an Isp range that spans several thousand seconds and a nearly 200X power throttling table, it is essentially seven different thrusters in one. This offers the mission planner flexibility in the different types of maneuvers that the

11

spacecraft is capable of undertaking given one propulsion unit and adds in a measure of redundancy—if one channel fails, there are still several viable thruster configurations available. Figure 1.6 below gives a representation of all of these various configurations.

| Maximum Exit Area (Low ISP—High T/P operation) | ISP Range (1400s-3200s) | Medium Exit Area (Mid ISP operation) | ISP Range (2000s-3600s) | Minimum Exit Area (High ISP Operation) | ISP Range (2000s-4600s) |
	Power Range		Power Range		Power Range
			20 kW–170 kW		10 kW–140 kW
	30 kW-240 kW		15 kW–120 kW		5 kW-90 kW
			10 kW-80kW		1 kW-50 kW

Figure 1.6 Figure illustrating the wide throttling range and multiple configurations of a three channel 200 kW NHT.

1.6. Why high-power EP matters outside academia

Having just discussed the relevance of EP and the suitability of NHTs for applications at high power, the natural next question that must be answered is: why do we care enough about high power applications to develop a thruster for it? Up until this point, the highest power HET mission flown has been 4.5 kW for a single device.[23] The largest commercial communications satellites flying specify *total onboard power*, that is to say all power available for every subsystem including propulsion, of approximately 20 kW,[34] and the International Space Station (ISS) has an approximately 260 kW available of power aggregated over batteries and solar arrays.[35] The only existing application that has the same order of magnitude of power available to fully utilize the X3 is the ISS, and the operators would never devote all of its power to a thruster for any steady-state period of time. That said, who is interested? As one might expect, the primary interested parties at

this stage are NASA and the United States Air Force (USAF), though private firms interested in long range spaceflight may one day invest in such high power trips[36].

1.6.1. A look at NASA's goals

At one end of the application spectrum lies NASA's interest in high power propulsion missions. The one that perhaps captures the public imagination the most is a manned mission to Mars. In order to take the first human explorers to the Red Planet, it has been put forth that a spacecraft outfitted with propulsion units capable of processing several hundred kilowatts would be required to make the journey in a timely manner[15,37,38]. Following the paper discussing the so-called "solar electric path" mission, NASA issued a broad agency announcement calling for the design of just such a propulsion unit[14].

However attention grabbing a mission to Mars might be, some would say that preliminary (and less costly) missions to objects nearer afield aught to be chosen both to test out the myriad of technologies for such a long-haul mission as well to achieve important tasks. Dr. John Brophy of the NASA Jet Propulsion Laboratory (JPL) proposed one such mission to Near-Earth Objects (NEO's) at the International Electric Propulsion Conference in 2011.[39] The idea of sending astronauts to asteroids has been discussed before with an eye towards scientific gain (understanding early solar system formation) as well as commercial profit (mining of precious metals)[35]. Dr. Brophy suggests that, rather than attempt the complicated maneuver of sending people and materiel to the asteroid, performing experiments and mining operations and returning, it would be far easier to send a smaller craft powered by electric propulsion to latch onto and steer the object back into Earth-orbit where it could be more conveniently exploited. The

complexity of such a maneuver and the lower bound size limit dictated by the target asteroid suggests the use of high-power propulsion.

Whether it is piloted mission to Mars or a trip to a NEO, there is general consensus that EP is a critical technology. NASA's Human Exploration Framework Team (HEFT) identified SEP as a key component of their transportation architecture.[40] Not only is it included as a main component of the in-space propulsion stages, but the HEFT study identified SEP as a required component for travel to the moons of Mars as well as a mission driven component in full capability missions to near-earth asteroids (NEA's) and a landing on Mars.[40] Building on the work of the HEFT study, Dr. Brophy suggests a 300-kW EP mission for human exploration of NEA's.[35] This mission is not to be confused with the asteroid-return mission discussed in the previous paragraph.

Beyond manned trips to Mars and NEO's, there exist a range of other suitable trips for a high-power EP missions. From cargo tugs for deployed astronauts to shuttles for sample and return vehicles to outer planets, to piloted missions to Mars, the missions for which using EP is plausible are numerous.

1.6.2. The interest of the Department of Defense

At the other end of the government lies the Department of Defense (DoD). The primary actor is the USAF, whose interest lies in high thrust-to-power devices with expansive Isp throttling at constant power for rapid on-orbit maneuvering of high-value assets,[41,42] for which high-power NHTs are ideally suited.[9] Further supporting the statement that the DoD is interested in high power propulsion units to help aid the missions of the USAF are public calls for such technology.[43] Moreover, the Defense Advance Research Projects Agency (DARPA) has initiated calls for advanced

technologies to support the development of high-power, highly throttleable SEP.[44] A high-power NHT that meets the power and high Isp requirements of a NASA high power mission may also have the ability to meet DoD needs to operate with wide throttleability at constant powers (~40-60 kW[45]), making it a very attractive technology.

1.6.3. Availability of space-based power

Mission-pull alone does not ensure the availability of high-power spacecraft that can fly high-power thrusters. A non-trivial hurdle that must be surpassed is the availability of in-space power. As stated earlier, the ISS has the largest amount of power available on-board a spacecraft. With recent advances in spaced based solar-arrays that generate more power per unit weight (high kW/kg), such as Boeing's FAST arrays[46,47] or competing technology from ATK,[48] the amount of power available on such spacecraft is increasing. There are also possibilities of using thermal-electric systems that reflect the sun's rays and using a Stirling engine conversion system to generate power.[49] Figure 1.7 illustrates the remarkable trends of increased available electricity onboard spacecraft, showing that if developments do follow these trends, we will have available power for a range of high-power missions (e.g. NASA piloted exploration missions to Mars) in the near-term (decade or so). With power doubling every four years, one can project that in as a little as a decade or so from the writing of this document (~2030) one can speculate that nearly 1 MW of power can be made available on a given spacecraft.
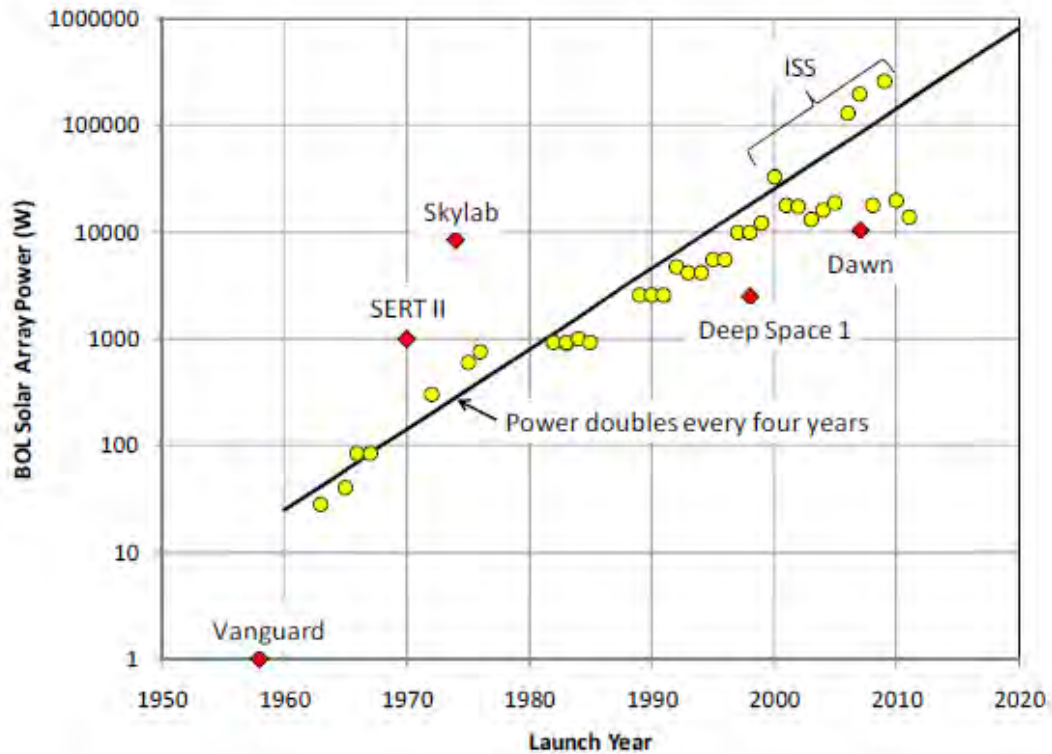
Figure 1.7. Figure showing trends in space-based power systems.[35]

All solar electric plans are well placed for missions whose reach does not extend

beyond Mars. While an NHT that can process 200 kW at Earth could still run efficiently

on the handful of kilowatts available by the time the craft reached an outer planet, say

Jupiter,[50] this level of available power would not allow for any extreme operation of a

large tug or human-rated craft. For such missions, nuclear reactors that can generate from

hundreds to thousands of kilowatts would have to be employed to power the propulsion

units, as they are not restricted by distance from the sun by the $\sim 1/r^2$ drop-off in available

power that solar arrays (or reflectors) are. In fact, NASA already planned out such a

mission in the early 2000's with the Jupiter Icy Moons Orbiter (JIMO), which had

onboard power of slightly greater than 200 kW supplied from a nuclear reactor.[51] While

this project was terminated due to dramatic cost increases, the reactor concept

16

nevertheless remains a viable benchmark for the method of power supply for high-power robotic exploration and sample-return missions to the outer planets.

1.6.4. Power-processing challenges for high-power applications

One of the costliest elements of any EP system is the development of the power processing unit (PPU) which controls all of the electrical telemetry for the thruster, both in terms of time and cost.[52] Unfortunately, as NASA GRC's chief PPU designer Mr. Luis Piñero notes, the attention given to this critical technology during the development cycle does not match its importance; "It's just a PPU, how hard can it be?" and "We can just leave it until the end" are common refrains from experienced thruster designer that PPU teams have to contend with.[53] Ultimately, this mismatch stems from a general ignorance of the inner-workings of PPUs by everyone except for the PPU designer. Simply put, PPUs are inherently complex pieces of technology which require more than a fundamental knowledge of power electronics to fully appreciate, something the non-electrical engineer does not commonly possess. While this section is by no means a primer on PPU design and operation (the reader is encouraged to refer to several design papers listed in the reference section for better detail[54,55,56]), it is meant as a launching point for future designs.

The primary challenges for designing a PPU for a 200-kW NHT are the expansive throttling range and the maximum current. The bigger of the two issues is the maximum expected output current, which for a thruster whose maximum operating condition occurs at a discharge current of 275 A forces the designer to employ a modular design approach. The inability to build a monolithic converter at this point in time stems primarily from the voltage and current limitations of semiconductor components.[57] There have been gains

recently made in PPU development with the employment of silicon-carbide (SiC) transistors instead of the traditional silicon (Si) devices,[54] but while SiC devices provide the ability to deal with higher switching voltages they are still limited in their current capacity.

There are advantages, however, to being forced to use a modular PPU. It should be noted that the following is not meant as a design solution but is instead simply an illustration of a possible path forward. It is further noted that the modular approach described in the next paragraph is a product of discussion with Mr. Piñero.[57]

One could conceivably build a ~200-kW supply out of 10-kW modules. To achieve 800 V of output voltage one could put four 200-V converters in series. In order to be able to supply a maximum of 275 A one would then parallel 5 of the 800-V strings of 55-A. This modular approach would allow one to throttle through the operating regime by terming modules on and off: to cut current one would turn off a parallel string and to reduce voltage modules in the series stack would be disabled. For example, if one wanted to run a thruster at 200 V and 275 A, all 5 parallel strings would be run with only one of the series stacked modules from each string engaged.

Even with a modular approach, one still runs into the difficult of balancing the demands of low cost, low weight, and high efficiency. One possible way to reduce the weight of the system is to switch to higher switching frequencies within the converter. Work has been done on DC-DC converters with switching in the ~13 MHz range that allows for the reduction/elimination of bulky ferrite cores and the printing of passive elements directly in the circuit board.[58,59] While these devices do not yet operate at the power levels associated with EP applications, they do have the potential for scalability.[60]

Through the application of SiC devices, these high-frequency converters should also be able to attain efficiencies on the order demanded of EP PPUs.[60]

In summary, the design of a PPU for an NHT that operates at or above 200 kW of discharge power and meets the demands of low-cost, low-weight, and high-efficiency is a distinct challenge. However, with flight model thrusters still years away, semiconductor technology (e.g. SiC or Galium Nitride devices) has the time to mature to the point where light weight, cost effective and efficient PPUs are a possibility. Such new devices would allow for the reduction in number and weight of modules needed to provide the full output current range. Moving to higher switching frequencies, while presenting its own set of challenges, may allow for further reduction in the weight of PPUs.

CHAPTER II

Background

"Vai chian chianu, e si va lontanu e arrive sanu."

"Un sacc' nente, nu vugliu sapere nente, ma so tutu."

Before embarking on the details of facility augmentation for, and the testing of, the largest and most powerful Hall-effect thruster built to date, it is useful to first establish a baseline of understanding of what exactly a HET is. The history of the development of HETs and their underlying physics are covered in depth in many other sources, with two seminal textbooks (Jahn's "Physics of Electric Propulsion"[61] and Goebel and Katz's "Fundamentals of Electric Propulsion"[62]) as well as several doctoral dissertations (Dr. Richard Hofer's is one example of a very complete description[63]). As such, the following description is written from a top-level perspective to give the reader the basis for an appreciation of the device tested for this work.

2.1. Exceptionally brief description of HET physics

There are five basic components of any HET: the anode (or positive electrode), the cathode (or negative electrode), the neutral gas distributor, the magnetic circuit, and the discharge channel. HETs can further be subdivided into two classes that share these common components. One subtype is the anode-layer thruster (TAL), whose prime distinguishing feature is that it typically has a shorter and proportionally wider discharge chamber with a length-width ratio typically less than 1; its anode, however, is generally

20

very long and hollow to ensure even propellant distribution.[64] The TAL was primarily

designed and investigated by the Russian Institute for Machine Building (TsNIIMASH),

and is not of the type investigated in this document. The interested reader is encouraged

to seek out papers on the TM-50 [65] and D-5[25], as well as other publications by

TSNiiMASH not here referenced.

The second subcategory, into which the X3 NHT falls, is that of the stationary

plasma-thruster (SPT). While the SPT was developed simultaneously in the US[66,67] and

Soviety Union in the early 1960's, the Soviets undertook the majority of the development,

with the design bureau Fakel being the major player.[68-70] It has comparatively longer

channels with larger length-width ratios than the TAL. The SPT also features channel

walls that are made up of insulating ceramic materials in contrast to the TAL's entirely

metal walls. Figure 2.1 provides cross sectional representations of a two stage TAL and

an SPT, highlighting their structural differences. To be sure, they differ from an

operational perspective as well, with the TAL's exhibiting significantly higher electron

temperatures than an SPT type.[63,71,72]
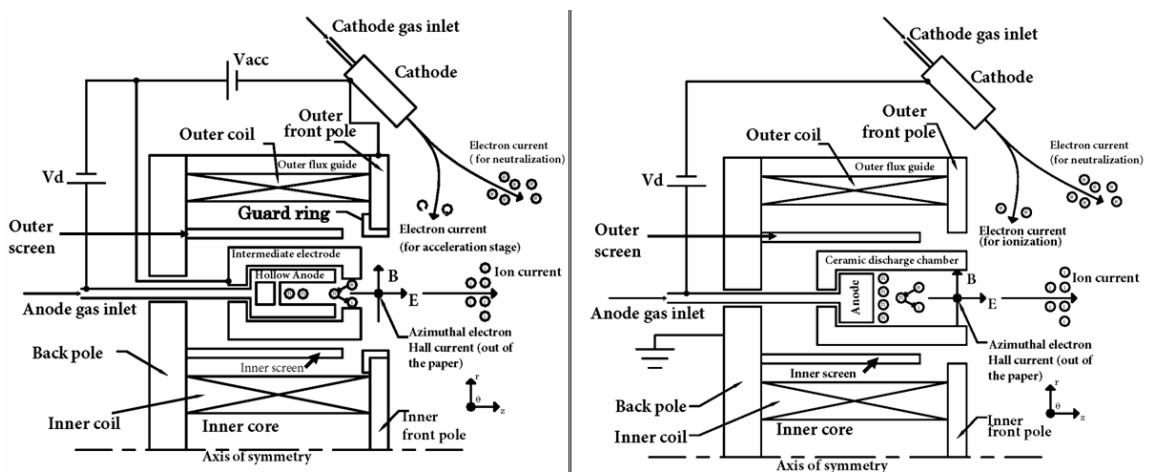
Figure 2.1. Cross Sectional Diagram of a two-stage anode-layer thruster (TAL) (left) side-by-side with a cross section of a single stationary plasma-thruster (SPT) (right). Note the differing aspect ratios of the channels as well as the difference in wall materials. Diagram slightly modified from original.[63]

21

From here-on out it can be assumed that when HET is written the SPT type of thruster is being discussed.

Having established how HETs are subdivided, it is worth briefly discussing the operating physics. As mentioned at the beginning of this section, these thrusters have five common components. Operationally, they come together in the following way. Neutral gas is injected into the back of the channel via the gas distributor. A strong electric field is established between the anode and the cathode, with potentials on the order of hundreds of volts producing a primarily axial electric field in the vicinity of the channel exit. The magnetic circuit provides a dominantly radial magnetic field in the vicinity of the channel exit. A small fraction of the main neutral gas flow into the channel is injected via the cathode, allowing for electron emission. A portion of these electrons are then guided into the channel where they enter into an ExB drift, flowing azimuthally about the channel. It is these electrons that collide with the neutral gas injected in the back of the channel by the gas distributor, ionizing them on impact. The newly formed ions are then accelerated out of the channel into space by the strong axial electric field (which until this point has had no effect on the neutral gas particles). Once the ionized gas (plasma), has exited the thruster it forms a structure known as the plume whose shape can be governed by the structure of the magnetic circuit and which is neutralized by the second portion of electrons emitted from the cathode, allowing the plasma to remain quasi-neutral (refer to Figure 2.2 for a graphical representation of the above described phenomena).
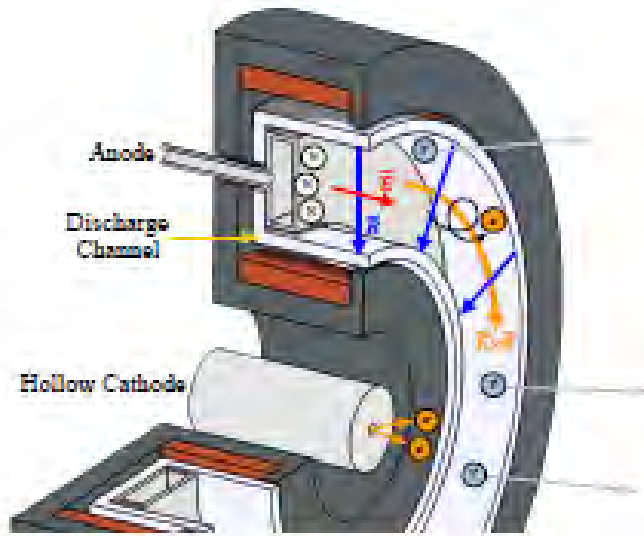
Figure 2.2. Graphical representation of the physics of Hall-effect thruster operation.[9]

This is merely a coarse top level explanation of the physics of an HET. There are many more detailed descriptions available[63], as well as several papers that have emerged in the last few years indicating that our understanding of electron physics (how those electrons manage to arrive in the channel) and general thruster operation as a whole may indeed by quite limited.[73,74] The reader is encouraged to delve into the references for a more detailed discussion of HET physics.

2.2. Design heritage of the X3

The X3 NHT owes its current form and its very existence to the thrusters (and designers) that came before it. At the beginning of the journey that was the design of the world's largest and most powerful Hall-effect thruster, it was determined that in order to succeed the design team had to leverage prior knowledge and the hard-won lessons of their predecessors. The H6 thruster, jointly developed by the Air Force Research laboratory (AFRL), NASA JPL, and PEPL, provided an excellent starting point for single channel design. However, the H6 is "only" a six kilowatt device, more than an order of magnitude below the desired operating range of the X3. Fortunately, NASA has already

had several forays into the realm of high-power EP, with thrusters like the NASA-300M, NASA-400M and the NASA-457Mv1 and -457Mv2 operating well into the 20-80 kW range. It was from these thrusters that important design and operational considerations were incorporated into the development of the X3. These considerations are not necessary in a smaller thruster such as the H6 due to its lower power and smaller physical size. Lastly, but perhaps most importantly, is the work done on the X2 NHT, developed by AFRL and PEPL, the first NHT to be documented in the open literature. True to its role as a proof-of-concept, not only did the X2 provide the data that showed that an NHT can be successfully designed and operated, but it addressed several challenges associated with nesting channels in vicinity to one another, both from a design as well as an operational standpoint. Images of all of these thrusters are included in Figure 2.3. This truly highlights that the X3 is the culmination of nearly two decades worth of American HET development.

Figure 2.3. The family of thrusters that influenced the X3, CW from top Left,: H6,[75] NASA-300M, [76]NASA-400M,[77] NASA-457Mv1,[24] NASA-457Mv2,[78] X2 NHT.[9]

CHAPTER III

X3 NHT design overview

"Se 'ddunisciuno u vue e la vacca e chine chiù po fare fa."

3.1. General notes

The design of the X3 NHT, pictured in Figure 3.1, was a multi-year effort that involved personel from PEPL, ElectroDynamic Applications, Inc., AFRL, NASA GRC, and NASA JPL. In this chapter, that process is distilled down to three main aspects. The design of the anode/gas distributor and the magnetic circuit will be covered in some measure of detail. Included in this will be presentation of experimental data used to verify the designs. The final aspect of the design process that will be briefly discussed is the thermal modeling effort.

Figure 3.1. The X3 NHT.

3.2. Anode design

3.2.1. Definitions and key parameters

One of the critical components of any hall thruster is its anode. Typically the gas distributor for the channel flow has the dual functionality of being the anode as well. In this section, any time that the term 'anode' is used it refers only to the gas distribution functionality of the part.

The primary metric used to evaluate the efficacy of a given anode design is the neutral flow uniformity. In the context of the X3 design process, this encompassed the anodes ability to produce a neutral flow that posed both radial uniformity across the width of the discharge channel as well as azimuthal uniformity throughout all 360 degrees of the channel. The main quantity used in the evaluation of this uniformity was normalized mass flux (Equation 3.1 and 3.2).

$$\Gamma = \rho \cdot v_{axial} \qquad\qquad \textbf{[3.1]}$$

$$\Gamma_{norm} = \frac{\Gamma}{\Gamma_{max,cl}} \qquad\qquad \textbf{[3.2]}$$

where ρ is local mass density, v_{axial} is local axial velocity, Γ is local mass flux, $\Gamma_{max,cl}$ is the maximum mass flux along channel centerline, and Γ_{norm} is the normalized mass flux.

As the one of the main attributes of the X3 is its expansive throttling range, the anodes had to be designed not to one nominal flow rate but instead to operate over a range of flowrates. A table showcasing the spread of flowrates considered for each channel in terms of the average of the spread is given (Table 3.1).

Table 3.1. Spread of flowrates considered in terms of the average rate, $\dot{m}_{avg,X}$ for each channel. Where X indicates the channel in question. I=inner, M=middle, O=outer.

Channel	Low Flow Limit	High Flow limit
Inner	0.2 $\dot{m}_{avg,I}$	1.8 $\dot{m}_{avg,I}$
Middle	0.2 $\dot{m}_{avg,I}$	1.8 $\dot{m}_{avg,I}$
Outer	0.2 $\dot{m}_{avg,I}$	1.8 $\dot{m}_{avg,I}$

The main computational tool used for evaluation of various designs was the FLUENT

CFD tool from Ansys.

3.2.2. General design flow

Three main design concepts for the anode of the X3 were evaluated. They were the

porous, drop-in orifice design, and the integrated orifice design. Notional cross sections

of each are given in.
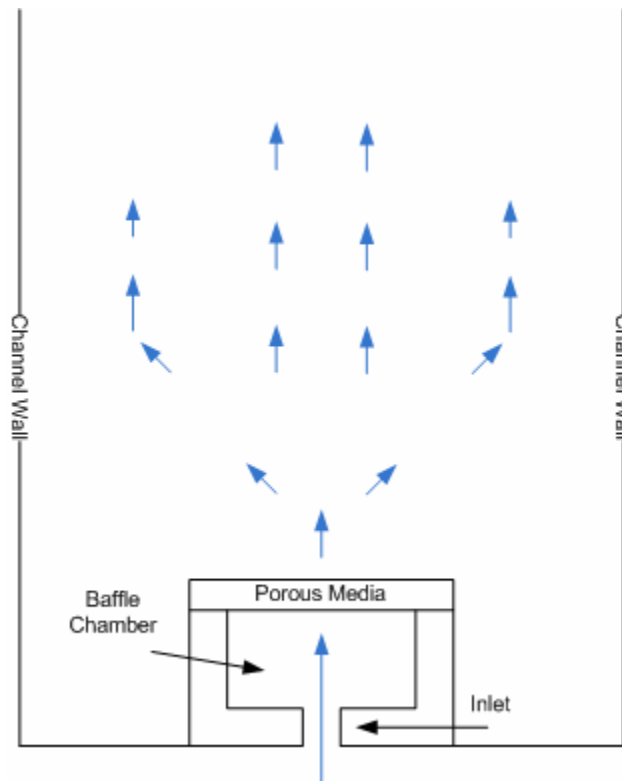
Figure 3.2. Notional cross section showing flow evolution in a porous anode design. Blue arrows indicate flow.

27
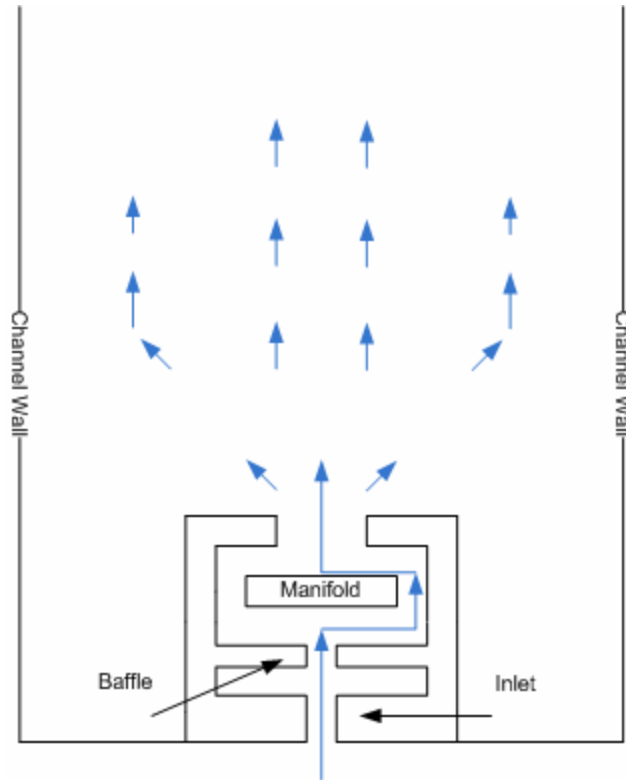
Figure 3.3. Notional cross section showing flow evolution in a drop-in orifice-based anode design. Blue arrows indicate flow.
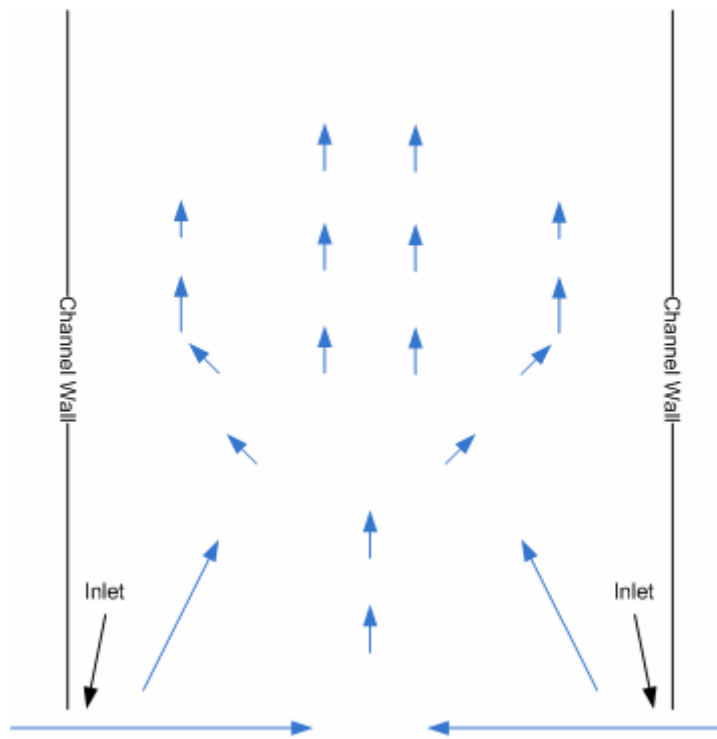
Figure 3.4. Notional cross section showing flow evolution in an integrated orifice-based anode design. Blue arrows indicate flow.

The porous design concept utilizes a porous material place over a propellant reservoir, the idea being that a uniform flow can be developed without the need for complicated machining. The integrated design builds the propellant distribution into the channel walls of the discharge chamber in an attempt to reduce parts count. The drop-in design has the most heritage and works by using a series of baffle and manifold holes to evenly distribute the propellant throughout the channel. In the end, the drop-in design was chosen primarily due to risk-mitigation factors.

The FLUENT CFD tool from Ansys was used to evaluate the validity of all three design concepts. Based on the work of Reid,[79] the design team identified FLUENT as a valid tool in the flow regimes that can be expected in an HET. To reduce computational expense, only the outer channel was simulated when deciding between the three design concepts. The outer channel was chosen because it was the most extreme case because of its size and expected flow range. Once the drop-in design was chosen, anodes for all three channels were iteratively designed and simulated. The results of the final simulations are presented in section 3.2.3.

3.2.3. Results of FLUENT simulations

Herein are presented the results of the FLUENT simulations of the drop-in anode designs for all three channels of the X3. They were obtained using double-precision, pressure-based simulations on 64-bit Windows machines with mesh sizes on the order of 1-3 million tetrahedral elements. Simulations were determined converged when the residuals from all three Cartesian components of velocity as well as mass flowrate reached levels at or below $1x10^{-5}$, domain outlet pressures were in the range of physically possible, and inlet and outlet mass flow rates matched. Radial uniformity results for both

the low and high flow regimes of each channel are given in Figure 3.5 and Figure 3.6 respectively. Azimuthal uniformity results are tabulated in Table 3.2. All data indicate designs that are capable of producing both radial and azimuthally uniform flowfields.
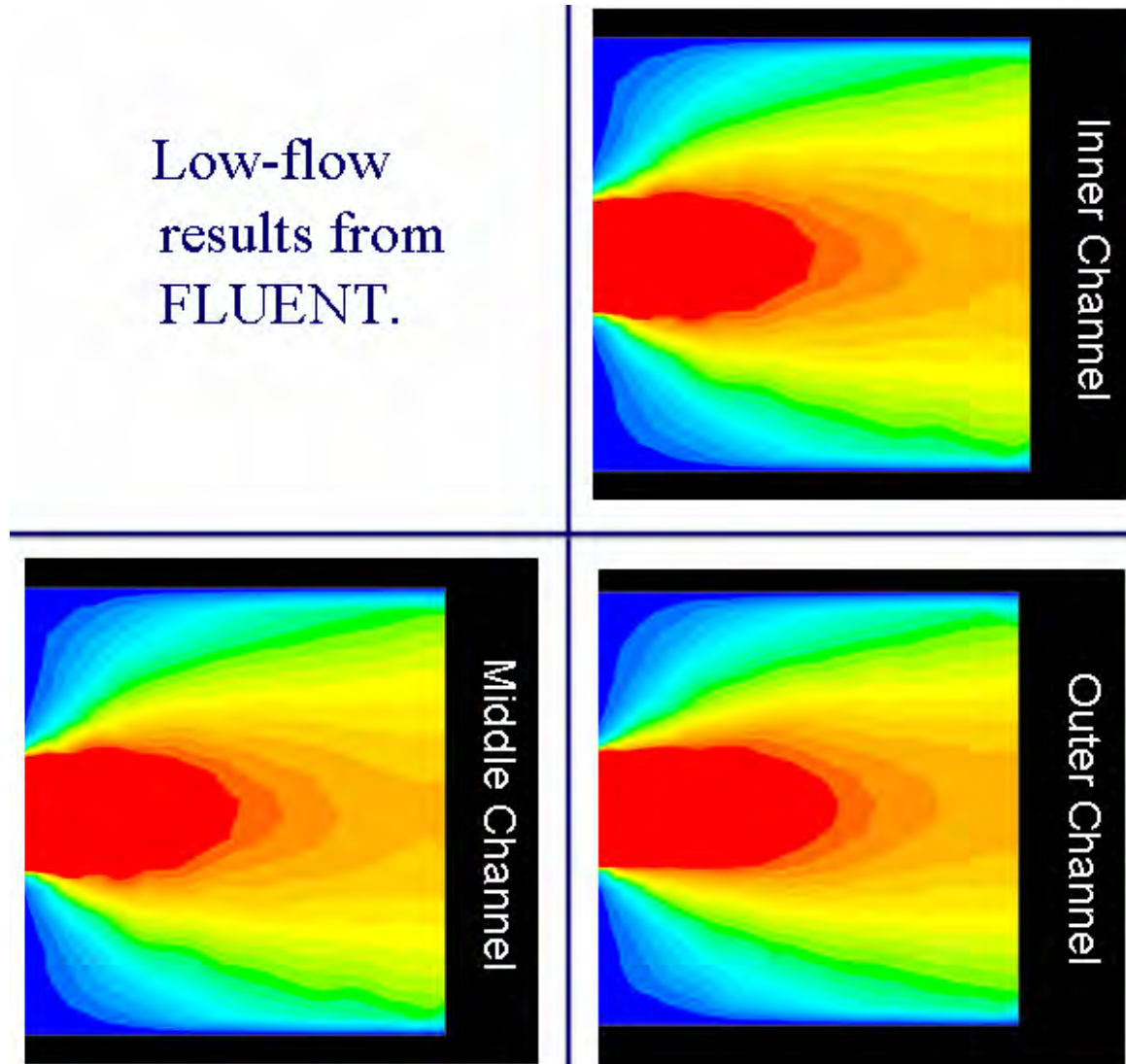
Figure 3.5. Cross-sectional normalized mass-flux contours for low-flow simulation all three designs used for determination of radial uniformity. Clockwise from Upper left: title, inner channel, middle channel, outer channel.
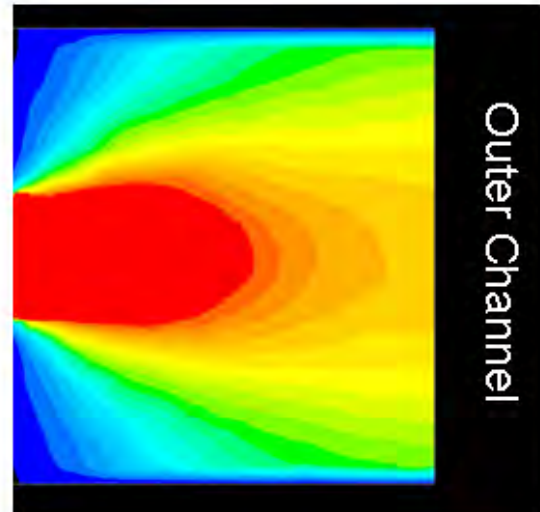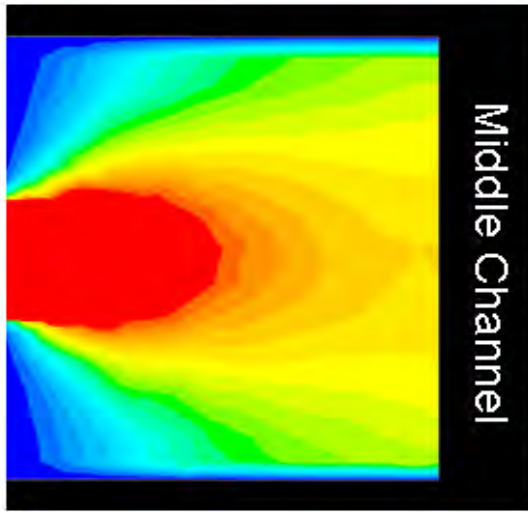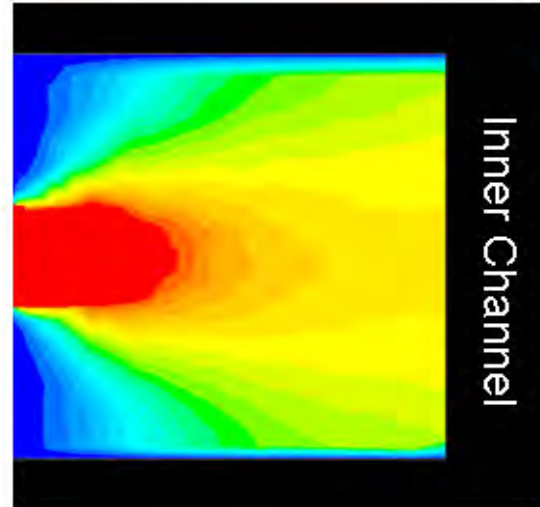
Figure 3.6. Cross-sectional normalized mass-flux contours for high-flow simulation all three designs used for determination of radial uniformity. Clockwise from Upper left: title, inner channel, middle channel, outer channel.

Table 3.2. Table of simulation results showing azimuthal uniformity. L is length of the channel.

Parameter	Inner Channel	Middle Channel	Outer Channel
Flux uniformity over center quarter of channel @ distance 0.07L, 0.14L, 0.29L upstream of channel exit (from FLUENT, low-flow)	+/- 1.9% (0.07L) +/- 2.4% (0.14L) +/- 3.3% (0.29L) standard deviation	+/- 2.0% (0.07L) +/- 2.5% (0.14L) +/- 3.8% (0.29L) standard deviation	+/- 2.4% (0.07L) +/- 2.9 % (0.14L) +/- 4.3% (0.29L) standard deviation
Flux uniformity over center quarter of channel @ distance 0.07L, 0.14L, 0.29L upstream of channel exit (from FLUENT, high-flow)	+/- 1.3% (0.07L) +/- 1.7% (0.14L) +/- 3.3% (0.29L) standard deviation	+/- 1.6% (0.07L) +/- 2.1% (0.14L) +/- 4.1% (0.29L) standard deviation	+/- 1.7% (0.07L) +/- 2.3 % (0.14L) +/- 4.3% (0.29L) standard deviation

3.2.4. Verification of design/acceptance test

Prior to final thruster assembly, the anodes' ability to produce a uniform flowfield were experimentally verified (Figure 3.7) within the framework of an acceptance test. All three anodes were interrogated while flowing cold neutral gas via the use of linear and rortary motion stages, a pressure probe, and a LabVIEW code,
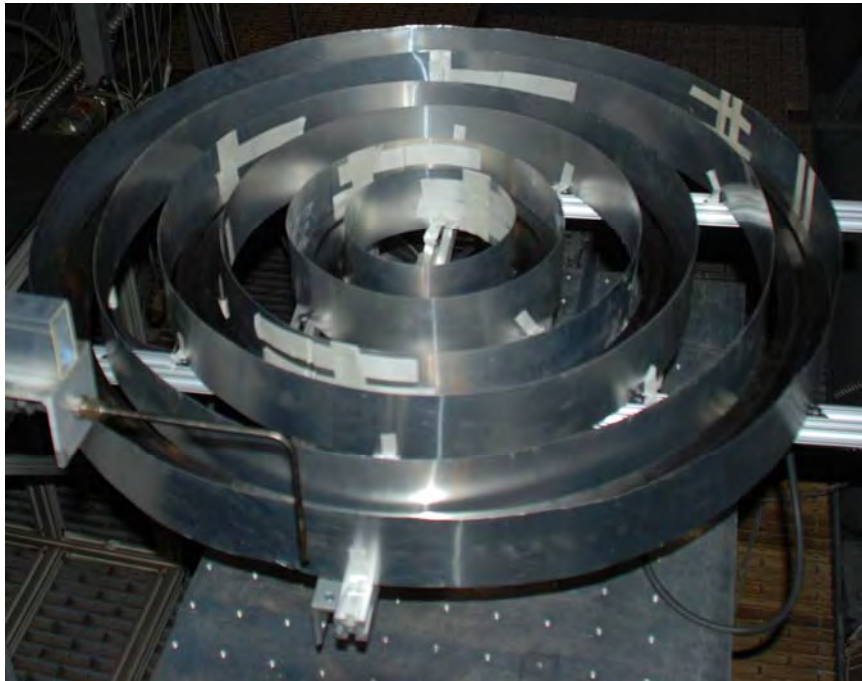
Figure 3.7. Picture of anode flow verification setup. Mock channel walls constructed of sheet metal to provide more accurate setup.

The primary goal of this testing was to verify pressure profile shape radially across the channel and to ensure that an azimuthally uniform flow was being produced. A representative radial profile is presented in. Normalized data showing azimuthal uniformity are presented in.
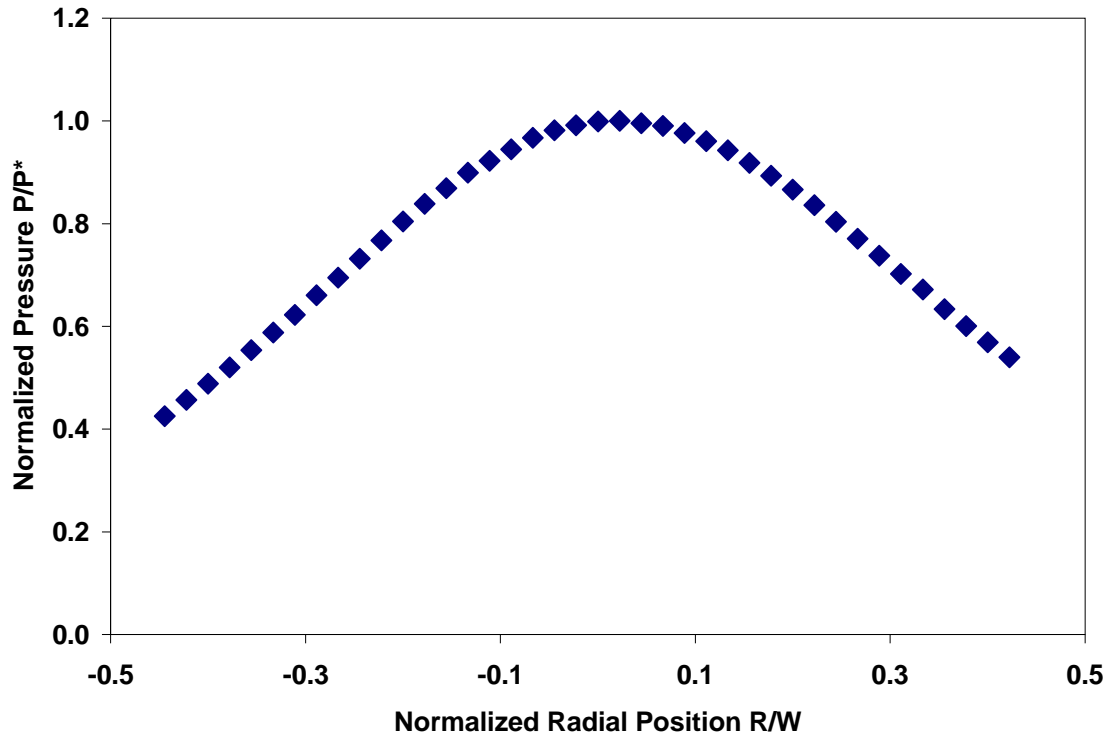
Figure 3.8. Representative radial pressure profile. Pressure P is normalized by maximum value in profile, P*. Radial position R is normalized by channel width W.

Table 3.3. Table giving normalized azimuthal uniformity data. L= channel length. I=inner, M=middle, O=outer. Flow rates for given data were in the upper half of the range given in Table 3.1. The % error reported here is the percent standard deviation of the pressure measured throughout all 360 degrees of a given channel. Azimuthal steps were 3.75 degrees for the middle and outer channels and 9 degrees for the inner channel.

Channel	Distance upstream of channel exit	% Error Std Dev	Gauge Error (+/-%)
I	0.29L	5	5
M	0.29L	13	10
O	0.29L	13	10

. All radial profiles followed the trend outlined in Figure 3.8 indicating radially uniform flow. The percent standard deviations in the pressure data presented in Table 3.3 are all within the gauge error, indicating azimuthally uniform flow. It was thus concluded that the anodes were developing the flow as expected and that they all passed the acceptance test.

33

3.3. Magnetic circuit design

3.3.1. General notes and simulation results

The magnetic circuit of the X3 was designed to support three simultaneously operating concentrically nested discharge channels. As with the X2,[9] this means that the circuit was designed to support three simultaneous magnetic lens topologies with magnetic field directions flipping in between channels to maintain quasi-radial fields within the channels. This means that if the fields of the inner and outer channel are pointing radially outwards, the field of the middle channel is pointing radially inwards. Also as with the X2,[9] cusps form at the middle two poles of the thruster causing the direction of the hall current to flip with the change in ExB direction between channels. This means that if the Hall current is moving clockwise in the inner channel, it moves counter-clockwise in the middle channel, and clockwise again in the outer channel. The resulting magnetic field topology is presented in ; the field was simulated using the MagNet 7 design tool from Infolytica.
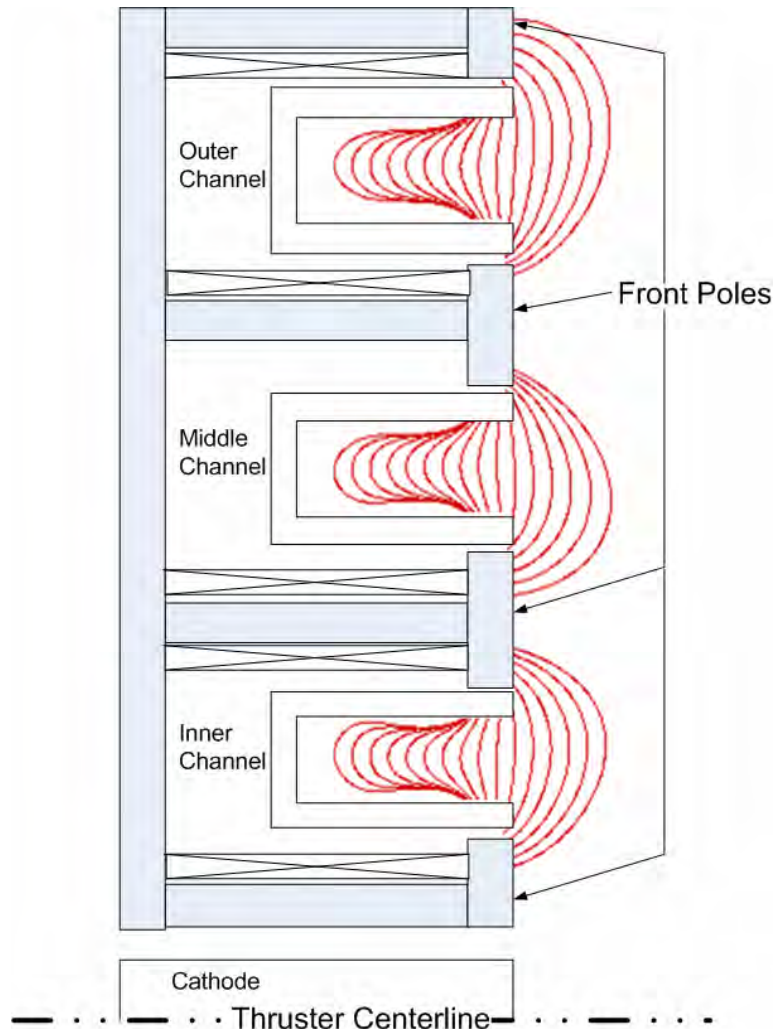
Figure 3.9. X3 design magnetic field topology; simulated results from Infolytica's MagNet 7.

3.3.2. Experimental Verification

Through the use of linear and rotary motion stages, a magnetic field probe, and a LabVIEW code, the magnetic field of the thruster was verified prior to operation of the X3. No pictures of the setup are available for release at this time. The goals of this experimental verification were to:

- Ensure field attains desired strength (Table 3.4)

- Ensure r-z profiles match (Figure 3.10-Figure 3.12)

Ensure azimuthal uniformity (

- Table 3.5)

Table 3.4. Table showing deviation from design value for each channel's peak radial magnetic field strength. Data is presented as fraction of each individual channel's individual design value. For example, a value of 0.5 for the column labeled "fraction" would indicate that the measured value was half the design value.

Channel	Fraction
Inner	1.0
Middle	1.1
Outer	1.1
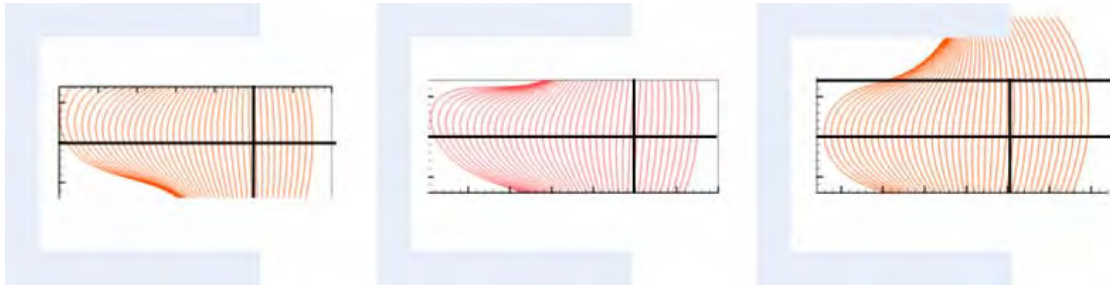
Figure 3.10. Side-by-side comparison R-Z radial cross-section magnetic field profiles for the inner channel. Left-right: measured 3 o'clock, measured 9 o'clock, simulated 9 o'clock. Clocking is defined as looking along the thrust axis of the thruster into the discharge channels. Cross lines (bold black) indicate common coordinates. Gray boxes represent notional discharge channel walls (not to scale).
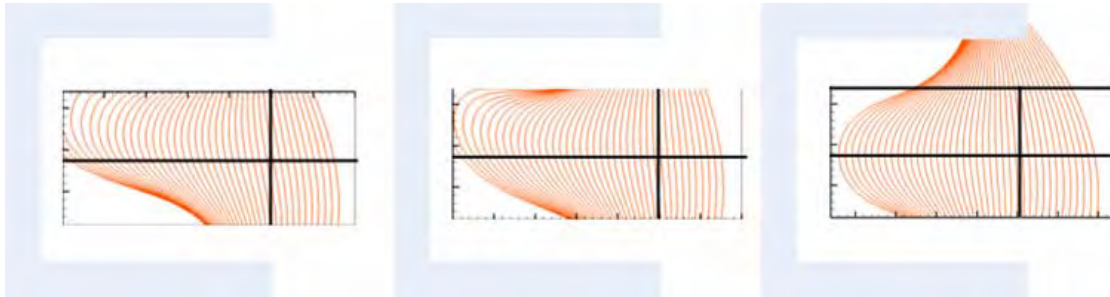
Figure 3.11. Side-by-side comparison R-Z radial cross-section magnetic field profiles for the middle channel. Left-right: measured 3 o'clock, measured 9 o'clock, simulated 9 o'clock. Clocking is defined as looking along the thrust axis of the thruster into the discharge channels. Cross lines (bold black) indicate common coordinates. Gray boxes represent notional discharge channel walls (not to scale).
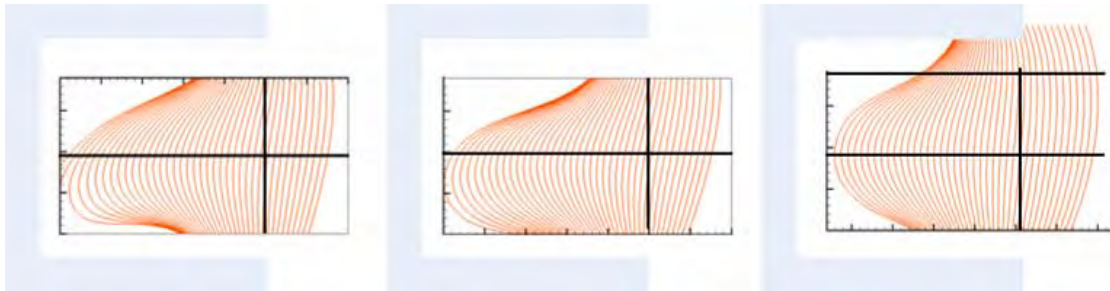
Figure 3.12. Side-by-side comparison R-Z radial cross-section magnetic field profiles for the outer channel. Left-right: measured 3 o'clock, measured 9 o'clock, simulated 9 o'clock. Clocking is defined as looking along the thrust axis of the thruster into the discharge channels. Cross lines (bold black) indicate common coordinates. Gray boxes represent notional discharge channel walls (not to scale).

Table 3.5. Summary of deviation of peak radial magnetic field across full 360 degrees of each channel. Data presented as percent standard deviation from mean (% Std. Dev).

Channel	% Std. Dev [%]
Inner	1.7
Middle	4.3
Outer	3.4

The data in Table 3.4 indicates that the magnetic circuit is able to produce, and even slightly exceed, the design values magnetic field magnitude. The percent deviation given in

Table 3.5 is below a threshold value of 5% and within the experimental error. As the data indicated that the magnetic circuit was performing within acceptable margins of the design, testing of the X3 was allowed to proceed.

3.4. Brief notes on thermal design

Due to X3's unprecedented size and power level, a thermal modeling effort was undertaken. All simulations were conducted by Dr. James Polk of the NASA Jet Propulsion Laboratory (JPL). As the work for this effort was carried out by a third party and not the author of this document, the primary purpose of this section is to relay the impact of the simulations to the reader.

The thruster was simulated at power levels between 70 kW and 200 kW in order to bracket the operational regime of greatest thermal stress. The simulations were carried out in full 3-D and representative image of the model and results is provide in.
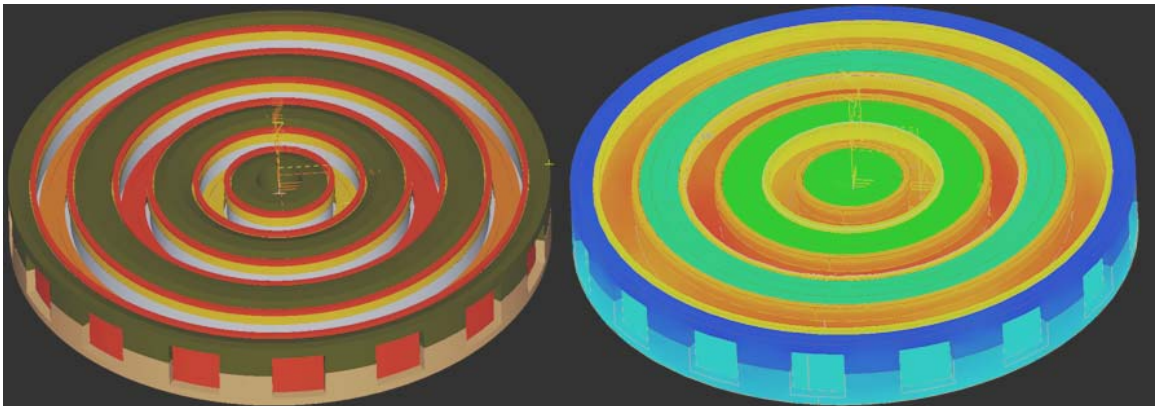
Figure 3.13. Representative 3-D rendering of X3 in thermal modeling software (Left) alongside representative results (Right).

The thermal modeling had two main impacts on the design process. First, the results of the modeling effort helped guide the material selection process for various components. The ability to select materials that will not loser strength nor melt at operating temperatures is not insignificant for the designer. Second, just as important as material selection is the ability to account for thermal growth when considering parts tolerancing. The design team realized the basic fact that all material properties being equal, by increasing part size to the scale of the X3 and the temperature change that parts undergo to the levels X3 was anticipated to experience, thermal growth of parts could very well approach appreciable amounts (e.g. at or greater than machining tolerances). Predicting dimensional changes at temperature afforded the designers the ability to incorporate thermal expansion into the design prior to fabrication.

CHAPTER IV

Facility upgrades and experimental setups

"Se biellu vo' pari, gran dulure de pa'ti."

At the initial design stages of this thruster, when the team was looking for facilities where the X3 could be tested, an important fact was realized: substantial infrastructure upgrades would need to take place in order to perform any kind of meaningful test with the device. Discussed herein are the various upgrades that have been performed at PEPL to prepare for the arrival of the world's largest HET parsed out into the following categories: electrical, gas flow system(s), mechanical upgrades, and thermal management.

The chapter is organized as follows. First, details on the large vacuum test facility (LVTF) itself are given (section 4.1). Next, the electrical and gas flow system(s) upgrades are presented (sections 4.2 and 4.3). A summary section is then given (section 4.4) that describes how these systems are part of the experimental setup for krypton and xenon operation. Included in this summary are the subsystems that allow for photographic evaluation of the thruster as well as high-speed monitoring of the discharge current. The mechanical upgrades are then presented in section 4.5. Section 4.6 details thruster installation steps for both krypton and xenon operation. Section 4.7 gives a description of thrust stand operation during xenon operation of the X3. Section 4.8 discusses thermal management in LVTF. Finally, a summary of upgrades undertaken is given in 4.9.

The X3 is the only thruster used in the experimental setups in this document. As the X3 is introduced in Chapters II and III, no sub-section is given to it in this chapter.

4.1. Large Vacuum Test Facility

The X3 NHT was installed and tested in the LVTF (Figure 4.1) for all of the krypton and xenon operation presented in this document. The LVTF is a 200 m^3 stainless-steel-clad vacuum chamber 9 m long and 6 m in diameter. Rough vacuum is achieved using two 2000 CFM blowers backed by four 400 CFM mechanical roughing pumps with an ultimate base pressure in the low 10^{-7} Torr achieved through the use of seven CVI-TM1200 internal cryopumps with LN2 shrouds that provide a nominal pumping speed of about 500,000 l/s on air 250,000 l/s on xenon, and 300,000 l/s on krypton. During operation, chamber pressure is measured by an external ion gauge at the top of the chamber axially co-located with the thruster exit plane with an uncertainty of ±20% according to the manufacturer.[80] The pressure varied in the chamber during testing due to changing anode and cathode flow rates with a fixed pumping speed. As the ion gauge is calibrated for N2, pressure is corrected for the propellant gas via Equation 4.1:[81]

$$P = \frac{P_{ob} - P_b}{x} + P_b \qquad \text{[4.1]}$$

where P is the corrected pressure, P_{ob} is the observed pressure, P_b is the ultimate pressure before propellant flow is initiated, and x is a propellant-dependent constant (1.96 for Kr and 2.87 for Xe).
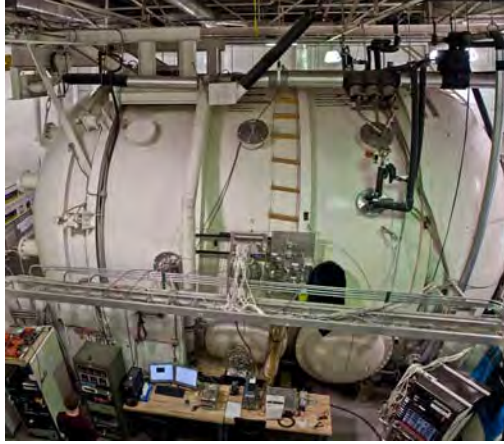
Figure 4.1. Large Vacuum Test Facility at PEPL.

4.2. Electrical infrastructure

In order to process 200 kW of applied DC power, significant upgrades had to be performed at PEPL. These can be sub-divided into three sub-categories: power distribution, the thrust stand waterfall (referred to as such or simply as "the waterfall"), and measurement circuitry.

A note on nomenclature: all voltages and currents are DC unless otherwise noted.

4.2.1. Power Distribution

4.2.1.1. Power Supplies

The discharge power supply is that DC output unit which applies the discharge voltage between the anode and the cathode. Discharge power is defined in Equation 4.2:

$$P_D = V_D \cdot I_D \qquad\qquad \textbf{[4.2]}$$

where P_D is discharge power, V_D is discharge voltage, and I_D is discharge current.

All three channels of the X3 required supplies that could reach up to 1000 V. This, however, is not the main challenge for the supplies. In fact, it is the need to also output from 60 A to 150 A while providing a potential difference of 1 kV that makes these devices large and expensive. Many 1 kV/1 mA and 1 mV/ 150 A power supplies exist in

the world, and their input power requirements are not difficult to meet in the average laboratory setting. Here the notation XX V/ YY A indicates the maximum output capacity of the supply. At the time of the inception of the X3, PEPL already possessed a 100-kW (1000 V/100 A) DC output power supply from Amrel (HPS1000-100). As this is only sufficient to operate one channel at max power, two other supplies were obtained. A 60-kW unit (1000 V/ 60 A) and a 150-kW unit (1000 V/150 A) were purchased from Magnapower Electronics in order to supply the other two channels (MSD1000-60/480 and MTD1000-150/480 respectively). While the work of the X2 showed that an NHT can be run off of a single power supply,[82] this brings one into a realm of power supplies for the X3 that was not convenient in a laboratory setting as well as prohibitively expensive. The operation of these power supplies required the installation of approximately 330 kW of 480 VAC three-phase power into PEPL. This is no small undertaking, and it is recommended that anyone considering installation of such devices careful examine the power available at their facility before embarking on such an endeavor. Often, 480 VAC power is available at laboratories, but either not enough is available in one place—necessitating the installation of new transmission/feeder lines--or there is not enough free power in aggregate—necessitating additional high voltage building service, which requires coordination with the utility company.

Figure 4.2. The three discharge power supplies for the X3 (left-to-right): 60 kW (Magnapower MSD1000-60/480), 100 kW (Amrel HPS1000-100), and 150kW (Magnapower MTD1000-150/480).

4.2.1.2. Cabling

The next challenge that had to be met was the method of delivering the power from the supplies to the thruster inside the chamber at vacuum. While previously existing cable met requirements for voltage isolation, it was undersized for the amount of current that needed to be pushed through it. The 12 AWG 150 C silicone rubber insolated wire in common use at PEPL has a max individual cable ampacity of 20 A at vacuum.[83] Bundling the wires together, when accounting for wire de-rating in a bundle, meant that in order to handle 250 A of current for the cathode return line, over 12 wires would have been required. Equation 4.3[83] gives the equation for de-rating wires in a bundle:

$$I_{BW} = I_{SW} \times \frac{29 - N}{28} \qquad \text{[4.3]}$$

where N is the number of wires in the bundle, I_{BW} is the current in a single wire in the bundle, and I_{SW} is the current in a single un-bundled wire.

Such a large number of wires presents a physical barrier to the setup, especially when in the context of vacuum feedthroughs. After extensive evaluation of high temperature

wire available from multiple vendors, the final selection that was made was for Cicoil brand 260 °C pure silicone insulated wire, which can hold its atmospheric ampacity rating all the way to the pressures seen inside LVTF. This is due to the fact that wire de-ratings are fundamentally based upon the thermal limitations of the wire insulation.[84] Experiments were performed to determine how hot the insulation would get using a 10 AWG wire from Cicoil. See below for the surface temperature of a coil of this wire as a function of elapsed time at a constant applied DC current that was chosen to be the maximum atmosphere rated current of 70 A. Background pressure was kept below 1×10^{-6} Torr.
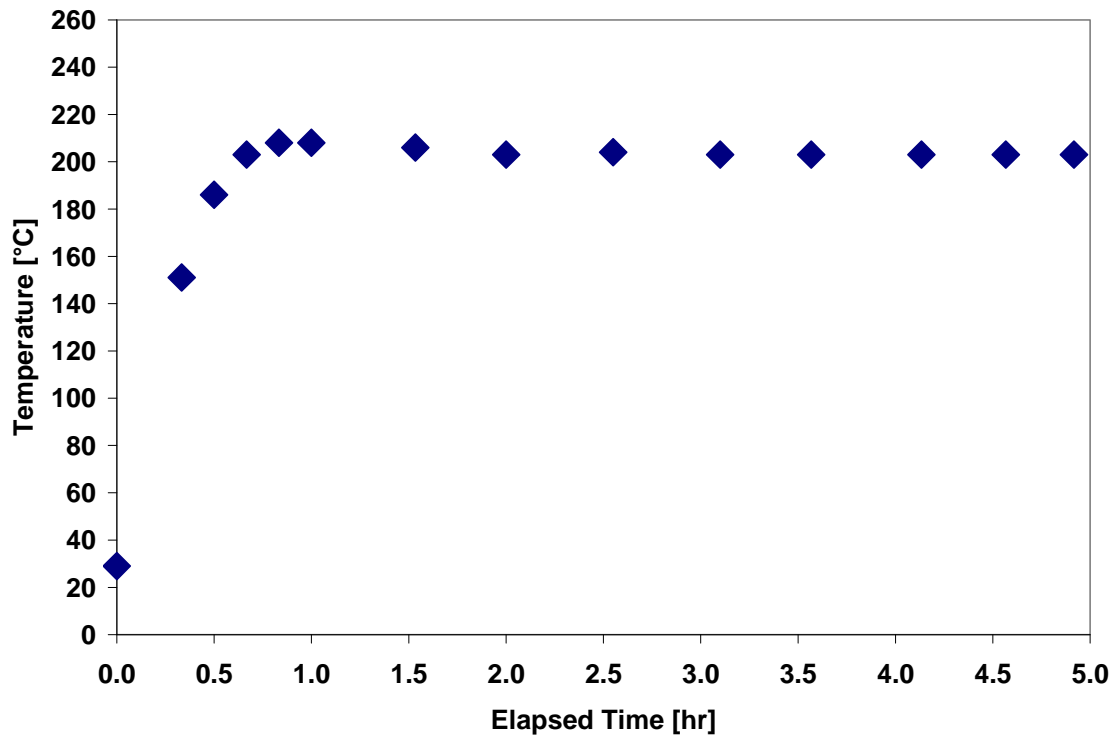
Figure 4.3. Wire surface temperature as a function of elapsed time for 10 AWG Cicoil wire under a vacuum of less than 1×10^{-6} Torr with an applied DC current of 70 A. Note: The upper bound of the graph, 260 °C, is the manufacturer rated temperature of the wire.[85]

Having proven that the insulation could perform at its atmospheric rated current down through the pressures that would be experienced during operation, discharge line bundles

44

were constructed with an eye at minimizing number of cables while maintaining roughly a factor of safety of two on allowable current. All discharge lines, at atmosphere and vacuum, were placed in grounded flexible aluminum conduit (grounded only at one the interface with the chamber) to act both as an EMI shield and to reduce overall line inductance by bringing the ground plane much closer to the transmission line. As it turned out that three wires was the optimum number per bundle, all conduit running from power supplies to the atmosphere side breakout box contained six cables each; positive and negative leads were twisted together to further reduce inductance. All conduit downstream of the breakout box contained three wires per run, for four runs of conduit total (three anodes and one cathode return).

Equation 4.4 below illustrates the need to reduce inductance in the lines as much as possible: coupling kHz oscillations that occur in thruster discharge currents with long wire length (higher L) and high currents, voltage oscillations at the thruster side can become a concern.

$$V_L = L\frac{dI}{dt} \qquad\qquad \textbf{[4.4]}$$

where V_L is the voltage oscillation magnitude, L is the inductance of the line, and $\frac{dI}{dt}$ represents the variation of the current through the line in time. In the figure below, a one-line electrical diagram has been provided that explains the power supply-breakout box-flange-thruster electrical arrangement (Figure 4.4). Further, a cross sectional view of three- and six-wire conduit is provided for illustrative purposes and is not to scale (Figure 4.5).
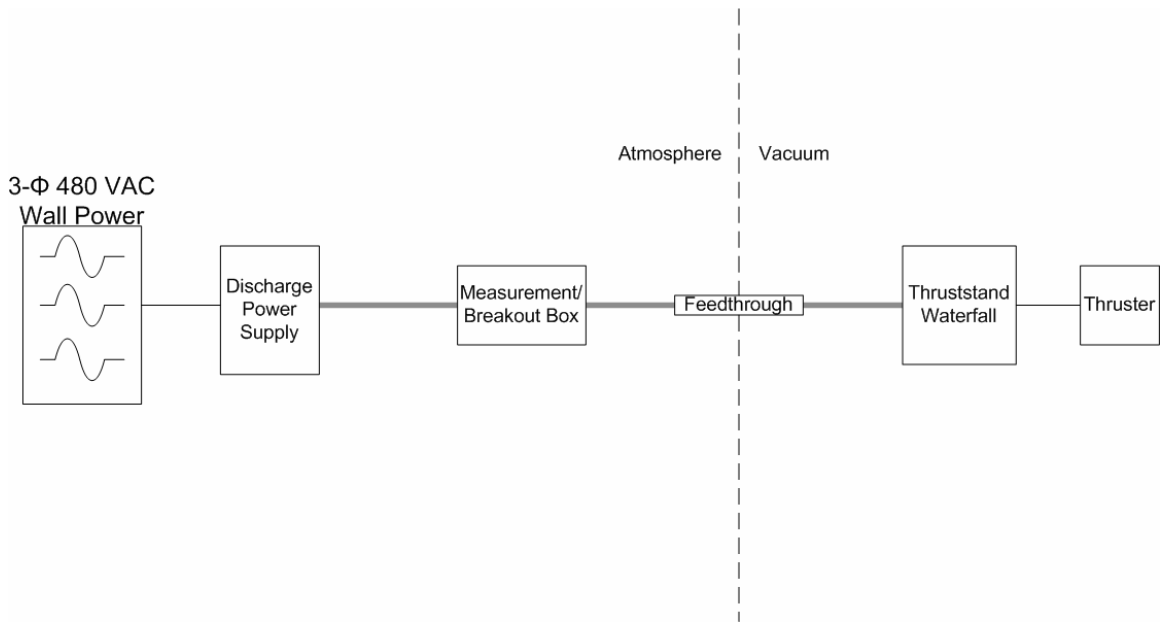
Figure 4.4. One-line diagram of discharge line delivery scheme. Thick grey lines indicate wiring inside grounded conduit.
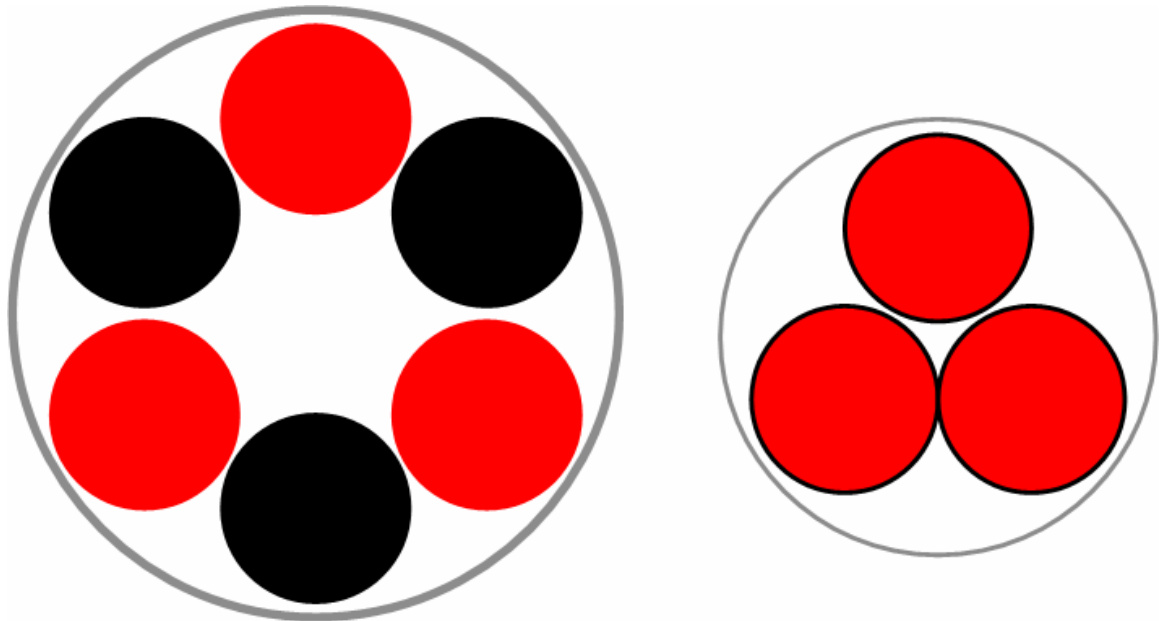
Figure 4.5. Six-wire (left) and three-wire (right) conduit configurations. Red circles (with and without black outline; the black outline is simply a visual aid and has no meaning) represent positive lines, black circles represent negative lines. The larger grey circles are the conduit.

4.2.1.3. Voltage Isolation

Previously existing discharge lines were assembled with a maximum voltage of 600

V in mind. This is not to say that higher voltages have not been run at PEPL before--

several kV have been fed into the chamber for gridded ion thrusters.[86] The point is that "existing" refers to infrastructure that was in place at the time that upgrades began, not something that had previously existed but had since been removed.

As the X3 initial run plans included voltages up to 800 V, with options to extend to 1000 V, the existing isolation scheme was insufficient. The point of contention was not the standoff of the wire insulation (previous lines were good to 15 kV) but the way they were isolated at bare wire points. This primarily includes where they connect to copper lug feedthroughs at the flange (Figure 4.6) as well as where they connect at the waterfall and thruster.
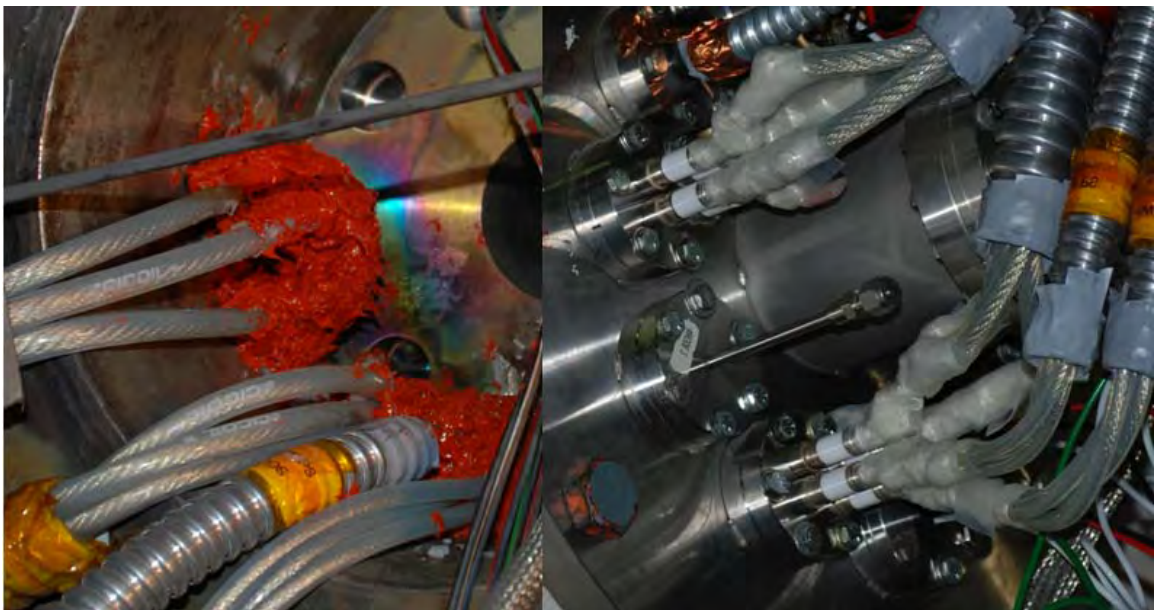
Figure 4.6. Four-stud copper feedthrough from MDC vacuum taped over atmosphere side of LVTF (right). Silicone isolating adhesive applied to vacuum side of feedthrough (left).

What this comes down to is taping schemes. While this is not a very glamorous topic for a PhD dissertation, it is somewhat critical to the operations that allow for such a dissertation to become possible. Ion thruster operators were consulted for the best taping scheme to isolate at 800 V and above, and it was concluded that a mixture of fiberglass and fusion tape is the best course of action. As one might gather from Figure 4.6, space at

the flange was at a premium. As such, high-grade, high-temperature 100% silicone insulating material with a very low volatile organic compound (VOC) content was employed to encase the entirety of the exposed lugs in an isolating material. Again, this is a method that can be considered a lesson learned by individuals who had to isolate at high voltage in tight spaces in vacuum.

4.2.2. Thrust stand waterfall

A waterfall in the context of thruster operation refers to the cable bundle that is draped over a fixed structural frame above the thrust stand down to connection points for the thruster. It is assembled in such a way as to provide strain relief on the wiring while allowing them to also flex properly without impeding the motion of the inverted-pendulum thrust stand which would introduce non-repeatable error in the thrust measurements. Please see the cartoon below for a visual conceptual description of a waterfall (Figure 4.7).

Rather than follow the PEPL tradition of creating a waterfall with each thruster setup, it was decided that as part of the upgrades a universal waterfall would be constructed.
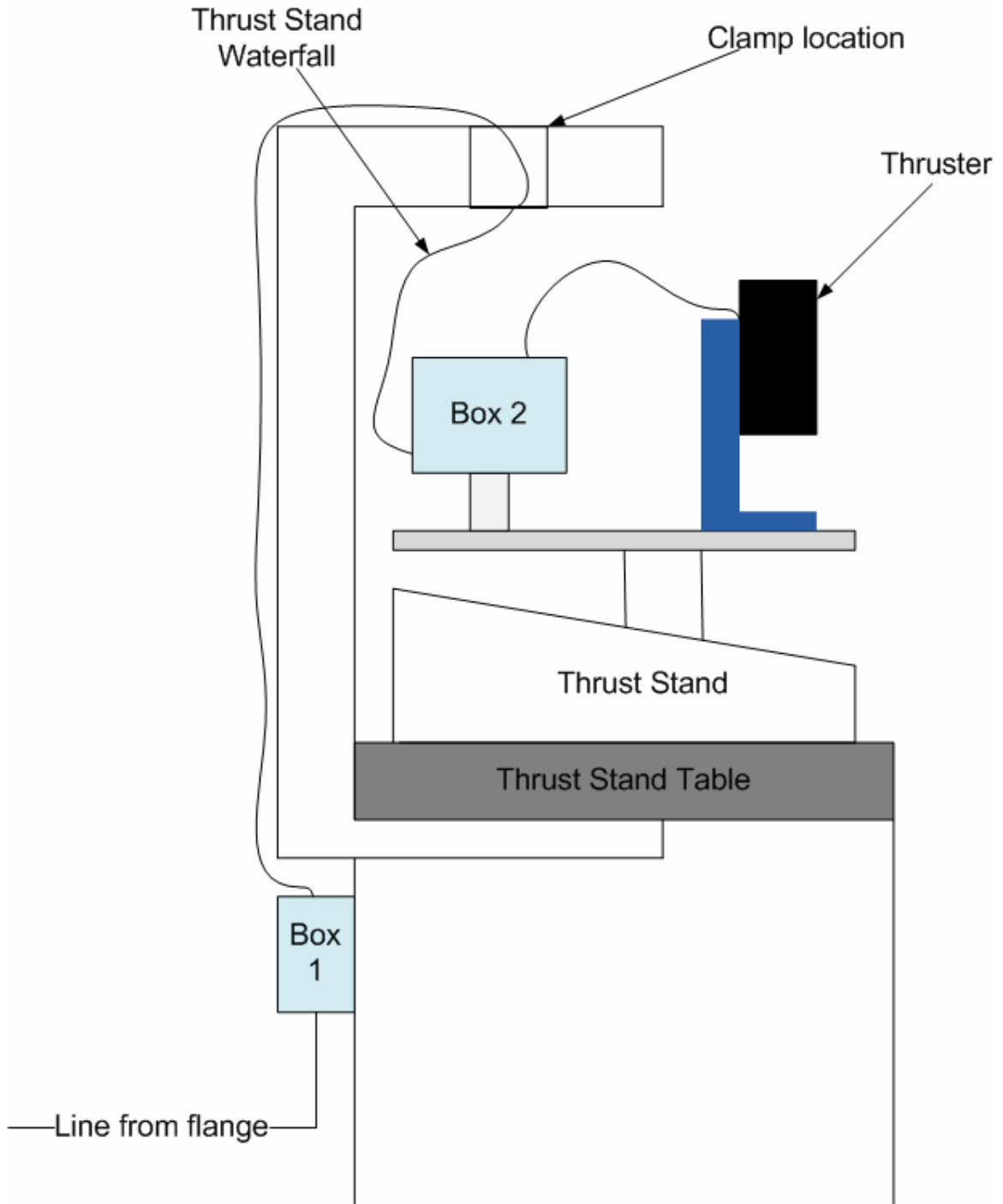
Figure 4.7. Cartoon of waterfall.

The primary advantages of a 'universal' waterfall are expediency and survivability. Diagnostics aside, the most time intensive portion of any test setup is thruster installation on the thrust stand. This stems from the need to carefully string and re-string the waterfall with each thruster setup. For a thruster like the X3, which has two to three times the

amount of wiring of nearly any other individual thruster, this would amount to many hours of work. With a universal waterfall, the idea is that the wire is already draped and terminated in breakout boxes such that all one has to do is fasten the thruster to the thrust stand and plug it in. The other issue is long term survivability of wiring. Previously, the wire had to be uncoiled, draped, clamped, unclamped, un-draped, and coiled up again. This scraping and bending wears at the integrity of the insulation and the conductors, as well as creates an unnecessary large umbilical of wire that must be organic to the thruster.

The design for the waterfall at PEPL is based upon the system in-place at NASA Glenn Research Center (GRC) at their Vacuum Facility-5 (VF5) test facility. The general requirements of the waterfall were as follows:

- Easy quick disconnects, via SuperCons

- Be able to support wiring for any thruster to conceivably be tested at PEPL, driven by the X3 as well as the BHT-600 4X cluster

- Wiring must be high-flex, high-temperature

- Modular for easy repair (wires do fail eventually)

- May not impede thruster installation

- Must accommodate sense lines

- Must accommodate a large number (>20) k-type thermocouple wires

The same Cicoil wiring used for discharge wire delivery was used for all lines with the exception of the sense lines and the thermocouple wires. Sense lines were 15-kV 150-°C wire from Allied Wire Company. The total electrical wire count is: 250-A lines (6X), 50-A lines (4X), 25-A lines (24X), low current (~3 A) sense lines (8X).

There are 36 complete k-type thermocouple wires. As of the writing of this document, they are not currently integrated into the waterfall, but stop just short of 'Box 1' from Figure 4.7. See Figure 4.8 below for a picture of the PEPL's new, universal waterfall.

Figure 4.8. PEPL's universal waterfall, sans thruster. The boxes which accept the wires from the flange are not pictured here.

4.2.3. Measurement Circuits

In order to monitor the extra telemetry of the X3, a new breakout box modeled on the one built by Dr. Raymond Liang for the X2 (Figure 4.9) was constructed.

51

Figure 4.9. Photograph of X2 NHTs breakout box.

This is the same breakout box that is referred to in Figure 4.4. What follows is a description of the various measurement circuits that exist within. The clearest way to do

this is to provide a list of the telemetry items accounted for and representative circuit diagrams/PCB layouts for each.

The list of categories is as follow:

- Discharge voltage

- Discharge current

- Cathode-to-ground voltage

- Heater voltage and current

- Keeper voltage and current

- Magnet voltage and current

- Cathode-to-ground protection (not a measurement)

Measurement Methods:

- Voltage Dividers: Discharge voltage, keeper voltage, cathode-to-ground voltage (Figure 4.10).

- Current Shunts: Magnet, heater and keeper current (Figure 4.11).

- Magneto-resistive sensors: Discharge current (Figure 4.12).

- Direct measurement: Magnet and heater voltage (Figure 4.13).
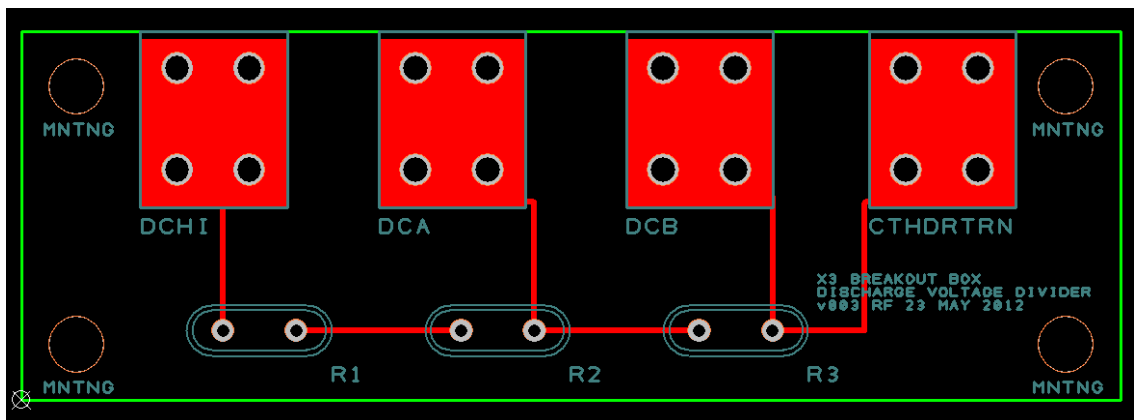
Figure 4.10. Sample voltage divider PCB layout. All resistors, indicated by R#, are thin-film metal-oxide resistors for minimal inductance. Labels are: DCHI-anode voltage, DCA-high end of divider fed to DAQ, DCB-low end of divider fed to DAQ, CTHDRTRN-cathode potential.
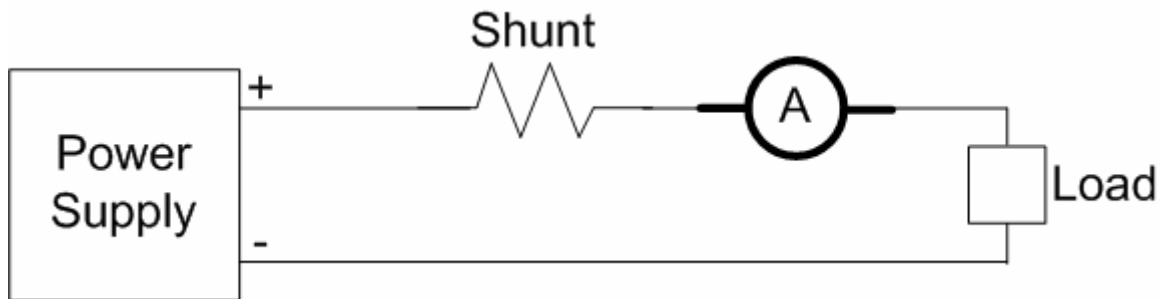
Figure 4.11. Sample current shunt setup. The ammeter symbol can be taken to be the DAQ, where the voltage read off the shunt is converted to a current by a scaling factor related to the resistance of said shunt.
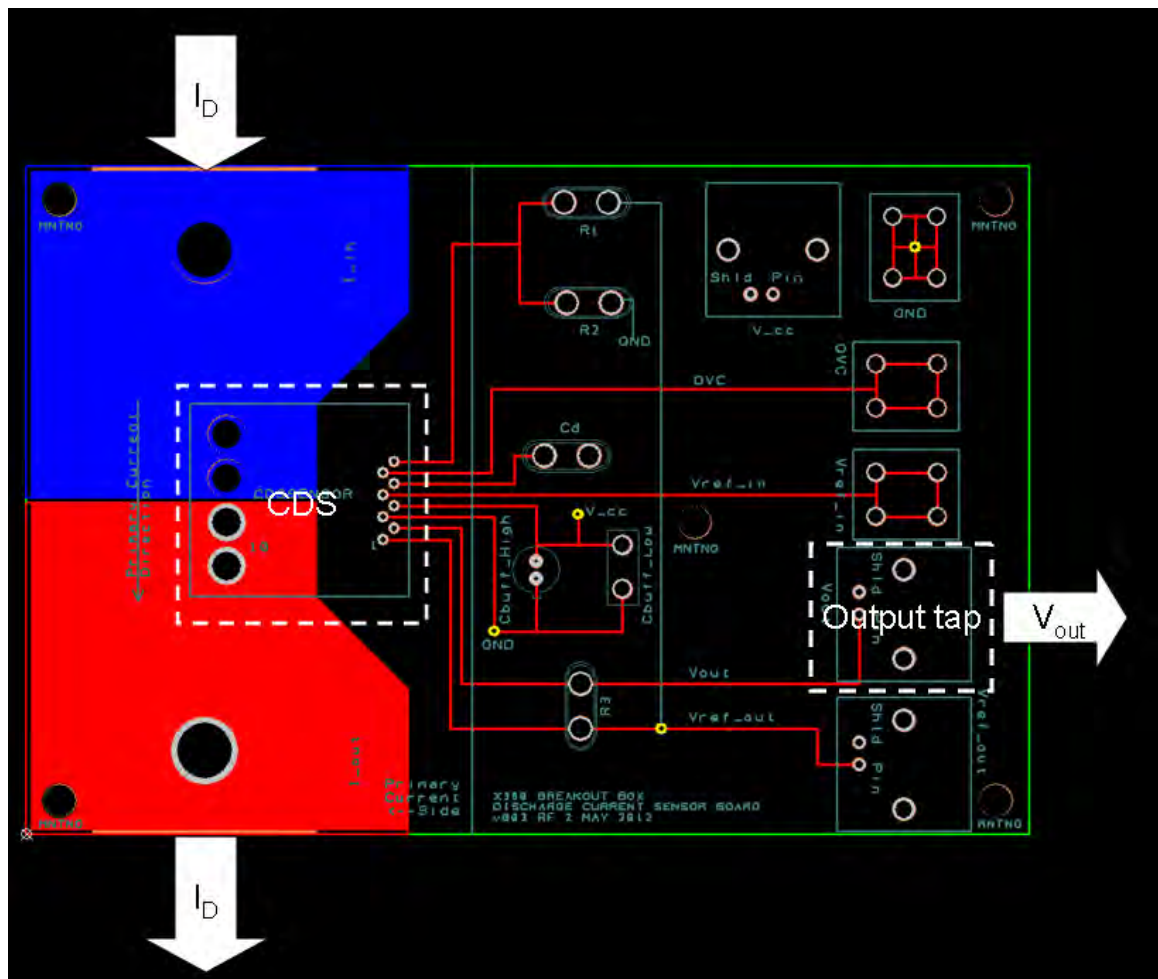
Figure 4.12. FW Bell CDS series magneto-resistive current sensor PCB layout, used for measuring discharge currents. Key component locations are highlighted I_D is the discharge current and V_{out} is the output voltage from the sensor fed to the DAQ. Note: this is a 4-layer board, only the top pour layer is pictured here. This sensors have a bandwidth from DC-100 kHz.[87]

Figure 4.13. Direct measurement sample circuit. The voltmeter represents the DAQ unit.

4.3. Gas flow system

The mass flow system in place at the LVTF prior to the development of the X3 had mass flow controllers (MFC's) that were sufficient to handle a single channel at 50 A or a dual channel device operating up to 70 A across both channels. The X3, with its double requirement of high flow and multiple controllers pushed us to augment the existing system. As with other upgrades that sprang up as a result of this project, an attempt was made to also improve the general operation of the facility as a whole.

4.3.1. High-flow MFC's

The following is a list of the available MFC's attached to LVTF prior to the upgrade (all ratings are for Xe, 1 mg/s of Xe is 10.24 SCCM):

- 500 SCCM (1x)

- 200 SCCM (1x)

- 50 SCCM (1x)

- 20 SCCM (1x)

The next list constitutes the requirements of the X3:

- 5000 SCCM (1x)

- 1000 SCCM (2x)

- 500 SCCM (1X)

It was decided to create an entirely new flow control system, with 'high-flow' units that met the X3's requirements in parallel with the pre-existing 'low flow' units; 20, 50, 200 and 500 SCCM. A system that ensured maximum flexibility and selectability was constructed and is pictured below (Figure 4.14); the credit for implementation and construction of the unit goes to fellow PEPL PhD student Michael Sekerak.
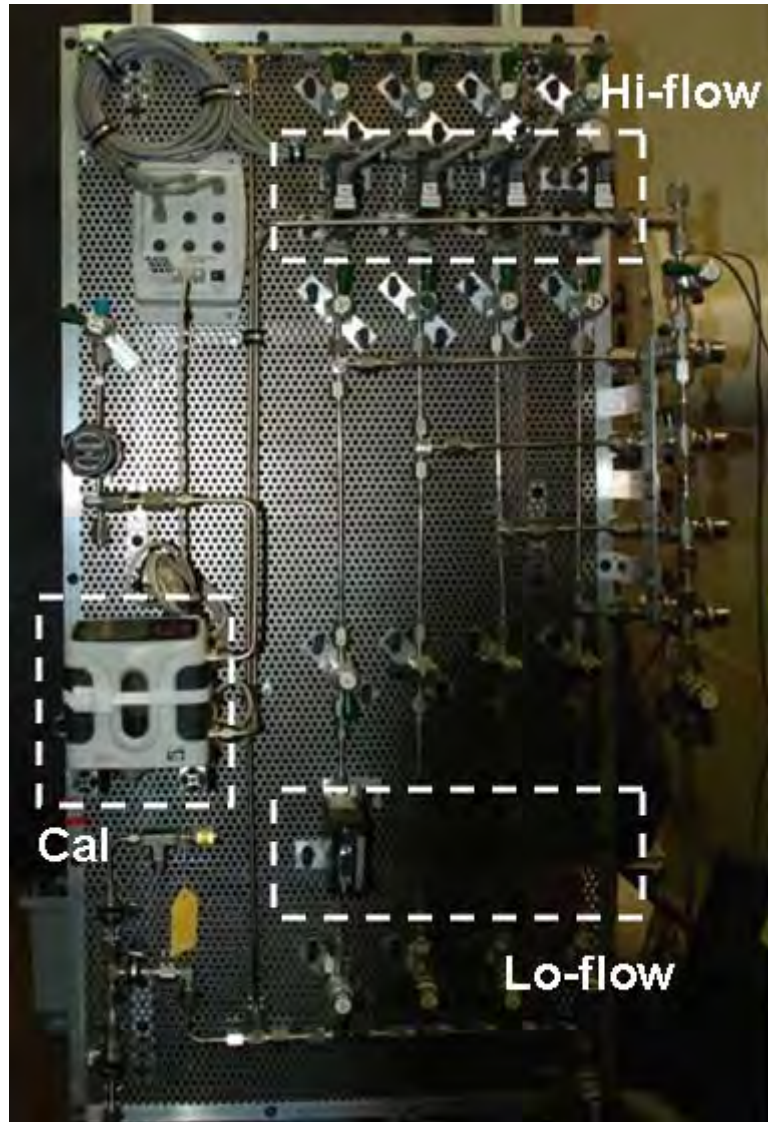
Figure 4.14. LVTF MFC manifold.

4.3.2. Calibration Units

Previously, the process of calibrating the MFC's was a laborious process that required the use of a control volume, temperature and pressure sensors and a LabVIEW code. As a

new system was being constructed, it was decided that it was worth the investment to purchase a highly accurate push-button system that would fulfill the same role. Two Bios Definer (Figure 4.15) units were purchased, one middle range unit to be used with the higher flow units (>200 SCCM) and a low range unit for the smaller cathode controllers (50 SCCM and 20 SCCM), both with a quoted accuracy of +/- 1% of the reading.[88] While the mid-range unit functions at the low range described, a unit specifically for those flow rates increases the accuracy of the calibration as well as reduces the time it takes to perform it.

Figure 4.15. Bios Definer MFC calibration unit Low- and mid-range units are identical in appearance except for a different sized piston. Hence only one unit is shown here. [88].

The units function by compressing the inlet gas inside a piston and measuring the time of travel as well as temperature, and have a programmable standard temperature. This allows a calibration curve to be produced.

4.4. Experimental setup—power, mass flow control, telemetry monitoring

Power was supplied to the inner, middle and outer channels of the thruster by a Magnapower 60-kW DC power supply, an Amrel 100-kW DC power supply, and a Magnapower 150-kW DC power supply, respectively. This discharge power was supplied across two 160-µF 1000-V Cornell Dubilier polypropylene film capacitors connected in

parallel per channel. The mean discharge currents for the inner and middle channel were each measured with a separate CDR-100 FW-Bell magneto-resistive current sensor, while the outer channel discharge current was measured by a CDR-150 magneto-resistive current sensor. Discharge voltages were measured via sense lines attached directly to the anodes and cathode and fed into 201:1 voltage dividers comprised of low-inductance metal-oxide film resistors. Magnet coil currents were read across 30-A, 100-mV current shunts (Deltec WB-30-100). Magnet voltages were read directly off of the output side of the power/telemetry breakout box pictured in Figure 4.16.

Figure 4.16. X3 NHT power and telemetry breakout box.

Keeper current was measured across a 10-A, 100-mV current shunt (Deltec WB-10-100) and its voltage was put through a 101:1 voltage divider. Heater current was measured across a 30-A, 100-mV current shunt (Deltec WB-30-100) and voltage was measured directly at the output side of the power/telemetry breakout box. All telemetry signals were routed to an Agilent 34970A Data Acquisition/Switching unit. Voltage

measurements were calibrated using a BK precision 5491A multimeter. Current measurements were calibrated using a precision 10-mOhm resistor accurate to 0.1% and a BK precision 5491A multimeter. Plume photographs were taken with a Nikon D3200 (camera 1 in following chapters), a Nikon D80 digital camera (camera 2 in following chapters) and a Sanyo VCC-HD2300 high-definition (HD) video camera (HDcam in following chapters). Details on photographic evaluation of the thruster during krypton operation and xenon operation that pertain to the two different setups are given in Chapter V and Chapter VI respectively.

Alicat Scientific MC Series mass flow controllers are used to deliver the krypton propellant to the X3 through electro-polished stainless steel lines. A Bios Definer 220L DryCal system plumbed in parallel to the anode and cathode feed lines, with a measurement accuracy of 1% of the reading between 5 and 500 sccm, is used for mass flow calibration. Mass flow calibration is done for each controller at multiple points and a linear fit is performed. This linear fit is used to determine the flow at any arbitrary set point. The AC component of each channel's discharge current, $I_{D,AC}(t)$, was measured with a Tektronix TCP 303 (DC to 15-MHz bandwidth) split-core Hall current sensor through a Tektronix TCPA 300 current probe amplifier. The signal was measured on the discharge current line external to the chamber on the anode side for each respective channel.

4.5. Mechanical upgrades

The largest thrusters assembled and tested in LVTF in recent memory have not exceeded approximately a half meter across and weighed less than 70 kg. They are of a size that they can be constructed using existing lab tables and space, and installed by

hand without any modifications to the chamber's steady-state configuration. This is not the case for the X3, weighing in at over three times anything previously installed with a girth that dwarfs anything else, the sheer physical reality is that new methods were required that would allow safe (both for the thruster and the operators) and secure methods of assembly and installation.

4.5.1. Rail System

The internal floor grating of LVTF sits on framework that has rails that run along the long axis of the chamber. There are three rails in total, all running more or less parallel to each other. The additions to the rails system therefore were required to compensate for approximately the inch of deviation across the length of the chamber. See Figure 4.17 below for a cad model of the flooring inside of LVTF.
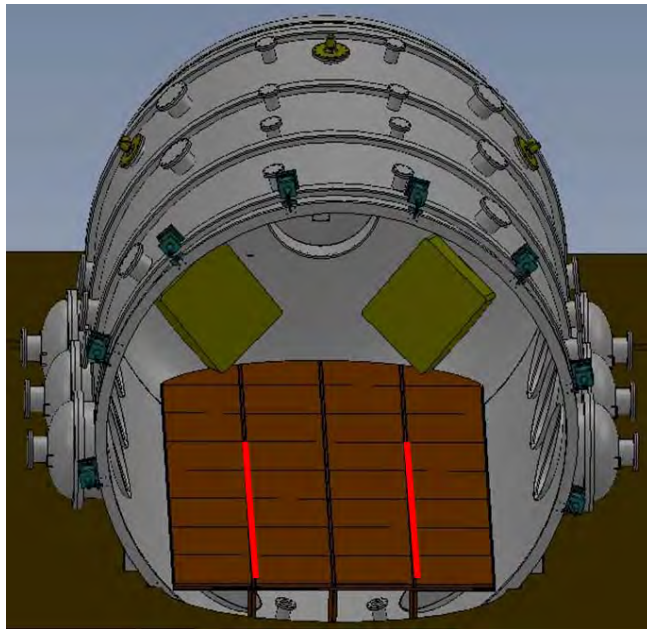
Figure 4.17. CAD model of flooring inside of LVTF with rail network and grating shown.

In the original configuration of the chamber, these rails can only be used to slide objects (or roll flat wheels) over and do not provide any guidance for the objects that are being transported along them. While two of these rails straddle the thrust stand table

(Figure 4.18), this was deemed insufficient to be used as a reliable piece of transport infrastructure for the X3, an object that is heavy, delicate, and expensive.
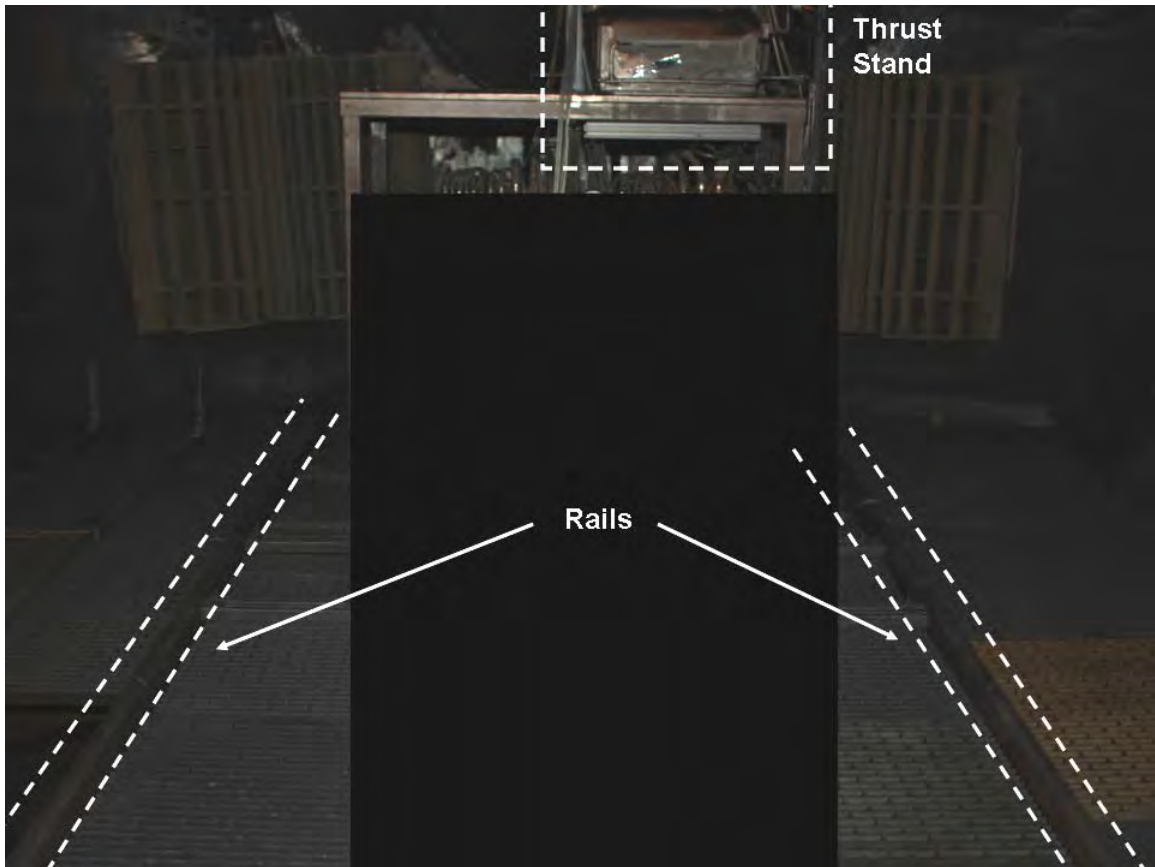
Figure 4.18. Picture of inside of LVTF showing rails straddling thrust stand.

A rail system that provides boundaries for the thruster to travel along and can act as a rigid guide is desired. It was decided that a V-track modified rail system be employed. This concept allows whatever rig the thruster is attached to follow a single path as it is transported inside the chamber as long as it is equipped with the appropriate V-groove type wheels. See Figure 4.19 below for a sketch of the wheel-track combination.
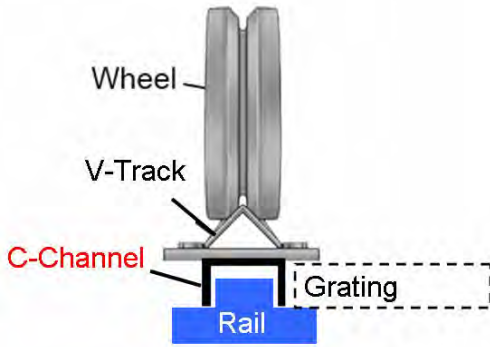
Figure 4.19. Conceptual rendering of v-groove wheels on v-track.

In order to clear the supports for the thrust stand table, the V-track, which is just a simple angle iron on its side, had to be raised above the level of the existing rail while maintaining structural integrity of the assembly. A stack of C-channel, square tubing, and angle irons, all made of carbon steel, was chosen as the optimum configuration. See below for a CAD model of the assembly showing weld locations and fasteners.
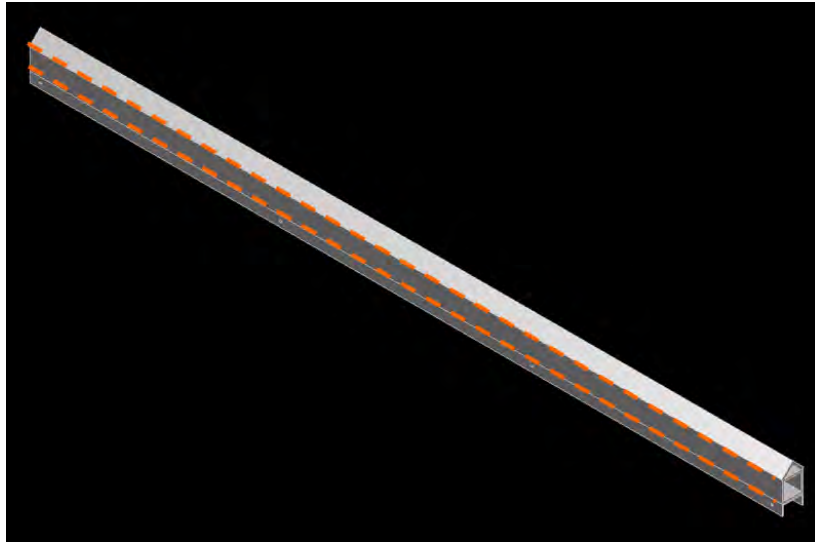
Figure 4.20. Isometric view of CAD model modular rail system showing weld locations as dashed orange lines. The bottom-right of the image has the exposed cross-section of the assembly.

Rather than create an assembly that was a single unit spanning the length of the chamber, it was determined that it would be more practical to make the rails modular. This way, they would both be easier to manufacture and install as well as would be removable. The removable aspect is important because unless some structure is in

residence on top of the rails, they can present a trip hazard (they are raised several inches above the level of the grating and are the same color). Each segment was kept to a manageable length of approximately six feet, with set screws placed at regular intervals in order to stabilize the rails and allow for compensation for the skewed nature of the underlying frames. As one can notice from the cross section in Figure 4.19, the c-channel was sized to allow for margin on either side of the underlying rail to accomplish just this goal of proper alignment.

4.5.2. Assembly Rig

At the time of assembly of the X3 there were two types of tables available at PEPL (Figure 4.21).

Figure 4.21. Pre-existing thruster assembly surfaces, metal table (left) and wood table (right).

In the case of all other thrusters at PEPL, these surfaces would be sufficient. While thrusters need to be assembled in the horizontal with the exit plane parallel to the floor, the size of thrusters like the H6 and X2 make it possible to assemble a simple jig of unistrut or other steel bars and place them on the table. Their weight makes it possible to manually right them again and take them inside the chamber.

At nearly a meter of girth and weighing as much as several grown men of moderate build, the X3's sheer size makes the physicality of using the standard assembly surfaces

all but impossible. It was recognized that what we had was a solved problem. Someone or some organization had need to assemble a heavy object safely with access to multiple orientations (i.e. having the ability to rotate the workpiece). It was discovered that a large "assembly rig" could be used for the X3. Flotron Inc is a vendor of choice in the community, and with their help an articulating unit was selected that allowed for the practical and safe assembly of the thruster (Figure 4.22).
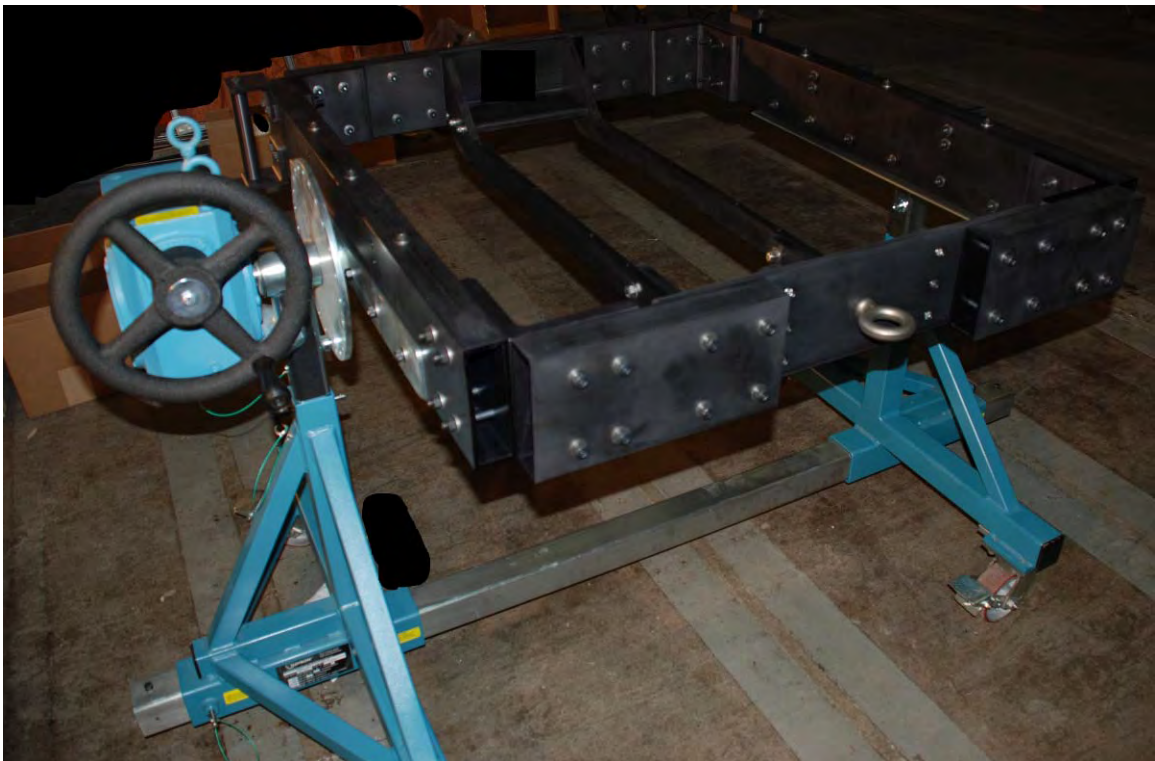
Figure 4.22. Flotron assembly rig with frame prior to thruster assembly in the horizontal position.

This unit is fully mobile and can be brought inside the chamber as needed, or to the edge of the endcap, to facilitate thruster installation.

4.5.3. Gantry Crane

The assembly rig has a maximum height of approximately 1 meter. The thrust stand is elevated above the level of the grating and the fastening point is approximately at 2 meters. This height differential coupled with the weight of the thruster necessitates a

structure that can aid in the transition of the thruster from the assembly rig to the thrust stand. A gantry crane of the type shown below (Figure 4.23) was chosen as the solution to this particular challenge. The crane is could support the weight of the thruster within appropriate factors of safety. It was also it is tall enough such that it could suspend the thruster from its main beam while clearing the thrust stand, and has a wide enough base such that it can be wheeled along the rail system describe earlier in this chapter. The crane was equipped with a manual chain hoist as electric ones tend to catch and is mounted on v-groove casters which can mate with the v-track rail system. It is modular and made of aluminum, allowing for manual assembly with a minimum number of people. There is the added benefit that because it is a non-magnetic structure, it can be left inside the chamber in the vicinity of the thruster should the need arise.

Figure 4.23. Vestil Manufacturing modular aluminum gantry crane with hoist and v-groove casters.[89]

4.5.3.1. Fortification and modification of the thrust stand

The structural components of thrust stand situated in the LVTF at PEPL have remained unchanged since it was constructed nearly a decade ago. While of sound

construction, it was deemed incapable of safely supporting the X3's substantial weight. As such, with the help of personnel at AFRL Edwards AFB, the thrust stand was upgraded to have stouter mechanical construction. Leaving all measurement and control interfaces the same, the support mechanism was altered to be a column and torsional bearing unit. In below we see the thrust stand with its previous flexure setup compared side-by-side to the new torsional bearing fixture.
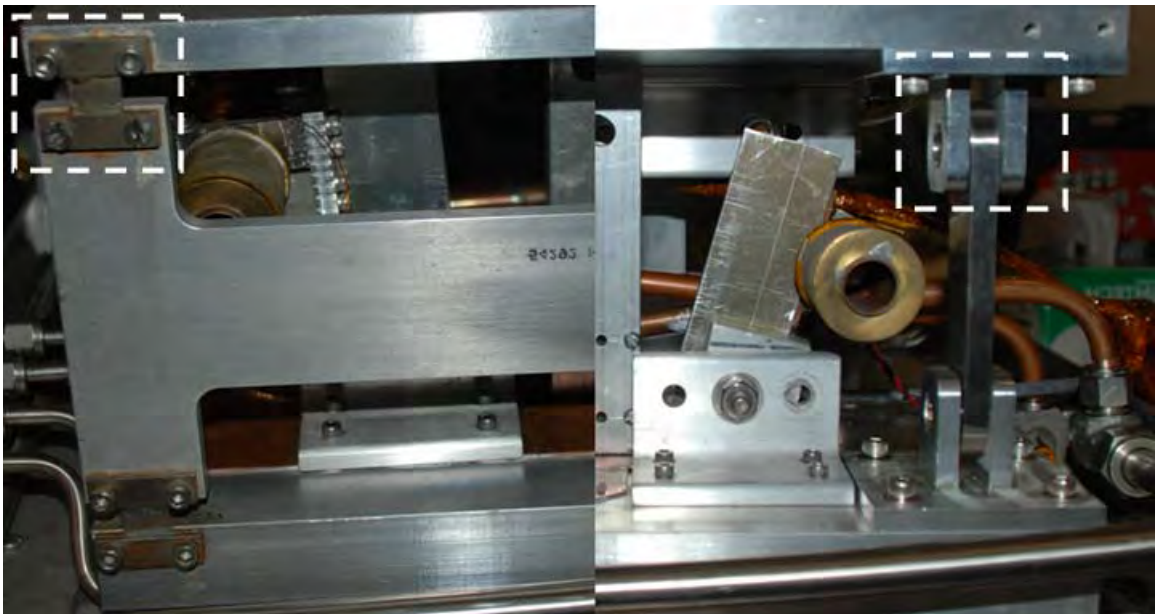
Figure 4.24. Thrust stand pre-modification support structure with flexures (left) and post-modification with torsional bearing structure (right). A flexure and torsional bearing assembly are highlighted by a white dashed box in their respective images.

Aside from offering a higher factor of safety, the new supports are more directly in the load bath than the previous design.

An additional modification to the thrust stand was the addition of a fifth gas line to the internal workings of the stand to allow for more flexible operation with a variety of cathodes for the X3.

It should be noted that as of the writing of this work the thrust stand has not yet been checked out with an existing thruster whose performance is already characterized to provide a direct quantitative assessments of impacts on accuracy of the measurements.

4.6. Experimental setup—mechanical systems

4.6.1. Thruster installation—krypton operation

The first firing of the X3 constituted the highest power thruster operation to date at PEPL. As noted in this chapter, in reaching for the incredible power of the X3 we crossed over the threshold of thruster that could be handled by two people and installed through a personnel hatch and into the realm of specialized equipment and structures. Figure 4.25-Figure 4.28 below show the installation procedure of the world's largest Hall thruster.

Figure 4.25. Representative photograph of the LVTF with its endcap open.

Figure 4.26. Steel grating required to bridge the gap between concrete floor outside LVTF and interior grating (stowed in this picture). Each unit weighs over 45 kg.

Figure 4.27. Photograph of gantry crane on the portion of the rail system that extends onto the flat paneled grating of Figure 4.26.
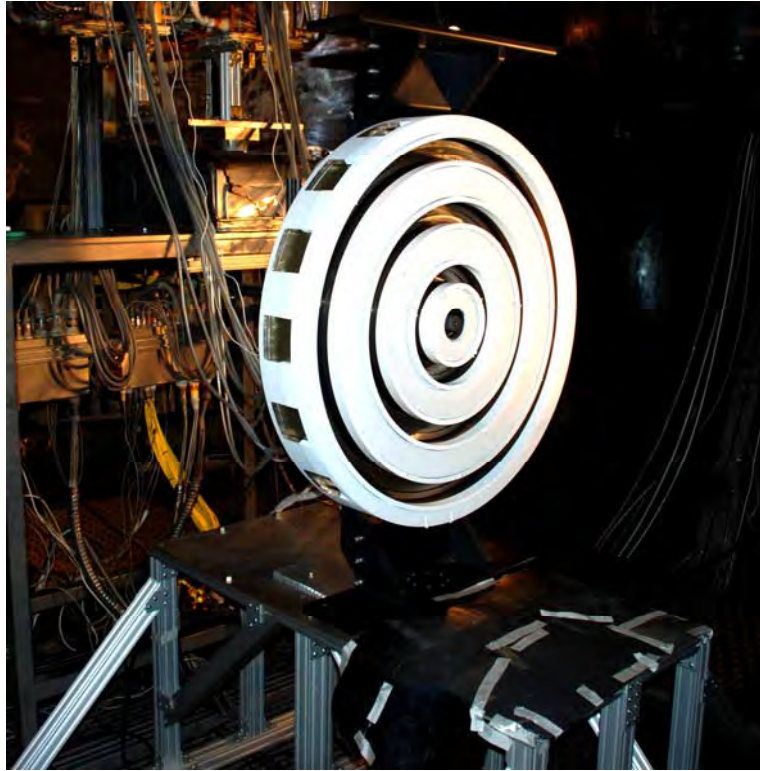
Figure 4.28. Photograph of X3 installed on its table.

In order to install the thruster, first it has to be positioned on the steel grating pictured in Figure 4.26 between the two parallel rails, which run all the way into the LVTF. Prior to this, the gantry crane is pre-positioned on the rails. The gantry crane winch then attaches to the mounting eyebolt on the thruster frame. Once the load is taken by the crane, the thruster can be separated from its assembly rig. From here, the thruster is transported as low to the ground as possible to its final destination. In the case of this test, that was on top of a specially constructed table made of 80/20 (Figure 4.28). This table was significantly over-engineered with large cross-section 80/20 in order to ensure that the structure did not give way under load. To verify the design, the structure was subjected to a load test with a test mass in excess of the thruster weight. As the structure passed the load test, the installation process was able to proceed.

4.6.2. Thruster installation—xenon operation

The xenon operation of the X3 presented in this document occurred chronologically right after the krypton operation. Where the X3 was on a table in front of the thrust stand for krypton operation, the thruster was on the thrust stand for the entirety of the xenon operating points. However, as the thruster was already inside of the chamber and electrically connected to the waterfall, installation was greatly simplified. Using the gantry crane and rail system, the thruster was transitioned from its table up and onto the thrust stand. Figure 4.29 show the X3 mounted on the thrust stand inside of LVTF.

Figure 4.29. The X3 mounted on the thrust stand in LVTF.

4.7. Experimental setup—thrust stand operation

For the set of experiments whose results are presented in Chapter VI, the X3 was mounted on the inverted pendulum NASA GRC[90] type thrust stand in LVTF. To accommodate the higher range of thrust of the X3, two new calibration weight sets were assembled. One that ranged to approximately three newtons for the lower current testing and another that ranged to approximately eighteen newtons for the higher current testing to be done.

It should here be noted that all points at 300 V and lower current operation were done with the thrust stand in null-mode. The higher current points were run in displacement mode as thrust was anticipated to be higher and PID controller unit coupled with the current null-coil were not expected to properly control the thruster position.

Presented here is a basic diagram representing the functionality of the thrust stand (Figure 4.30), where all of the components are utilized in both null- and displacement-mode. The difference is that in null-mode the PID circuitry that is connected to the electromagnetic coil ("damper" in Figure 4.30) uses the LVDT reference signal and attempts to keep it at a given setpoint that is usually the zero-thrust neutral point. In this mode, all three elements of gain are used: proportional (P), integral (I), and differential (D). In displacement-mode, the PID controller is still fed the LVDT reference signal and is also given a setpoint to compare it to. However, instead of manipulating the coil current to keep the LVDT signal at the given setpoint, the controller attempts to dampen out high-frequency oscillations in the position—essentially the rate of change of position is managed, not the change itself. This is achieved by using the controller in PD-mode (only P and D gain used) and turning the proportional gain to a much lower value than the settings for null-mode and turning the differential gain up to a higher value such that

their product is roughly the same. The null-coil now acts as a damper, hence the labeling in the diagram.
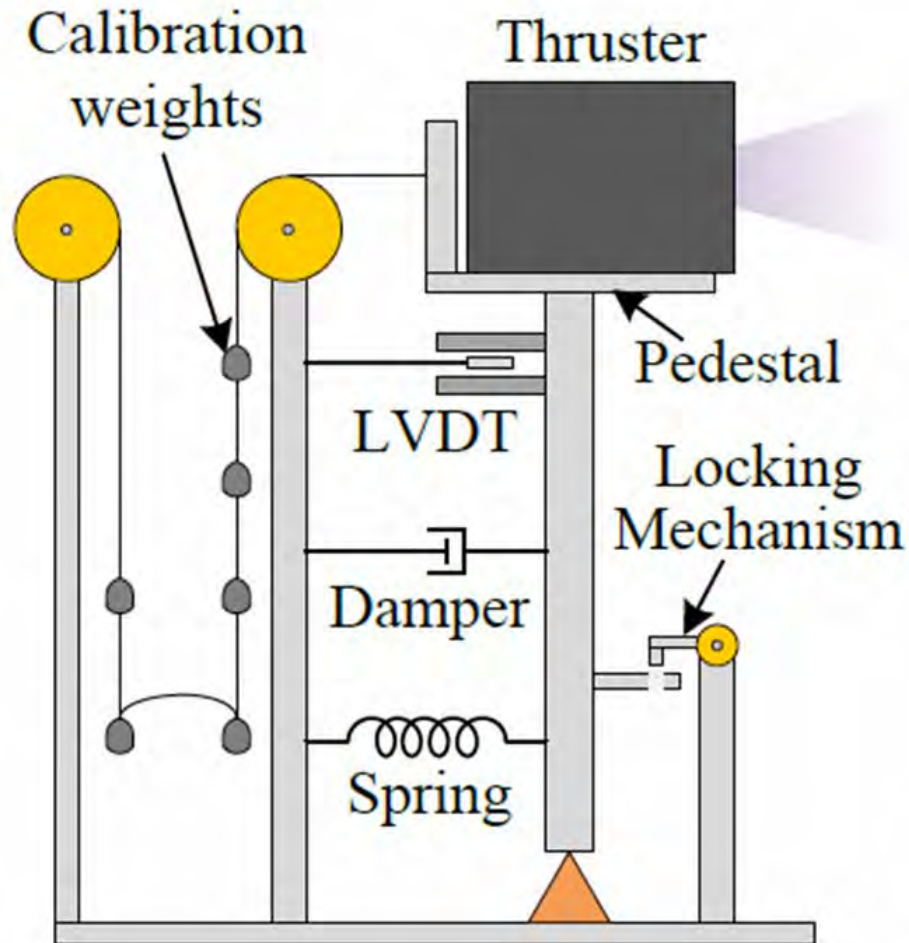
Figure 4.30. Graphical representation of the thrust stand with calibration weights. Courtesy of Shabshelowitz,[91] The damper is an electromagnetic coil with magnetic plunger that can be used to either (a) maintain a given position or (b) to only damp out high-frequency oscillations.

4.8. Thermal management

The X3 is expected to process eight times as much power as any engine ever tested at PEPL. Existing thermal management systems such as carbon beam dumps and chillers can handle tens of kilowatts of energy deposition. What happens, however when the power level is increased by an order of magnitude? As with everything involving this

thruster, scale has made what was once taken for granted something that must be looked at carefully.

4.8.1. Water-cooled beam dump

When thrusters are operated in LVTF they are pointed down the long axis of the chamber (Figure 4.31) towards the large endcap. To prevent the beam from overheating and eroding the chamber, there is a target consisting of five ~0.3 m x ~1.8 m graphite panels that function as a "beam dump" (Figure 4.32).
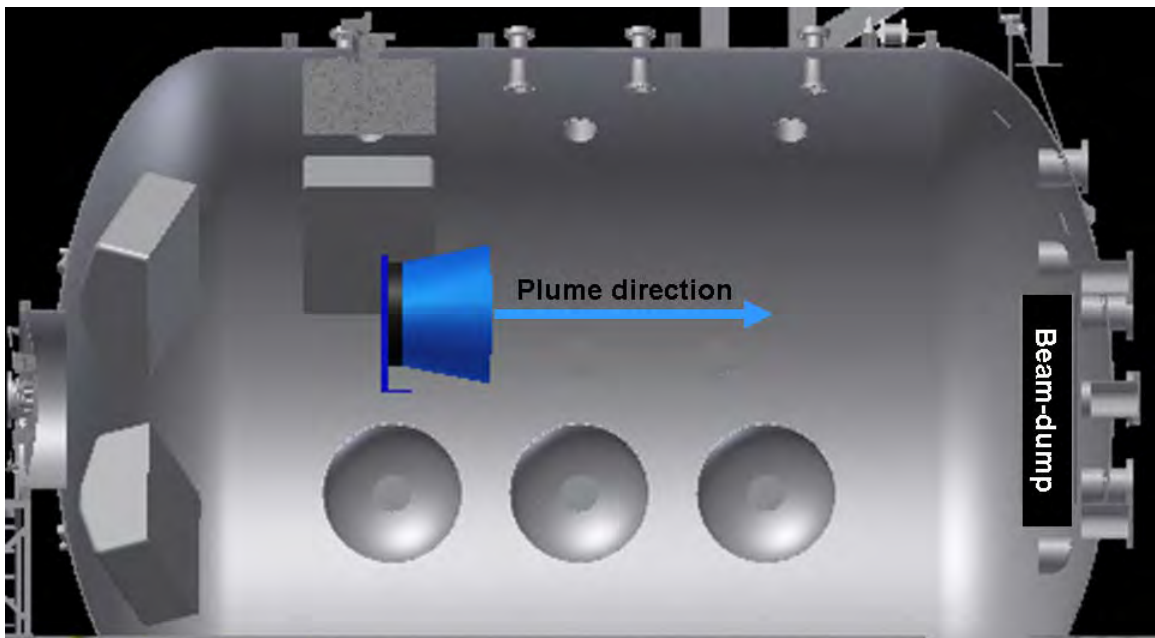
Figure 4.31. Schematic of LVTF showing representative thruster firing direction.

Figure 4.32. PEPL LVTF graphite beam dump mounted on the endcap.

As an entirely precautionary measure, a water cooling system has been deemed necessary for the graphite panels. The preliminary design is herein presented and it should be noted that while the modifications have not yet been undertaken, they are scheduled to take place.

The design takes advantage of the fact that city water is readily available in the lab, and with the aid of a pressure regulator, one can ensure no pressure spikes in the lines. Simple copper serpentine pipe on the back of each panel, with each panel connected in parallel as to not impede the rotation of each individual panel, was selected as the design solution. See Figure 4.33 below for simplified schematic of the proposed setup. As the beam dump is on the endcap, which must be moved over 6 m when installing the thruster, quick disconnect plugs will be employed to connect to the supply and drain on the fixed chamber wall, as recommended by NASA GRC.

Rear View
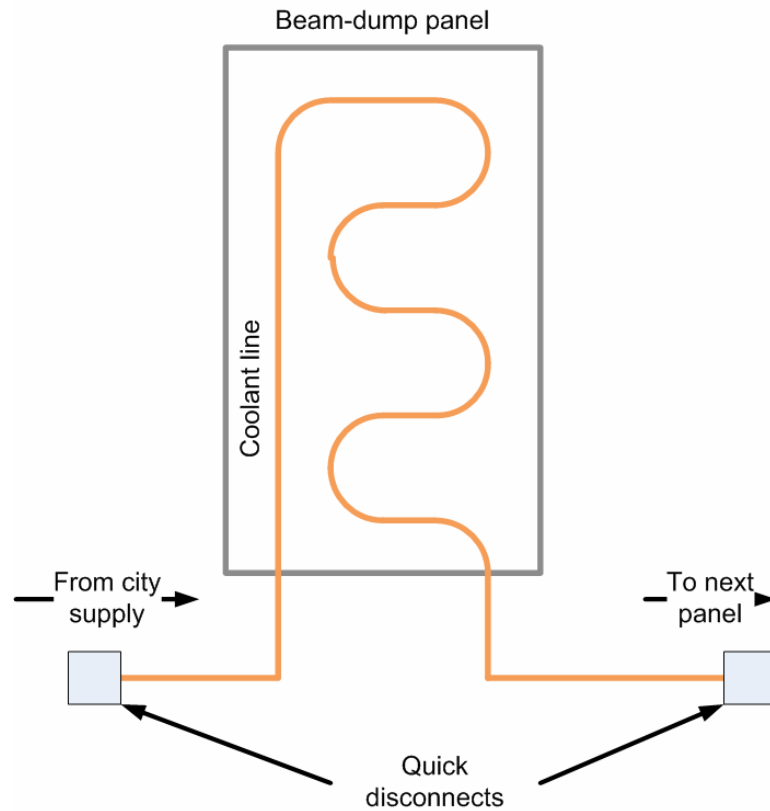
Figure 4.33. LVTF beam-dump cooling scheme, single-panel schematic.

4.8.2. Extended beam-dump

In addition to water cooling the beam dump it was determined that it should also be extended. While these extensions will not be water-cooled, they do offer substantial protection for the bare metal endcap beyond the limits of the current beam-dump (see Figure 4.32). In order to achieve maximum coverage while maintaining flexibility of the setup inside the chamber, a tower system was designed by fellow PEPL PhD student Scott Hall to the author's specifications that would allow for the mounting of graphite panels much in a modular way that bears a similarity to the existing beam dump. As a preliminary proof-of-concept, the 80/20 underlying framework was assembled and outfitted with Grafoil graphite sheeting to test its composition. A photograph of the first

implementation of this extended beam dump is shown in Figure 4.34. This version increases the area of the beam dump to approximately 2.5 times its original size.
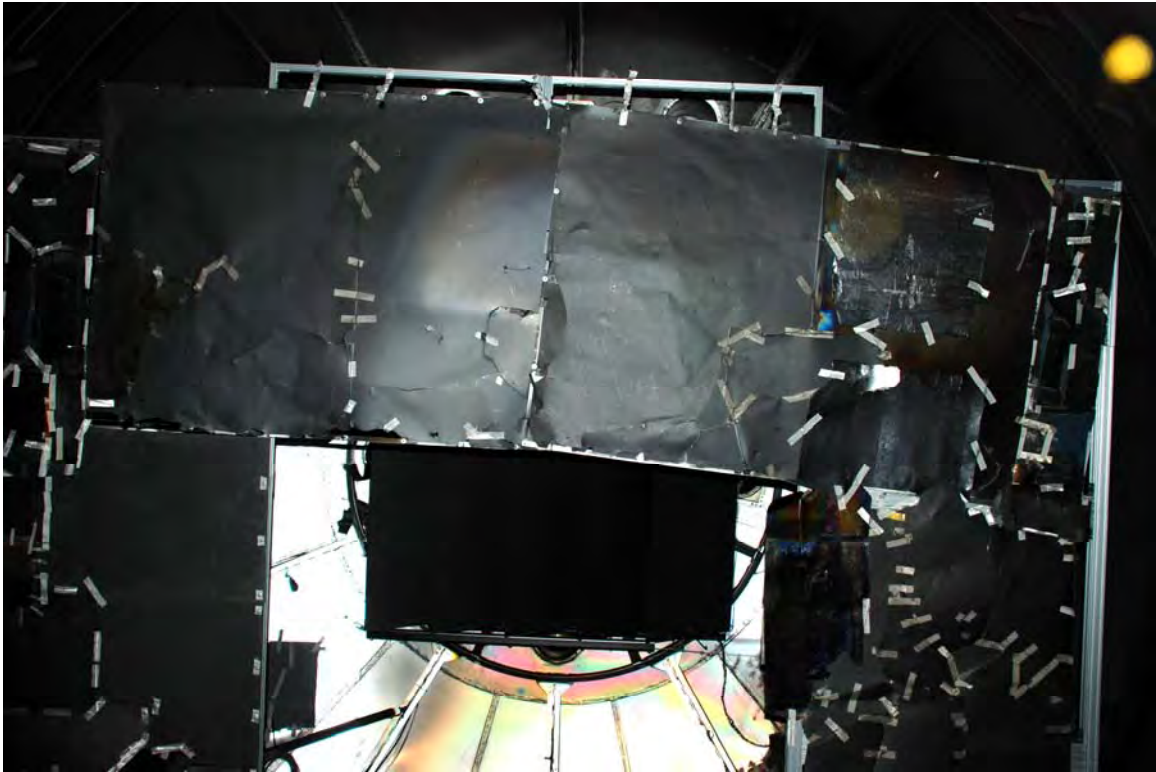
Figure 4.34. Photograph of first implementation of extended beam-dump inside of LVTF.

4.9. Summary

Extensive facility modifications were needed to properly prepare for the X3. This included power, mechanical, and thermal needs. The power modifications encompassed electrical service infrastructure, power supplies, and telemetry. New structures for thruster assembly and installation were procured and/or assembled. Finally, methods of mitigating the exceptional thermal load that the X3 is expected to impinge on the chamber and its systems have been investigated and their implementation begun. Table 4.1 gives a summary of key facility attributes and capabilities before and after upgrades undertaken for the X3 project. Pumping capability is not listed as it was not altered during the upgrade process.

Table 4.1. Summary of facility capabilities, pre- and post- upgrades undertaken for the X3 project. Main capabilities are herein listed. Specifications of the waterfall are omitted for brevity. *Note: for pre-upgrade values, parenthetical value is theoretical max capacity; for post upgrade, given value is the load tested value.

Attribute/capability	Pre-Upgrade	Post-Upgrade
Available discharge power supplies	(1x) 1000 V/ 100 A, (1x) 600 V/ 16 A	(1x) 1000 V/ 150 A, (1x) 1000 V/ 100 A, (1x) 1000 V, 60 A
#/Ampacity of anode power lines	(1x) 50 A, (1x) 30 A	(1x) >150 A, (1x) >100 A, (1x) >60 A
Ampacity of cathode return line	80 A	>300 A
# of thruster side thermocouple feedthroughs	0	36
# of discharge sense wires	4	8
Universal waterfall	no	yes
Shielding of discharge lines	n/a	single-end grounded conduit
Temperature rating of discharge lines	150 °C	260 °C
Discharge current sensors	(1x) 50 A, (1x) 15 A	(1x) 150 A, (2x) 100 A
# of Magnet current shunts	6	6
# of cathode keeper current shunts	2	3
# of cathode heater current shunts	2	3
Load capacity of thrust stand*	~90 kg (~230 kg)	> 295 kg
Load capacity of overhead gantry	n/a	>680 kg
Load capacity of articulating assembly rig	n/a	>295 kg
LVTF internal rail system	unguided, fixed	guided tracks, portable
Beam dump coverage area	3.8 m^2	9.3 m^2
Available mass flow controllers (ratings for Xe)	(1x) 20 SCCM, (1x) 50 SCCM, (1x) 200 SCCM, (1x) 500 SCCM	(1x) 20 SCCM, (2x) 50 SCCM, (1x) 200 SCCM, (2x) 500 SCCM, (2x) 1000 SCCM, (1x) 5000 SCCM
Mass flow controller calibration	control volume/ LabVIEW	(2x) Bios DryCal Definer push-button unit

CHAPTER V

Krypton operation of the X3

"L'aqua bulle ma lu puorcu a cosenza"

The first firing of the X3 NHT and indeed the first phase of its testing can be characterized as a shake-out test. The purpose of this shake-out was to test the very basics of thruster operation, ensure that all channels could operate independently and in concert, to burn-in each channel at given voltages, and to assess early-on weak points in the physical design that might fail.

The first portion of this testing was conducted with Krypton gas for both economic reasons (cost) and because proposed mission scenarios feature this gas. Krypton has been identified as a propellant suitable for use in HETs to be utilized on a certain set of NASA missions requiring high specific impulse (>4000 s).[77,92] The second reason centers on the fact that krypton is on average 1/5 to 1/10 the cost of xenon, the nominal propellant of choice for HET systems. Thruster channel burn-in (described in section 5.1) requires on average 2-4 hours of operation. Couple this with the current levels involved (upwards of 50 A for individual channels), the burn-in would quickly become an expensive enterprise if xenon were used.

To simplify the test, it was determined that it not take place on LVTF's thrust stand. As such, a specialized table was constructed and mounted axially directly downstream of the thrust stand. Due to facility effects, primarily negative response from the pumps,

Krypton was only used up to 550 V. In this section we will go over the entire shakeout plan but only cover the Krypton operation.

5.1. A brief explanation of thruster burn-in

Burn-in at a given voltage is considered achieved when visible wear bands are observed on the boron-nitride of the discharge chamber and is generally expected after 2-4 hours of operation. With some variation across channels, the X3 burned in after the expected amount of time. Thruster burn-in prior to performance measurements is important because the characteristics of operation during burn-in are different from the steady state configuration of the channel. Thruster discharge current oscillations are usually of higher amplitude and possibly different frequencies than if the channel is not burned in. Also, the discharge current is artificially higher during this burn-in process. This is not to be confused with the increased discharge current seen during moisture bake-out, which is usually shorter lived. Moisture bake-out can of course occur during the burn-in process if a thruster has been exposed to atmospheric air for any appreciable period of time, and must occur with each new pump-down (whereas burn-in at a given condition need only occur once for a given channel). Detection of burn-in was made via a set of binoculars used to look into the chamber while the thruster was running as well as via photographs taken using two DSLR cameras.

5.2. Experimental setup

5.2.1. Test matrix

The test matrix presented in this document covers only the initial 300-V operation of the thruster as well as additional single-channel operating points for the inner and outer channel (550-V condition) and middle channel (450-V condition). All seven

configurations of the thruster were tested, with the channels operating at a constant discharge current density. This current density is derived from all three channels operating simultaneously with a total discharge current of 100 A.

The test matrix for the thruster is provided in Table 5.1 below.

Table 5.1. Test matrix for Krypton operation of the X3. I= inner, M= middle, O= outer, I+M= inner and middle simultaneously, M+O= middle and outer simultaneously, I+O= inner and outer simultaneously, I+M+O= inner, middle, and outer simultaneously. V_D= is the discharge voltage, I_D =discharge current, P_D =discharge power. Kr= Krypton

Test Condition	Channel(s)	Total P_D [kW]	V_D [V]	Total I_D [A]	Propellant
Kr,1	I	3.9	300	13.1	Kr
Kr,2	M	9.6	300	31.9	Kr
Kr,3	O	16.5	300	55.1	Kr
Kr,4	I+M	13.5	300	45.0	Kr
Kr,5	M+O	26.1	300	87.0	Kr
Kr,6	I+O	20.5	300	68.2	Kr
Kr,7	I+M+O	30.0	300	100.1	Kr
Kr,8	I	7.2	550	13.1	Kr
Kr,9	M	14.4	450	31.9	Kr
Kr,10	O	30.3	550	55.1	Kr

5.2.2. Photographic evaluation

In order to provide a qualitative understanding of the structure of the plasma and the stability of the thruster, two DSLR cameras were employed in addition to a Sanyo HD Video camera. One DSLR was positioned looking down the thrust axis of the X3 at an acute angle less than 30° (camera 1) and the other DSLR providing a side view of the thruster (camera 2). The HD camera (HDcam) was positioned such that it provided a view of the discharge chamber at an angle between that of camera 1 and camera 2. This camera was only available for the data points after 300-V operation.

5.3. Results and discussion

5.3.1. Operational observations

The stated upper bound of discharge voltage for the X3 is 800 V. During the planning phase prior to initial operation, it was determined that a stepped approach would be used

in order to minimize risk while pushing the boundaries of the thruster. A waypoint

voltage of 550 V was picked to provide an opportunity to break vacuum and inspect the

thruster for any damage prior to going to 800 V. The logic in this case being to head off

any catastrophic failure at 800 V that might occur because of some weak point induced in

the thruster on the ramp-up from 300 V. For example, an electrical isolator which is

degraded at 550 V yet retains functionality might fail when the thruster is at 800 V,

arcing from anode to ground. At the higher power associated with such a higher voltage,

the arc would be that much more damaging to the thruster. It should be noted that this is a

conservative testing approach and that there is nothing inherent in the design that would

suggest failure might occur at 550 V.

During the initial testing of the X3, diagnostic evaluation of the thruster was limited

to two means. The first is that of photographic interrogation with the use of the DSLR

cameras (and later for higher voltage the HD video camera) as described in the section

above to assess the overall quality of the plume; e.g. identify hot spots. The second

avenue of approach is that of high-speed measurement of the discharge current to provide

a more quantitative evaluation of the stability of the discharge. The base telemetry for

each condition is presented in

Table 5.2 below. A more complete accounting of thruster telemetry is provided in

Appendix A (Table A.1- Table A.2).

Table 5.2. Telemetry of X3 at all operating conditions on krypton. I=inner, M=middle, O=outer. V_D = discharge voltage, I_D =discharge current, P_D =discharge power. $\dot{m}_T$ = total mass flow rate, m_dot,a= anode mass flow rate. I/(m_dot,a)=ratio of a channel's individual discharge current to that channel's individual m_dot,a. Test conditions Kr,1-Kr,7 constitute the 300 V/ 100 A conditions. *Note: P,Kr is pressure corrected for krypton.

Test Condition	Channel(s)	Total P_D [kW]	I_D [A]	V_D [V]	$\dot{m}_T$ [mg/s]	I/(m_dot,a) [A/(mg/s)]	*P,Kr [Torr]
Kr,1	I	3.9	13.0	300.5	9.2	1.6	1.0×10^{-5}

Test Condition	Channel(s)	Total P_D [kW]	I_D [A]	V_D [V]	$\dot{m}_T$ [mg/s]	I/(m_dot,a) [A/(mg/s)]	*P,Kr [Torr]
Kr,2	M	9.6	32.0	299.8	21.2	1.7	2.3×10^{-5}
Kr,3	O	16.5	55.1	299.6	36.1	1.7	3.6×10^{-5}
Kr,4	I+M	13.4	44.6	300.2	24.4	2.0 (I) 2.0 (M)	2.1×10^{-5}
Kr,5	I+O	21.1	70.3	300.6	40.7	1.8 (I) 1.9 (O)	3.5×10^{-5}
Kr,6	M+O	26.1	87.1	299.4	49.4	2.3 (M) 1.8 (O)	5.0×10^{-5}
Kr,7	I+M+O	30.0	100.1	299.7	53.9	2.3 (I) 2.3 (M) 1.9 (O)	6.1×10^{-5}
Kr,8	I	7.2	13.1	550.7	10.0	1.4	3.0×10^{-5}
Kr,9	M	14.4	32.1	449.3	21.8	1.6	2.2x10-5
Kr,10	O	28.4	51.6	549.6	29.1	2.0	1.3x10-5

An interesting observation that can be made from this table is that less mass flow is required to maintain a given channel mean discharge current as each additional channel is turned on. From

Table 5.2, it can be noted that the ratio of I/(m_dot,a) experiences anywhere from a ~10% increase (outer channel, at test condition Kr,6) to a 46% increase (inner channel, test condition Kr,7) when compared to 300-V, single-channel operation. The interior channels seem to benefit more from this apparent neutral ingestion (e.g. ~40% increase for middle channel in test condition Kr,6 versus ~10% increase for outer channel). This interior channel benefit was observed by Liang with the X2,[9] though in the X2 data the effect was not as pronounced when considered in the context of current measurement uncertainty. With an average uncertainty in the discharge current measurements of 0.8%, this trend observed in the X3 is far enough outside the uncertainty bounds to be considered more than negligible and indeed due to an actual physical phenomenon.

Further, when the combination of channels does not involve immediately adjacent ones, as in test condition Kr,5 operating condition in

Table 5.2, the benefit also appears to be reduced. Lastly, the gains seen by the I/(m_dot,a) ratio of the inner channel in three-channel mode (test condition Kr,7) beyond both two channel modes that it operates in may possibly be attributable to a substantial increase in absolute cathode flow increasing the neutral pressure in the vicinity of the inner channel even further. Without performance measurements on krypton, it is not possible to draw any conclusions about whether or not this is a positive or negative effect. However, these observations provide further support for the idea that this increase in I/(m_dot,a) in NHTs is due to neutral ingestion and in general is indicative of channel interactions as characterized by Liang.[9]

Another item to note is the differing pressures between the 300-V and the 550-V/450-V operating conditions. First, one notes that for the inner channel operating by itself the pressure is three times the 300-V case when operating at 550 V and the same flowrate. Second, for the outer channel case the flowrate was reduced by a third in the 550-V case compared to the rate of the 300-V case. While the facility backpressure is comparatively lower (as is the discharge current) at these lower flowrates, it should be noted that this reduction in flow rate was to keep the cryopumps from "running away" or "shedding". Pump run-away can be defined as the point when the pumps can no longer keep up with flow rate into the chamber and start releasing accumulated gas from their surfaces, increasing backpressure and discharge current of the thruster in a cascade effect. In both cases, it is hypothesized that the beam becomes energetic and does not accommodate on the walls as much as has been previously assumed. Further, it is suggested that these energetic particles make their way back to the pumps where they contribute to

overloading more than the average neutral particle—all the pumping calculations assume room temperature neutral gas, not hot energetic particles.

5.3.2. Photographic Evaluation

The purpose of camera 1 was to provide an understanding of any hot spots that might develop in the thruster as well as detect any azimuthal non-uniformities in the plume. Hot spots can be defined as any locations on the channel walls or anode itself that are substantially brighter than the rest of that given channel, and possibly might even glow red to indicate some form of preferential heating. Azimuthal non-uniformities could take the form of peaks and valleys of brightness in the discharge, either periodic or aperiodic. Referring to Figure 5.1, we can see that neither hot-spots nor azimuthal non-uniformities are present across all seven operating modes.
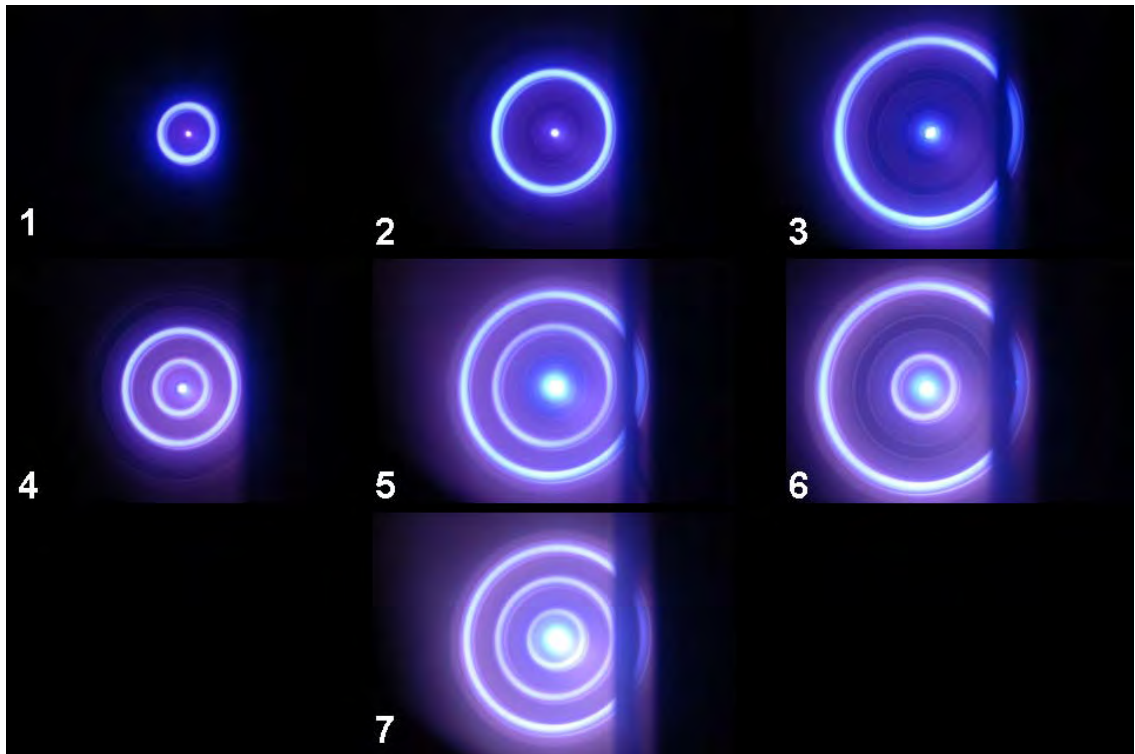
Figure 5.1 All operating modes of the X3 (front view). Operating points from top-left to bottom-right: (1) Inner (Kr,1), (2) Middle (Kr,2), (3) Outer (Kr,3), (4) Inner+Middle (Kr,4), (5) Middle+Outer

(Kr,5), (6) Inner+Outer (Kr,6), (7) Inner+Middle+Outer (Kr,7). All photographs were taken with the same camera settings. The black bar seen in (5), (6), and (7) is a physical part of the chamber (shutter-like beam dump at the downstream endcap).

Camera 2 was employed to give another perspective on the structure of the plume and to allow detection of any anomalous coupling of the plume to the facility. From this side-view, it would be possible to detect azimuthal non-uniformities in terms of discharge brightness that could signal the discharge favoring the top (thruster 12 o'clock) or bottom (thruster 6 o'clock) of the frame. An example of anomalous coupling of the plume to the facility would be the plume coupling to the metal grating directly downstream of the thruster, which would be evidenced by a distinct downward arc of the plume in any of the images from camera 2. None of these abnormalities were observed during thruster operation as one can see in Figure 5.2. The plume is qualitatively symmetric across all seven conditions.
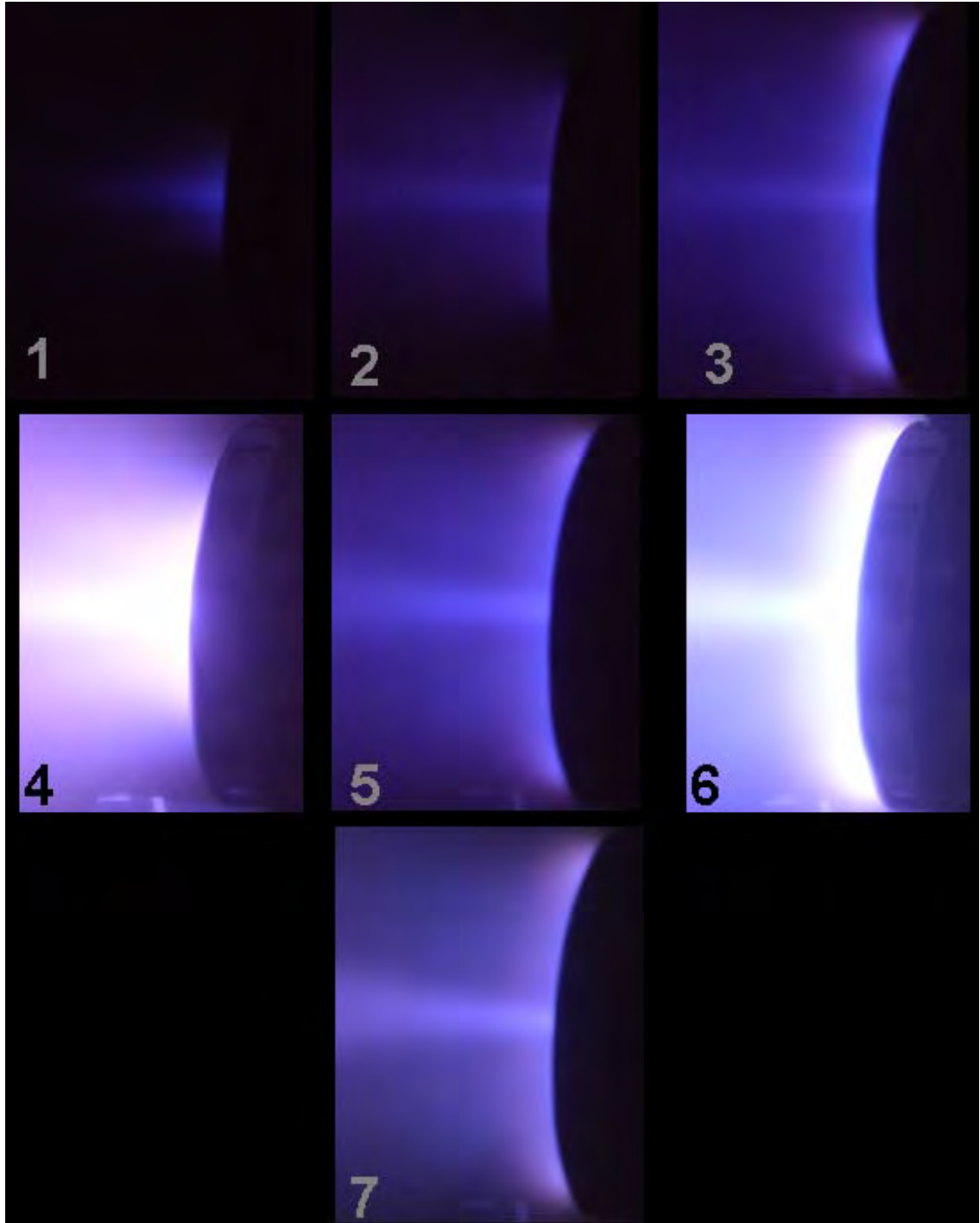
Figure 5.2 All operating modes of the X3 (side view) for the 300 V/100 A conditions. Operating points from top-left to bottom-right: (1) Inner (Kr,1), (2) Middle (Kr,2), (3) Outer (Kr,3), (4) Inner+Middle (Kr,4), (5) Middle+Outer (Kr,5), (6) Inner+Outer (Kr,6), (7) Inner+Middle+Outer (Kr,7). All photographs were taken with the same camera settings with the exception of those for operating points (4) and (6), which are over-exposed. In actuality, the plume brightness for operating points (4) and (6) is comparable to that of (5).
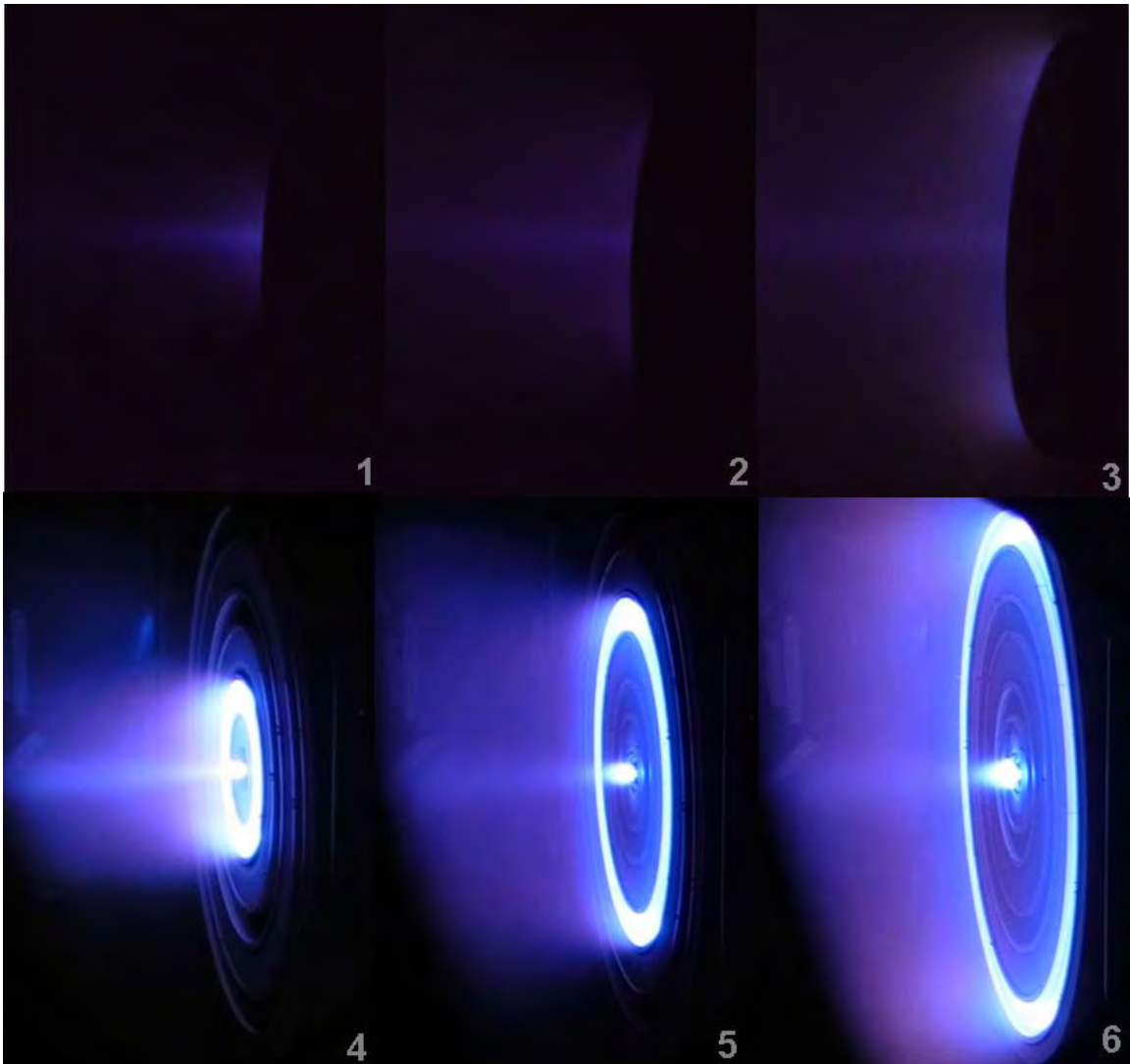
Figure 5.3. Single channel operation above 400 V of the X3 (side view). Top row (camera 2): (1) Inner (Kr,8), (2) Middle (Kr,9), (3) Outer (Kr,10). Bottom Row (HDcam): (4) Inner (Kr,8), (5) Middle (Kr,9), (6) Outer (Kr,10).

For the higher voltage operation, the use of the HDcam provided a much better means

of evaluating the thruster discharge chamber as well as the plume itself because of its

ability to see inside of the discharge channel while still providing more of a side view

than camera 1. We compare the views from camera 2 and HDcam in Figure 5.3 above.

While it is clear that HDcam's view is much more useful for evaluating the plume, the

view from camera 2 is included to compare the higher voltage operation to the 300-V

cases presented. The HDcam shows us that the plume is indeed uniform without hotspots.

Further, as it was determined that opening and closing the beam-dump at conditions above 300-V was detrimental to pump operation, the HDcam provides us with our only photographic record of the discharge chamber during these tests.

5.3.3. High-speed current probe evaluation

Through the independent monitoring of each discharge channel on the anode side of the circuit, we are able to observe high-frequency oscillations (kHz and above) that the naked eye and the three cameras cannot. This provides another tool for determining the stability of the thruster as well as offering a means for understanding interaction between channels.

Both qualitative and quantitative metrics were employed to determine stability during testing. The first is to say the less structure the oscillations had the better the thruster was operating in terms of lower peak-peak oscillation amplitudes. During these evaluations, the oscilloscope was sampling in the range of 1-2 giga-samples per second. Structure, in the case of discharge current, was a trace that approximated a sinusoid. When observing the post-processed power spectral densities (PSDs), this takes the form of a trace that has no prominent peak. From empirical observation, this was determined to be more stable because the more sinusoidal the oscillations became, it was found that there was a higher probability of the oscillations of the thruster growing to a damaging amplitude (e.g. a value that would cause the thruster to switch to "spot-mode", a low-voltage high-current mode where the potential for arcing is greater). Amplitudes were observed to increase by an additional 50%-100% of less structured value; as it was determined not desirous to leave the thruster in such a mode during this test, no oscilloscope traces exist for reference in this document. It should be noted that there are modes where the thruster will

not transition to an unstable mode even if the AC-coupled current trace takes a distinctly sinusoidal form. Quantitatively speaking, as long as the mean peak-peak oscillations are kept to under 15% of the mean discharge current, the thruster can be considered in a quasi-stable operating regime. This is a conservative percentage chosen for this testing, as other thrusters have been observed to operate at higher percentages and still remain very stable.[93] The exception to this rule is the inner channel, which seems to operate at an oscillation amplitude of higher magnitude. Further, there were extended periods of operation (>30 minutes) where the mean peak-peak oscillation was observed to be less than what shown here. No telemetry was taken at those points and thus they are not reported here.
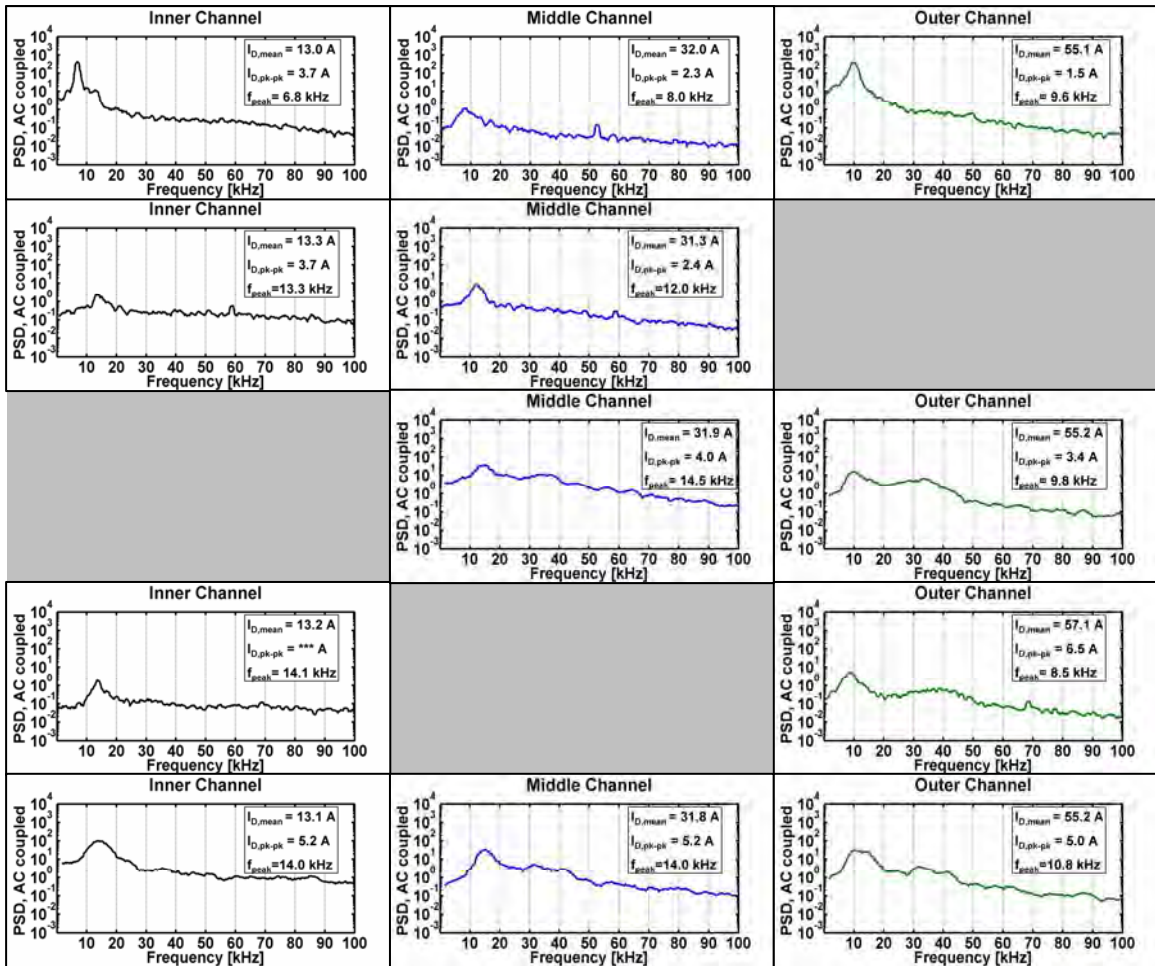
Figure 5.4 AC-coupled power spectral densities (PSDs) of the discharge currents for the 300 V/100 A conditions. The first row of plots show results from the independent operation of each channel operating by itself. The conditions for the following four rows are (top-to-bottom): I+M (Kr,4), M+O (Kr,5), I+O (Kr,6), I+M+O (Kr,7). Columns left-right are: inner, middle, outer channel respectively. Blank gray spaces in a row indicate that that channel was not on during that particular operating point.

The plots in Figure 5.4 above show the power spectral densities of the raw data from the oscilloscope with minimal smoothing. The post-processing was done in Matlab via the built-in PSD functionality.

A number of observations can be made from looking at these plots. First, we note that all three channels have a fundamental oscillation frequency in the 5-10 kHz range, increasing from inner to outer channel. Based on the peak-peak oscillation amplitude, we can also note that all three channels are remarkably "quiet", with the inner channel being

the "noisiest." Here "quiet" is defined as a having a peak-peak amplitude that is a relatively low percentage of mean discharge current.

Perhaps of greater interest, however, are the preliminary observations that can be made about channel interaction. As more channels are added, we can see that the PSD magnitude broadens across the frequency range with the damping out of any prominent peaks, with the greater broadening occurring when adjacent channels are turned on. The peak frequency tends to shift to frequencies higher than either of the independent channel oscillation frequencies. We can note that, for example, with all three channels running together the oscillations have shifted to approximately 15 kHz and that the magnitude of the oscillations appear to have synced up with peak-peak values at essentially 5 A. It seems that in this case, the amplitude of the outer channel's oscillations drive that of the inner two, while all three channels convolve together to form a new fundamental frequency not explicitly organic to any of them. Moreover, we further observe that while the oscillation frequencies of the inner and middle channels are shifted higher, the outer channel remains relatively untouched regardless of which combination of the other two it is operating with. In fact, it oscillation frequency remains lower than the other two.

The response of thruster behavior to increased discharge voltage was also investigated. The 300-V single channel PSD plots are shown alongside those for the higher voltage operation in Figure 5.5. From these plots, the outer channel peak-peak oscillation amplitude as recorded by the oscilloscope was found to have increased by nearly 50% while the inner channel's have dropped by half. Additionally, the fundamental frequencies also have shifted higher by several kHz. In addition to these two points, while the middle channel remains relatively unchanged in peak-peak oscillation, it

has had its PSD broadened along with the other three channels. As none of the channels have been since run on krypton at 300 V and the X3 is still very much at the beginning of life, it is hard to conclude with certainty if the observed trends are simply thruster wear-in characteristics or not. Yet, a simple re-test at the 300-V conditions would yield answers to this effect. It is hypothesized that in-fact it is not completely clean cut: while likely an effect of high-voltage operation, it will take hundreds of hours of operation to completely discount thruster wearing in effects.
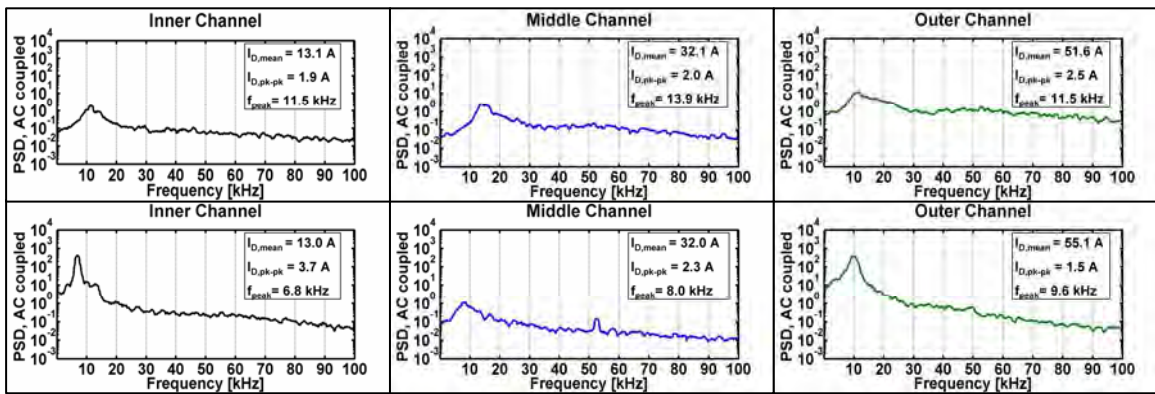
Figure 5.5. AC Coupled Power Spectral Densities (PSDS) of the discharge currents. These are individual channel operation plots in the top row (left-right): Inner at 550 V (Kr,8), Middle at 450 V (Kr,9), and Outer at 550 V (Kr,10). The 300-V operation points are re-displayed here for individual channels only (bottom row, left-right same as top).

5.3.4. Thermal behavior

Thermocouples were used to provide a valuable real-time ability to assess the thermal behavior of the X3. As three-channel thruster operation is the most unique mode of this thruster, and the most intense from a thermal load perspective, representative thermocouple data is presented in Figure 5.6 for the 300 V/100 A three-channel case (Kr,7). Alongside the thermocouple data are simulated values for the key components, linearly extrapolated from simulations conducted at higher powers. Only data for the magnets (zones z2-z7), the channel cups (zones z9,z10, and z11), and the outer radius of the thruster (zone z8) are available for the simulated case.
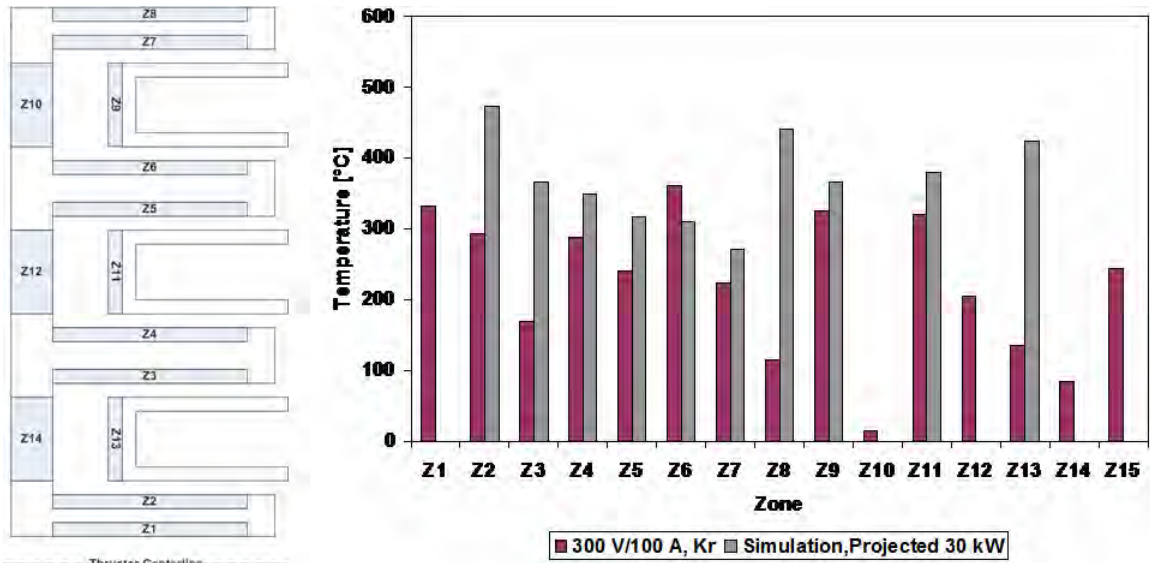
Figure 5.6. Thermal profile of the X3 with all three channels on, 300 V/100 A condition (Kr,7). (Left) Representative cross-section of the X3 with labeled zones where data were collected. (Right) Bargraph containing absolute temperature values. Krypton propellant.

From the above graphic, one can note three main things. We note that the temperature of components decreases as we reach the radial periphery of the thruster, where it is easier to reject heat via radiation. Also, as one moves axially upstream away from the channel cups (Z11 to Z12 for example) temperature decreases, as one might expect as one moves away from the heat generating magnetic coils and plasma discharge. The final and most important point is that all temperatures measured are well below the material soft-failure temperature (red or "1" on the scale).

5.4. Concluding remarks

Having successfully operated the thruster up to 550 V on krypton, the remainder of thruster burn in was put aside in favor of running performance testing on xenon. There were two reasons for this. One, the pumps were responding poorly to voltages above 550 V and further facility modification was needed. Second, the timeline for the work was such that xenon performance data at 550 V and below was required to occur before the > 550 V operation. These higher voltage burn-ins are planned for future testing.

93

CHAPTER VI

Preliminary xenon performance

Tuttu le cose c'e' repare menu 'u morre

While understanding fundamental plasma parameters is a crucial component of comprehending how EP devices function and indeed how to improve upon them, the keystone of a thruster is how it performs. How much thrust does it produce? What is its Isp? How efficient is it? These are all critical quantities that mission designers need to know to decide what technology they are going to put on their spacecraft.

The X3 is a thruster that came to exist with mission-pull in mind. That is to say that it was born of a desire both by NASA and the USAF to put a thruster into space that could meet their unique mission requirements. As such, performance of the X3 is the critical deliverable. With that said, it must be noted that the performance presented in this document is to be treated as preliminary only. There are a number of reasons for this outside of the obvious fact that they are the first data presented. First, for the higher current data set (i.e. discharge currents above the 300 V/ 100 A conditions' values), the facility background pressure is on the high end of acceptable. Second, the magnetic field settings were very roughly optimized for thruster stability and lowered discharge current. They should not be considered the final settings that will yield best performance. Lastly, the full range of thruster operation is simply not testable in the LVTF at PEPL. Higher

currents are possible, however, high current and high voltage are not possible without significant modifications to the facility (as discussed in an earlier chapter).

With all this in mind, the reader is encouraged to take the performance numbers presented as a conservative estimate of how well the X3 will perform as a thruster.

6.1. Experimental setup

6.1.1. Test matrix

The test matrix for these experiments is far from a complete representation of the operational range of the X3. As such a complete characterization was beyond the scope of this work (and facility), a data set was chosen that would allow for comparison between the seven different operational modes of the thruster as well as the krypton testing previously done. The comparison to krypton is done via the photographic diagnostics and high-speed current measurements. The target test points are summarized in Table 6.1 below.

Table 6.1. Test matrix for xenon performance test. Xe=xenon, I=inner, M=middle, O=outer. V_D= is the discharge voltage, I_D =discharge current, P_D =discharge power.

Test Condition	Channel	P_D [kW]	V_D [V]	I_D [A]	Propellant
Xe,1	I	3.9	300	13.1	Xe
Xe,2	M	9.6	300	31.9	Xe
Xe,3	O	16.5	300	55.1	Xe
Xe,4	I+M	13.5	300	45.0	Xe
Xe,5	M+O	26.1	300	87.0	Xe
Xe,6	I+O	20.5	300	68.2	Xe
Xe,7	I+M+O	30.0	300	100.1	Xe
Xe,8	I	8.6	300	28.6	Xe
Xe,9	M	20.9	300	69.5	Xe
Xe,10	O	33.0	300	110.0	Xe
Xe,11	I+M	29.4	300	98.2	Xe
Xe,12	M+O	53.9	300	179.5	Xe
Xe,13	I+O	41.6	300	138.6	Xe
Xe,14	I+M+O	62.4	300	208.1	Xe
Xe,15	I	7.2	550	13.1	Xe
Xe,16	I	10.6	300	35.3	Xe
Xe,17	O	36.0	300	120.0	Xe

The first series of 300-V points were chosen at the same power levels as the krypton test. In part to show the range of the thruster and in part to have testing more representative of nominal discharge current values, the second set of test points were chosen for a three-channel operating point of roughly 300 V and 200 A. Lastly, two operating conditions that achieved higher discharge currents on the inner and outer channels by themselves as well as a third that tested the 550-V condition of the inner channel previously studied under krypton were looked at as well to round out the data.

6.1.2. Photographic diagnostics

The same two DSLR cameras described in Chapter IV were available for use during this test as well as the HDcam. There are some differences in the setup for these data however. First, because the thruster was relocated axially upstream inside the chamber by approximately one meter, the viewport that camera 2 was located at in the krypton testing afforded a much better view of the front of the thruster than in the previous test. As such, the HDcam was relocated to the same flange and the viewport on the top of the chamber that it had been positioned at was replaced with the original blank flange. Camera 1 was positioned at the same location as in the krypton test as well yet was not used for the high current testing as the expanded beam-dump obscured too much of the field to be useful.

6.2. Operational observations, results and discussion

6.2.1. Telemetry

The basic thruster telemetry are presented in Table 6.2.

Table 6.2. Telemetry of X3 at all operating conditions for Xe operation. I=inner, M=middle, O=outer, V_D = discharge voltage, I_D =discharge current, P_D =discharge power, $\dot{m}_T$ = total mass flow rate, m_dot,a= anode mass flow rate, I/(m_dot,a)=ratio of a channel's individual discharge current to that channel's individual m_dot,a. Rows 1-7, not including the top header row, constitute the 300 V/ 100 A conditions. Rows 8-14 constitute the 300 V/ 200 A conditions. Rows 15-17 constitute the extreme conditions. *Note: corrected for xenon.

Test Condition	Channel	V_D [V]	I_D [A]	P_D [kW]	$\dot{m}_T$ [mg/s]	I/(m_dot,a) [A/(mg/s)]	*Pressure [Torr]
Xe,1	I	299.2	13.1	3.9	14.0	1.0	7.21×10^{-6}
Xe,2	M	299.1	31.7	9.5	32.3	1.1	1.60×10^{-5}
Xe,3	O	299.2	55.2	16.5	52.1	1.1	2.70×10^{-5}
Xe,4	I+M	299.6	45.1	13.6	38.0	1.6(I) 1.2 (M)	2.08×10^{-5}
Xe,5	M+O	298.1	86.9	25.9	68.2	1.5 (M) 1.4 (O)	3.47×10^{-5}
Xe,6	I+O	299.5	68.9	20.6	58.1	1.7 (I) 1.2 (O)	3.05×10^{-5}
Xe,7	I+M+O	299.2	100.3	30.1	73.3	1.7 (I) 1.7 (M) 1.4 (O)	3.50×10^{-5}
Xe,8	I	299.2	28.6	8.6	27.2	1.2	1.46×10^{-5}
Xe,9	M	294.3	69.7	20.5	57.4	1.4	2.85×10^{-5}
Xe,10	O	301.0	110.8	33.3	100.0	1.2	4.56×10^{-5}
Xe,11	I+M	296.0	98.6	29.1	70.0	1.9 (I) 1.4 (M)	3.51×10^{-5}
Xe,12	M+O	298.2	184.5	54.9	133.1	1.6 (M) 1.4 (O)	5.95×10^{-5}
Xe,13	I+O	299.5	140.0	42.0	114.3	2.7 (I) 1.2 (O)	5.26×10^{-5}
Xe,14	I+M+O	296.9	204.5	60.8	151.6	1.8 (I) 1.7 (M) 1.3 (O)	6.65×10^{-5}
Xe,15	I	549.9	13.5	7.4	12.9	1.2	7.95×10^{-6}
Xe,16	I	300.7	38.5	11.6	35.4	1.2	7.51×10^{-6}
Xe,17	O	298.0	122.2	36.5	108.7	1.2	4.91×10^{-5}

6.2.2. Thrust stand

Presented here are the thrust data in graphical format. Key calculated metrics are anode efficiency, thrust-to-power ratio where the power is the discharge power (T/P) and anode specific impulse (anode Isp). A more complete accounting of thruster telemetry

including cathode flow and magnet currents is provided in Appendix B (Table B.1- Table B.3). The basic equations for anode efficiency and anode specific impulse are defined below in Equation 6.1 and 6.2.

$$\eta_a = \frac{T^2}{\left(2 \cdot P_D \cdot \dot{m}_a\right)} \tag{6.1}$$

$$Isp_a = \frac{T}{\dot{m}_a \cdot g_o} \tag{6.2}$$

where η_a is the anode efficiency, T is the measured thrust, P_D is the applied discharge power as defined in Equation 4.2, $\dot{m}_a$ is the anode mass flowrate, Isp_a is the anode specific impulse, and g_o is the local gravitational constant.

It was determined that the best way to evaluate the X3 based done these preliminary performance data was to compare it to similar thrusters operating at similar fractions of their design current density and at the same discharge voltage. Only data for test conditions Xe,1-Xe,7 are presented. Data for Xe,16 and Xe,17 are included in Appendix B (Table B. 3). Data for Xe,8-Xe,15 was determined to be too inaccurate for presentation. The main sources uncertainties in these measurements are derived from the uncertainty in the LVDT signal, assumed constant based on observed noise in signal at 100 mN, and uncertainty in the mass flowrate (+/- 1 %) measurements as the dominant sources of error in the data.

The following is a series of figures that present the data in graphical format. First we examine T/P and anode efficiency versus anode Isp in Figure 6.1 and Figure 6.2.
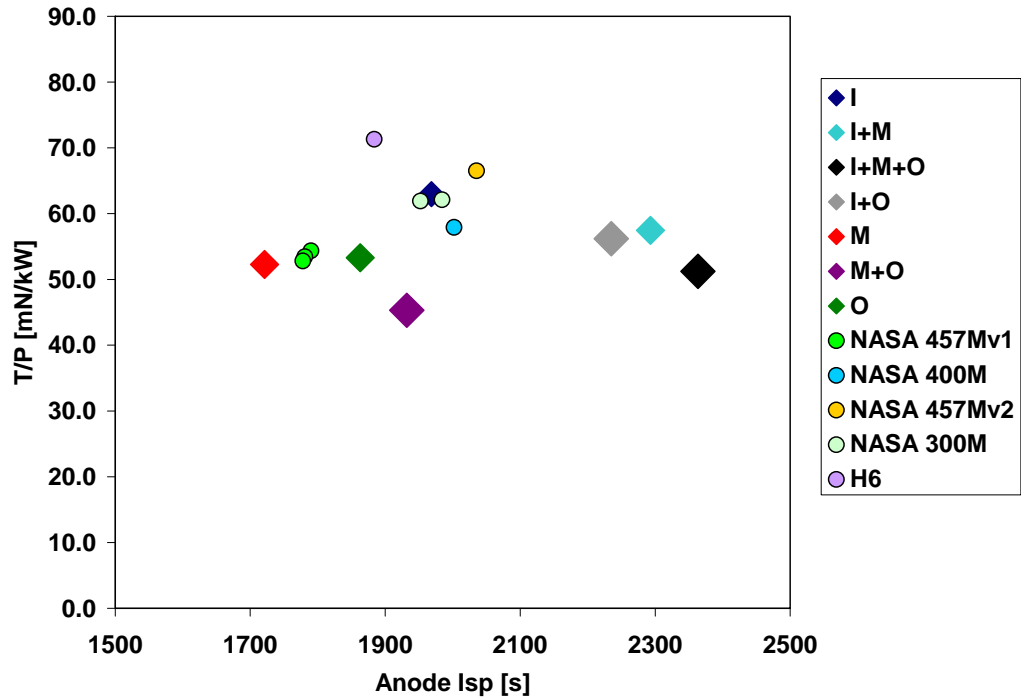
Figure 6.1. T/P ratio vs anode Isp for X3 at 300 V/100 A conditions (Xe,1-Xe,7) as compared to similar thrusters operating at a discharge voltage of 300V and a similar fraction of their respective design current densities: NASA 457Mv1,[24] NASA 400M,[77] NASA 457Mv2,[78] NASA 300M,[76] and H6.[94]
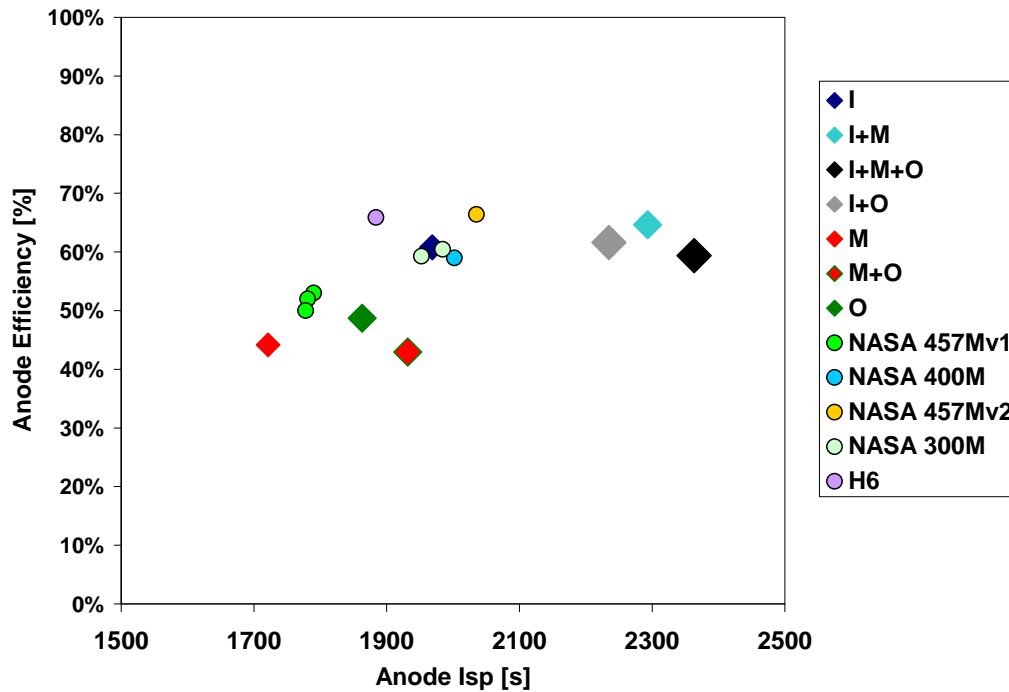
Figure 6.2. Anode efficiency vs anode Isp for X3 at 300 V/100 A conditions (Xe,1-Xe,7) as compared to similar thrusters operating at a discharge voltage of 300V and a similar fraction of their respective design current densities: NASA 457Mv1,[24] NASA 400M,[77] NASA 457Mv2,[78] NASA 300M,[76] and H6.[94]

When referring to Figure 6.1 and Figure 6.2, we note that the X3 is performing at as expected in terms of the metrics presented. That is to say, that T/P, anode efficiency, and anode Isp are comparable to other high-power thrusters operating at similar fractions of design discharge current density at the same discharge voltage. The anode Isp values for test conditions Xe,4 (I+M), Xe,6 (I+O), and Xe,7 (I+M+O) appears to be higher than expected. These points will have to be re-investigated for validation.

Next, as a second means of comparison to existing thrusters, we plot T/P and anode efficiency by a normalized current density j/j* (Figure 6.3 and Figure 6.4), where j is the operational current density of the thruster whose data is being plotted and j* is the average design current density of the NASA high-power thrusters.
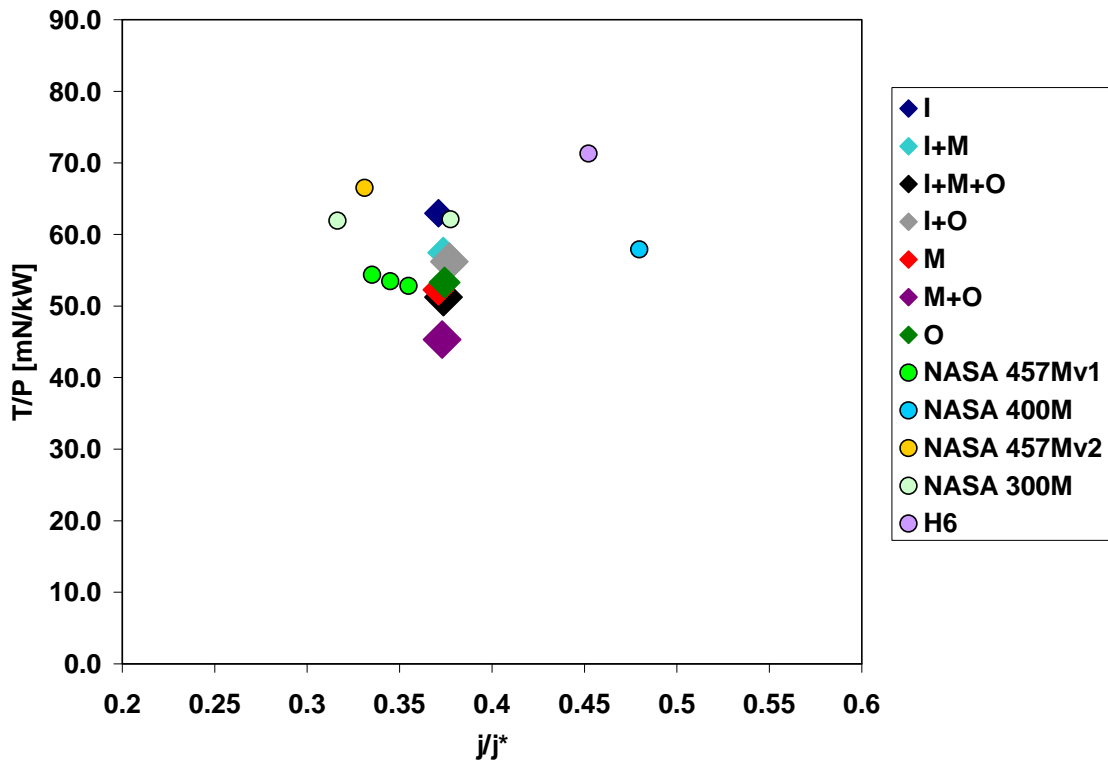
Figure 6.3. T/P vs j/j* for X3 at 300 V/100 A conditions (Xe,1-Xe,7) as compared to similar thrusters operating at a discharge voltage of 300V: NASA 457Mv1,[24] NASA 400M,[77] NASA 457Mv2,[78] NASA 300M,[76] and H6. [94]
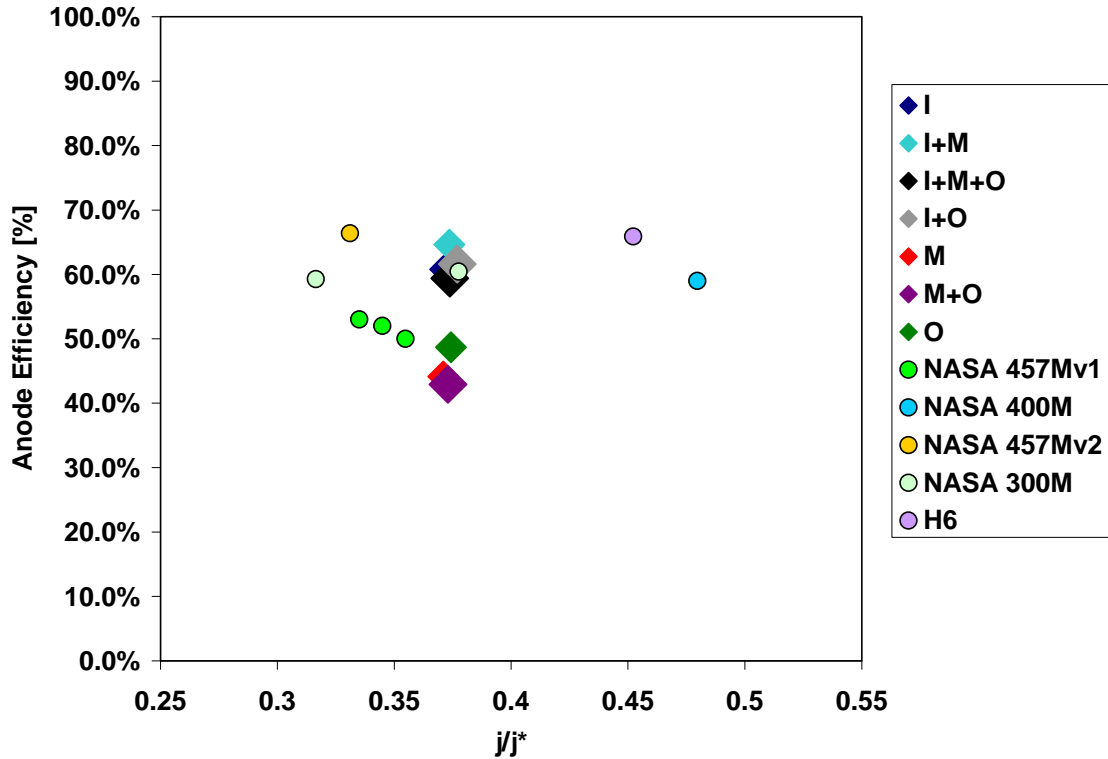
Figure 6.4. Anode efficiency vs j/j* for X3 at 300 V/100 A conditions (Xe,1-Xe,7) as compared to similar thrusters operating at a discharge voltage of 300V: NASA 457Mv1,[24] NASA 400M,[77] NASA 457Mv2,[78] NASA 300M,[76] and H6. [94]

There are two observations one can make when referring to Figure 6.3 and Figure 6.4. The first is to say that this method of presenting the data also shows the X3 in the same performance envelope as the other thrusters (better than some, worse than others). The second, and perhaps more useful observation, is that these figures showcase the benefits of a NHT. These figures show that with a single thruster (the X3), one can span the performance envelope of five distinct thrusters.

In order to help assess the impact of the different mass utilizations of multi-channel operations on performance, we plot T/P and anode efficiency versus I/(m_dot,a) in Figure 6.5 and Figure 6.6.

101
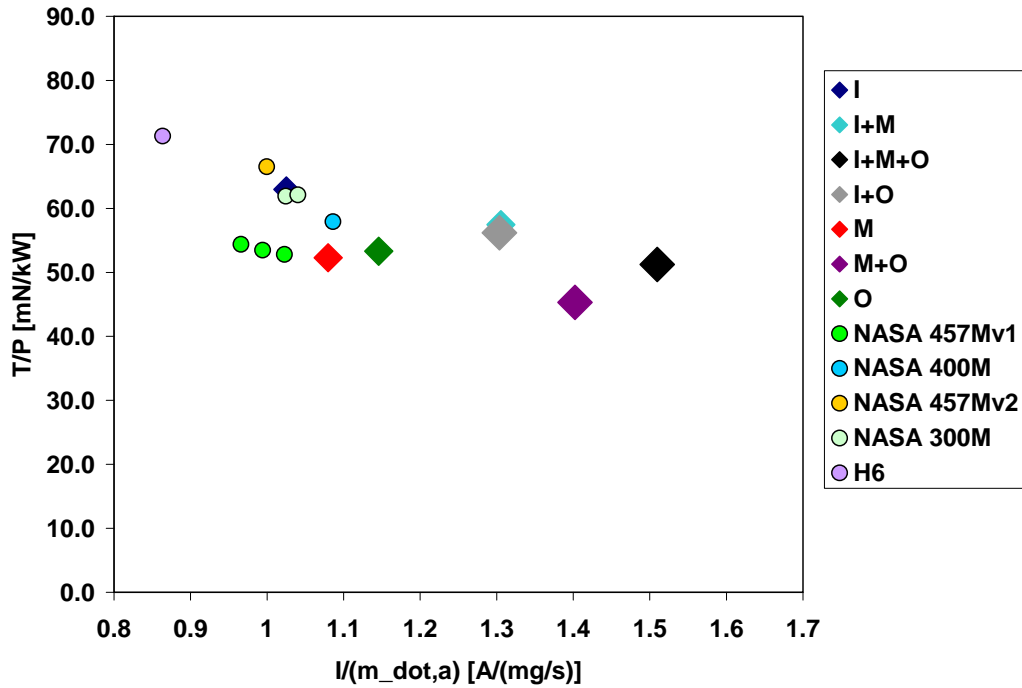
Figure 6.5. T/P vs I/(m_dot,a) for X3 at 300 V/100 A conditions (Xe,1-Xe,7) as compared to similar thrusters operating at a discharge voltage of 300V and a similar fraction of their respective design current densities: NASA 457Mv1,[24] NASA 400M,[77] NASA 457Mv2,[78] NASA 300M,[76] and H6. [94]
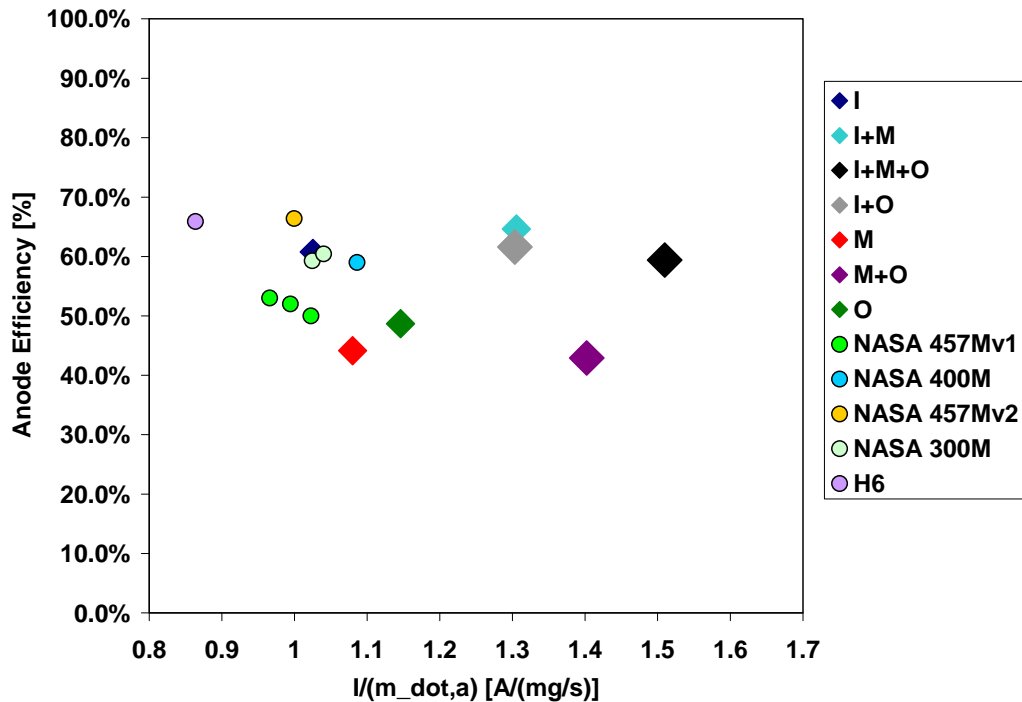
Figure 6.6. Anode efficiency vs I/(m_dot,a) for X3 at 300 V/100 A conditions (Xe,1-Xe,7) as compared to similar thrusters operating at a discharge voltage of 300V and a similar fraction of their respective design current densities: NASA 457Mv1,[24] NASA 400M,[77] NASA 457Mv2,[78] NASA 300M,[76] and H6. [94]

In Figure 6.5, we note a general downward trend in T/P with increasing values of the ratio of discharge current to anode mass flow rate. Intuitively, this is not entirely unexpected. As thrust generally follows mass flow rate in a linear fashion with HETs, increasing values of I/(m_dot,a) at a given discharge voltage would indicate that less thrust is being produced for a given amount of power. While the data presented occurs at varying discharge power levels, this observation still holds true.

Based on the data in Figure 6.6, there does not appear to be an overarching trend that anode efficiency follows with respect to I/(m_dot,a). Observing the values for single channel operation of the X3 when compared to the other thrusters, there seems to be a downward trend in anode efficiency with increasing I/(m_dot,a). However, when considering multi-channel operation of the X3, the trend is obscured to an indiscernible level. The useful observation that we make from this plot is that the increased I/(m_dot,a) values seen in multi-channel operation do not seem to hurt performance when considered from the angle of efficiency.

In order to be better discern a possible physical mechanism for the slightly out of range Isp seen in some of the multi-channel operations of the X3, we include a plot of anode Isp versus I/(m_dot,a) (Figure 6.7).
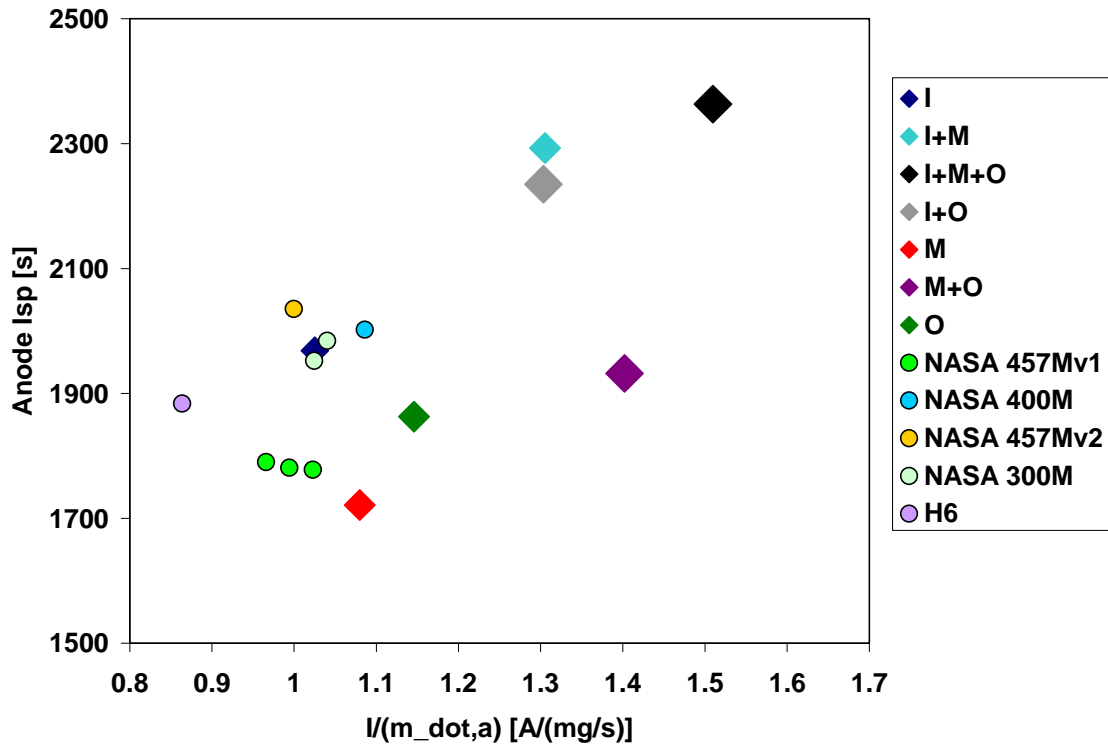
Figure 6.7. Anode Isp vs I/(m_dot,a) for X3 at 300 V/100 A conditions (Xe,1-Xe,7) as compared to similar thrusters operating at a discharge voltage of 300 V and a similar fraction of their respective design current densities: NASA 457Mv1,[24] NASA 400M,[77] NASA 457Mv2,[78] NASA 300M,[76] and H6. [94]

We can observe a general trend that anode Isp increases in value with increasing I/(m_dot,a). Referring back to Figure 6.1 and Figure 6.2, we note that the same points that were observed as outliers in terms of Isp are also at the higher end of the I/(m_dot,a) spectrum. In order to determine if the other thrusters exhibit similar trends, the data set for the NASA thrusters and H6 must be expanded to include a wider range of j/j*. This expanded data range is presented in Figure 6.7.
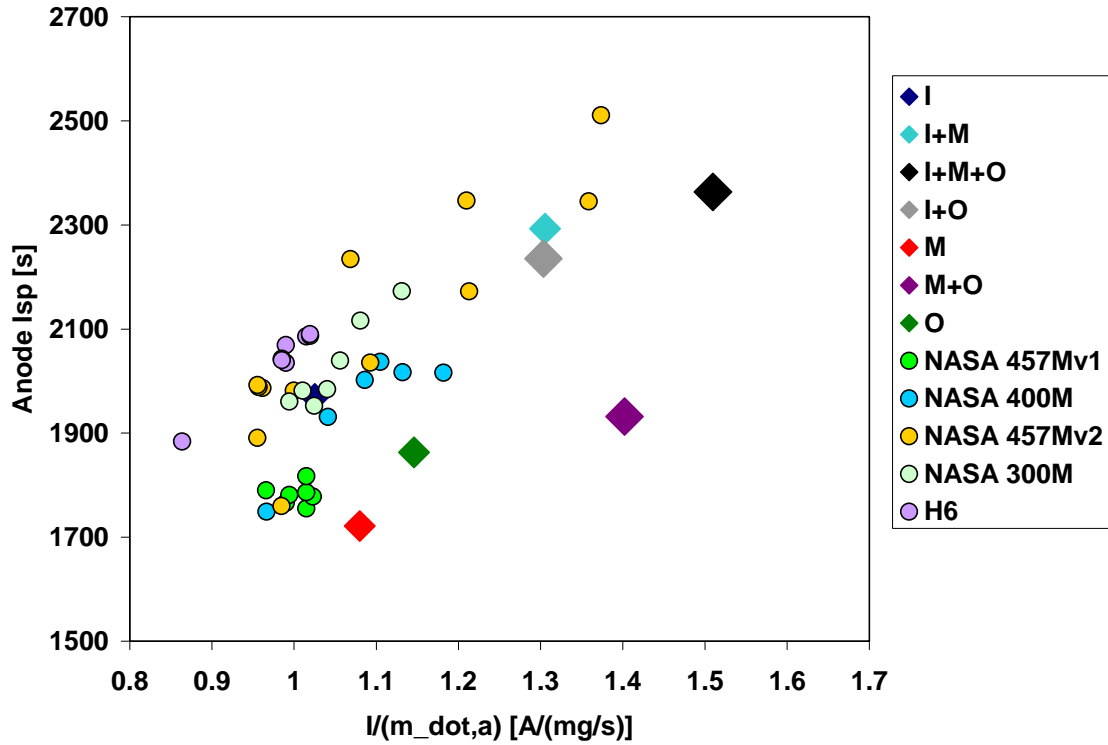
Figure 6.8. Anode Isp vs I/(m_dot,a) for X3 at 300 V/100 A conditions (Xe,1-Xe,7) as compared to similar thrusters operating at a discharge voltage of 300 V and over a range of j/j* that spans values of approximately 0.2-1.1: NASA 457Mv1,[24] NASA 400M,[77] NASA 457Mv2,[78] NASA 300M,[76] and H6.[94] Plot provided to help show trends across a wider range of I/(m_dot,a) for all of the thrusters.

From Figure 6.8, we can see that the NASA thrusters and the H6 all exhibit the same general linear upward trend in Isp with increasing I/(m_dot,a). While this by no means eliminates experimental uncertainties as a cause for this increased performance, it does point to a possible non-error based source of a boost in performance. To fully assess what the cause of this increased Isp in the X3 is testing on a fully validated thrust stand is required to reduce the level of uncertainty associated with thrust measurements and testing in a facility with higher pumping speed to help mitigate the possible impact of facility effects.

The final check of X3 performance is to see how the measured multi-channel performance compares to the superpositioned values of performance Figure 6.9. Superpositioned values are obtained by adding up the single channel performance values.

For example, superpositioned thrust for Xe,4 (I+M) is calculated by adding up the thrust generated by conditions Xe,1 and Xe,2. The values for I/(m_dot,a) are obtained the same way.
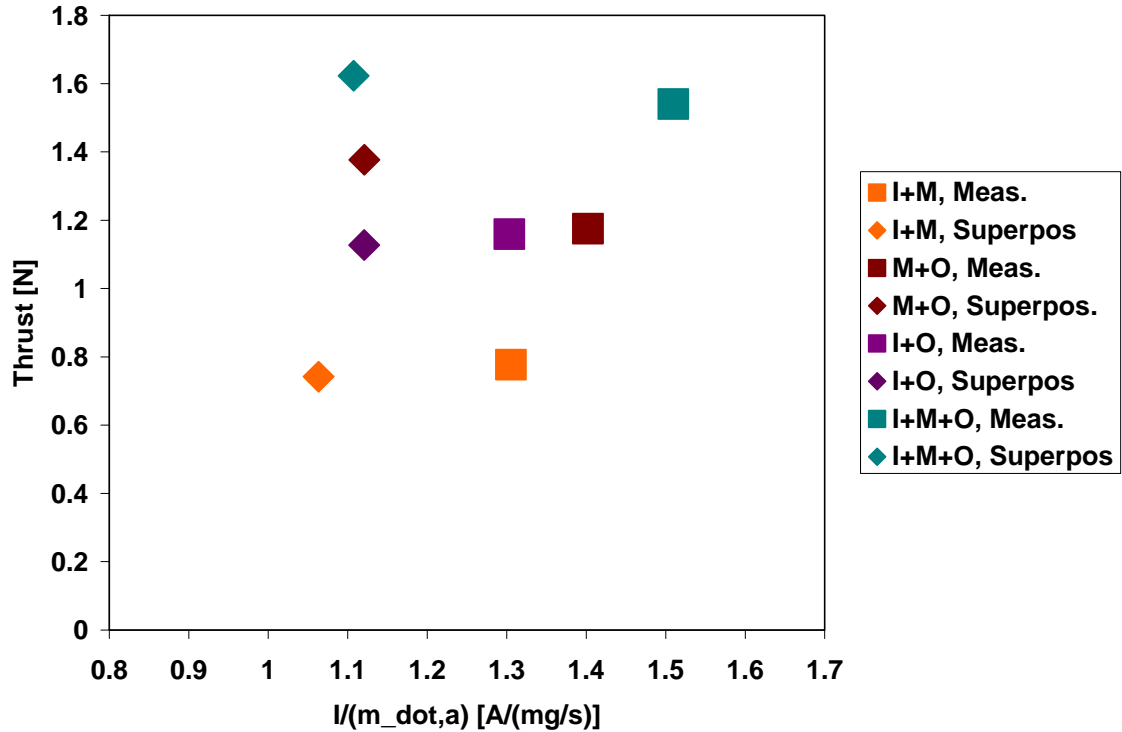
Figure 6.9. Thrust versus I/(m_dot,a) highlighting the difference between the measured performance of mutli-channel configurations and the calculated performance from the superposition of single-channel numbers. To obtain superpositioned ('Superpos') values of thrust and (I/m_dot,a), single channel values of thrust, discharge current, and anode mass flow were summed together respectively. Thrust uncertainty is +/- 0.100 N.

From the data presented in Figure 6.9, we note that in the context of the experimental uncertainty there is negligible performance gain or loss due to operating channels simultaneously versus superimposing their individual values. This matches with what Liang observed with the X2.[9]

6.2.2.1. Thrust data general observations and commentary

The thrust data obtained for this work is preliminary. With that in mind, there are a few key points from the data worth discussing. There is a possibility that thrust

performance is over-estimated due to elevated background pressure. We note that the corrected pressure falls within the established 5×10^{-5} Torr range of acceptability.[95,96] New evidence from testing at NASA GRC suggest, however, that even this to high and pressure effects are still seen below it.[97]

As noted at the beginning of section 6.2.2, data associated with test conditions Xe,8-Xe,15 are not presented in this document due to an unacceptably high level of uncertainty. While the LVDT and mass flowrate uncertainty remained unchanged from that present in the other data, another major source of uncertainty is also hypothesized for these data. The only explanation that can be offered at this time is that a facility effect is occurring which is causing the discharge current to be artificially high for a given flow rate. The following two paragraphs offer a suggestion for what is occurring and should be treated as conjecture as not enough data exists yet for the X3 to make a concrete statement.

What is hypothesized is that a combination of an energetic beam and a large amount of neutral input into the vacuum chamber is may be loading down the pumps. As this limit is reached, the pumps begin to release previously accumulated gas from their cold surfaces, raising the background pressure in the chamber and artificially increasing the discharge current. While it is possible to combat this effect with magnet tuning, in a sense one is not tuning to the thruster but to the facility, which is not a proper way to characterize a thruster. In order to maintain facility pressure and proper discharge currents, then, mass flowrates must be accordingly decreased to a sub-optimal level, negatively effecting performance.

At this point, it is worth pointing out that what is conjectured is that the problem is not due to the change in pressure but the rate of increase of the pressure in time. The

problem appears to be one of a cascade effect where once the pumps begin to release/shed their accumulated gases, the pressure in the chamber will continue to rise until the pumps can no longer pump any gas (pump "run-away"). During that process the discharge current of the thruster will rise at an unacceptably fast rate to a point where the magnets can not keep up with it. It is thus submitted that to properly assess the performance of the X3 at nominal and above-nominal discharge currents, testing must take place in a facility with higher pumping capacity (e.g. NASA GRC's VF-5[97]).

6.2.3. High-speed current probe evaluation

Power spectral densities (PSDs) of the AC-coupled discharge current trace are presented. Aside from presenting these data in graphical format, a table is provided that summarizes peak frequency and peak-peak oscillation amplitude for each operating condition. The PSD's plots are presented in three separate figures for ease of viewing, split up by two groupings that combine for three-channel operation (Figure 6.10 and Figure 6.11) as well as the three extreme data points for the inner and outer channel (Figure 6.12).
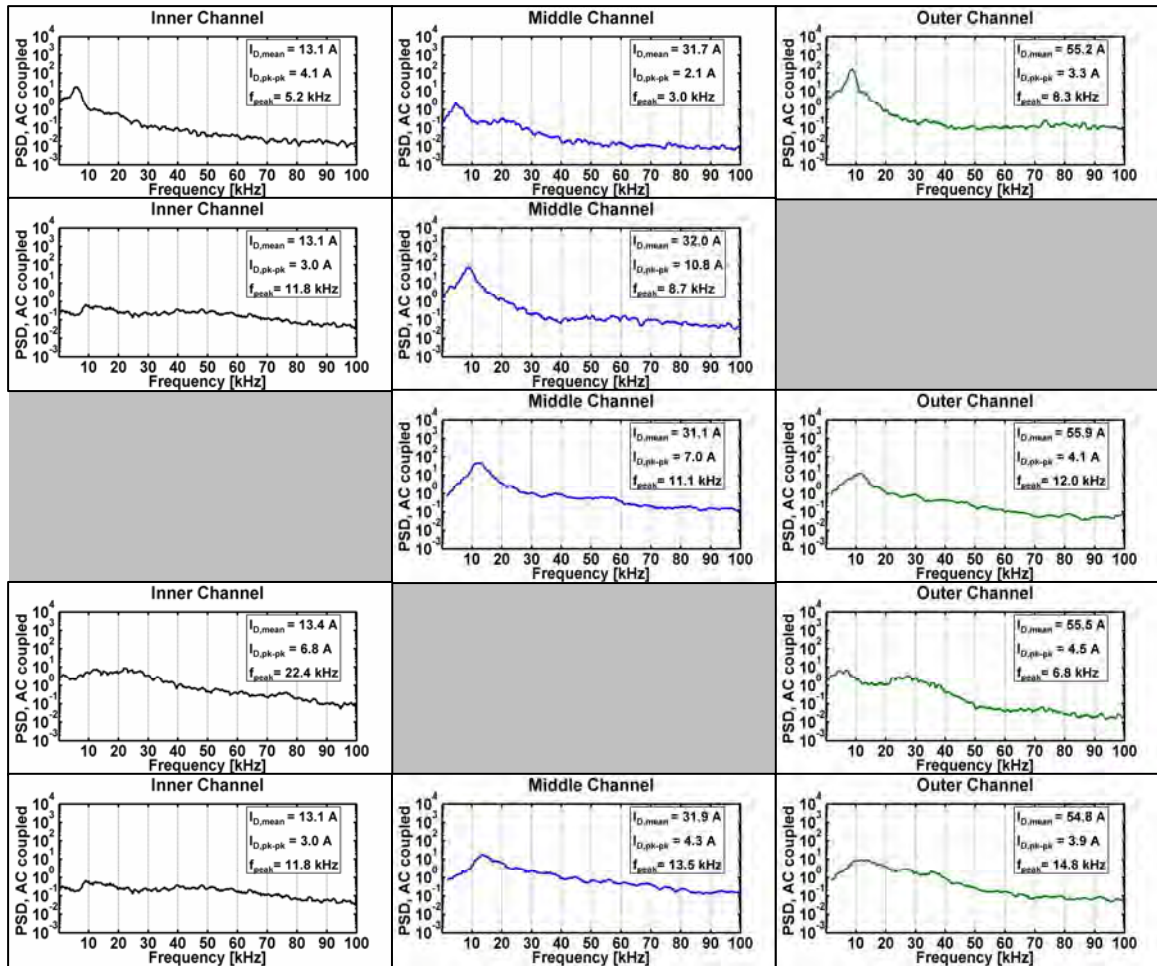
Figure 6.10. AC-coupled power spectral densities (PSDs) of the discharge currents for the 300 V/100 A three-channel set of conditions (Xe,1-Xe,7). The first row of plots is each individual channel operating by itself. The conditions for the following four rows are top to bottom are: I+M (Xe,4), M+O (Xe,5), I+O (Xe,6), I+M+O (Xe,7). Columns left-right are: inner, middle, outer channel respectively.

Several of the trends seen in the krypton performance are repeated in the xenon performance testing. The data suggest that the outer channel is the "quietest" of the three channels with the lowest peak-peak oscillation amplitude as percentage of mean discharge current. Secondly, when additional channels are turned on, the oscillation frequency does shift to slightly higher registers. However, the degree to which oscillation amplitudes and frequencies synchronize in two channel operation is not as significant as in the krypton operating points. That said, adjacent channels appear to have the greatest impact on each other.
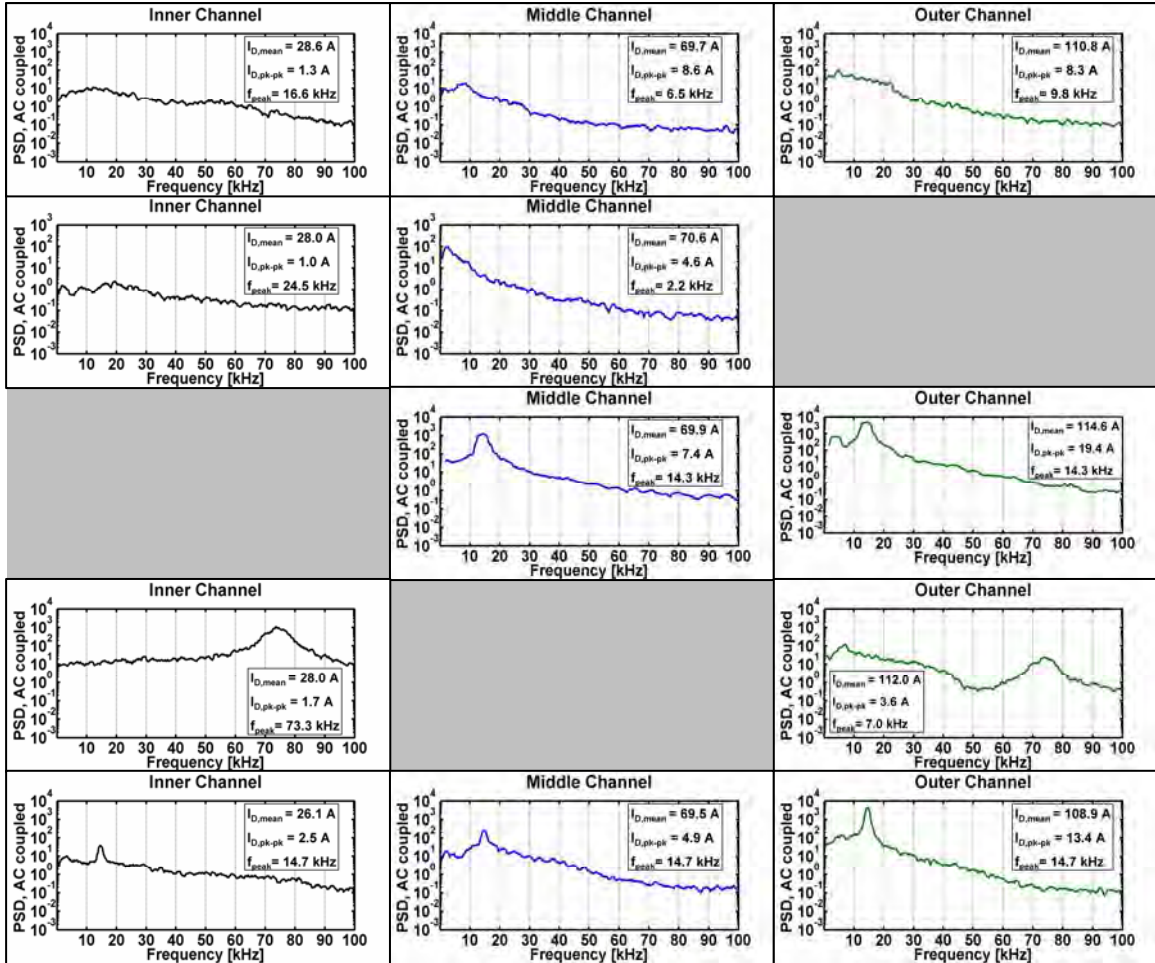
Figure 6.11. AC-coupled power spectral densities (PSDs) of the discharge currents for the 300 V/200 A three-channel set of conditions (Xe,8-Xe,14). The first row of plots is each individual channel operating by itself. The conditions for the following four rows are top to bottom are: I+M (Xe,11), M+O (Xe,12), I+O (Xe,13), I+M+O (Xe,14). Columns left-right are: inner, middle, outer channel respectively.

At the higher discharge current ranges, for example the I+O combination (Xe,13) shown in Figure 6.11, it is observed that if one channel (the inner one in this case) has a dominant frequency well above another channel that this significantly higher frequency will not shift the dominant frequency of the other channel. That said, one can see in the PSD of the outer channel in that combination that the dominant peak of the inner channel shows up as a secondary peak at the same frequency in the outer channel's trace.

110
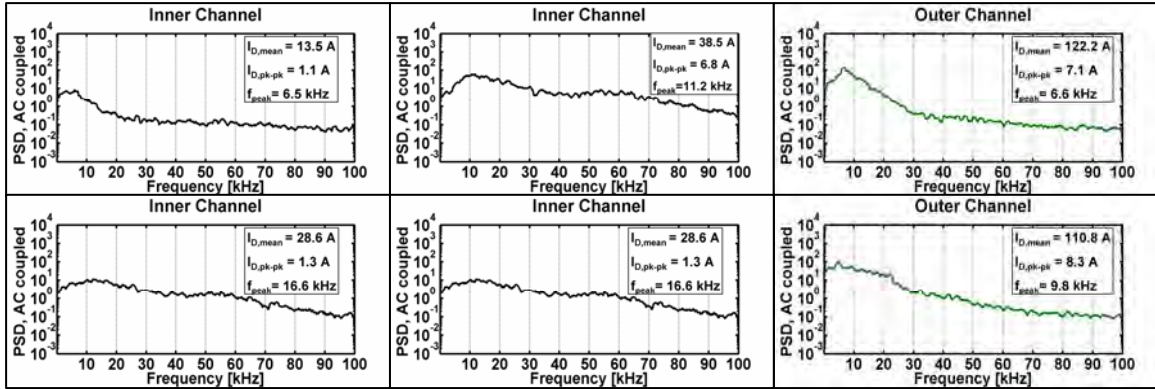
Figure 6.12. AC-coupled power spectral densities (PSDs) of the discharge currents for three remaining data points (extreme ends, Xe,15-Xe,17) in the top row, with the 300 V/100 A single-channel data (Xe,1-Xe,3) in the bottom row for comparison. Columns left-right are: inner, inner, outer channel.

In both three-channel cases, the oscillation frequencies synchronize across all three channels at values above their independent peak frequencies. In the 100-A case, one can see that even the oscillation amplitudes coalesce to the value of the outer channel's peak-peak oscillations. However, in the 200-A case this no longer seems to occur. Regardless, taken as percentages of the mean discharge current, the peak-peak values do fall within the same range of 7-13%.

A final trend of note is that in the one 550-V operating condition presented, the same response that was seen with krypton is repeated: by increasing the discharge voltage, the frequency shifts higher and the overall oscillation magnitude drops. All of the results for the high-speed current probe evaluation are summarized in Table 6.3.

Table 6.3. High-speed current probe data summary table. TC#= test condition, Ch= channels, V_D= average discharge voltage, $I_{D,X}$ = Channel X mean discharge current, $I_{D,PP,X}$ = Channel X peak-peak current amplitude, $f_{pk,X}$= Channel X peak/dominant frequency. I=inner, M= Middle, O= Outer,

TC#	Ch	V_D [V]	$I_{D,I}$ [A]	$I_{D,M}$ [A]	$I_{D,O}$ [A]	$I_{D,PP,I}$ [A]	$I_{D,PP,M}$ [A]	$I_{D,PP,O}$ [A]	$f_{pk,I}$ [kHz]	$f_{pk,M}$ [kHz]	$f_{pk,O}$ [kHz]
Xe,1	I	299.2	13.1	-	-	4.1	-	-	5.2	-	-
Xe,2	M	299.1	-	31.7	-	-	2.1	-	-	3.0	-
Xe,3	O	299.3	-	-	55.2	-	-	3.3	-	-	8.26
Xe,4	I+M	299.6	13.1	32.0	-	3.0	10.8	-	11.8	8.7	-
Xe,5	M+O	298.2	-	31.1	55.9	-	7.0	4.1	-	11.1	12
Xe,6	I+O	299.5	13.4	-	55.5	6.8	-	4.5	22.4	-	6.76
Xe,7	I+M+O	299.2	13.6	31.9	54.8	3.4	4.3	3.9	13.5	13.5	14.8
Xe,8	I	299.2	28.6	-	-	1.3	-	-	16.6	-	-
Xe,9	M	294.3	-	69.7	-	-	8.6	-	-	6.5	-
Xe,10	O	301.0	-	-	110.8	-	-	8.3	-	-	9.84
Xe,11	I+M	296.0	28.0	70.6	-	1.0	4.6	-	24.5	2.2	-
Xe,12	M+O	298.2	-	69.9	114.6	-	7.4	19.4	-	14.3	14.25
Xe,13	I+O	299.5	28.0	-	112.0	1.7	-	3.6	73.3	-	6.96
Xe,14	I+M+O	296.9	26.1	69.5	108.9	2.5	4.9	13.4	14.7	14.7	14.66
Xe,15	I	300.7	38.5	-	-	6.8	-	-	11.2	-	-
Xe,16	I	549.9	13.5	-	-	1.1	-	-	6.5	-	-
Xe,17	O	298.0	-	-	122.2	-	-	7.1	-	-	6.56

All of the observations pointed out should be considered points for further studies on channel interactions. While the data suggest some level of channel cross-talk, it is not clear what the driving factors might be. For example, the shifts to higher frequencies that are observed may in some part be related to the cathode oscillations which are in general of higher frequency than channel breathing modes.[98] It was observed that altering magnet settings could change cathode coupling voltages by a significant amount (e.g. from -20 V to -30 V); perhaps, then, the extent to which the cathode oscillations influence the behavior of the channels also changes. Further, while the points presented herein show oscillation amplitudes at 20% of mean discharge current and below (relatively "quiet" operation) with frequencies in an expected range of 5 kHz-15 kHz, that does not preclude these values changing with performance-optimized operation of flow rates, cathode flow fractions, and magnet field settings.

6.2.4. Photographic evaluation

Side views for the data points taken are presented in Figure 6.13-Figure 6.16. All camera settings are the same in a given figure. However, the settings of camera 2 were adjusted to prevent over-saturation of the image in the photographs presented in Figure 6.14.
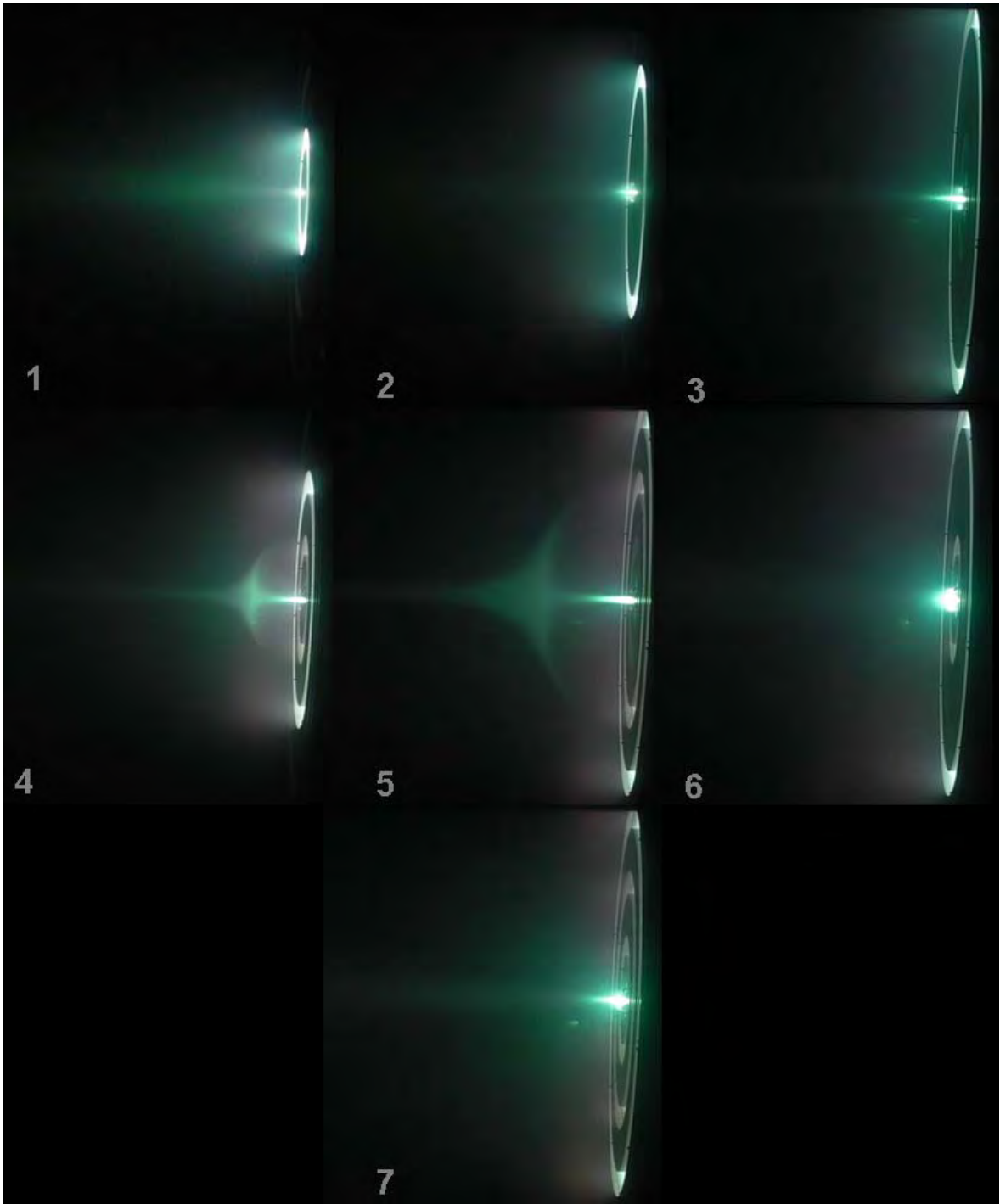
Figure 6.13. All operating modes of the X3 (side view, HDcam). 300 V/100 A three-channel conditions. Operating points from top-left to bottom-right: (1) Inner (Xe,1), (2) Middle (Xe,2), (3) Outer (Xe,3), (4) Inner+Middle (Xe,4), (5) Middle+Outer (Xe,5), (6) Inner+Outer (Xe,6), (7) Inner+Middle+Outer (Xe,7). All photographs were taken with the same camera settings.
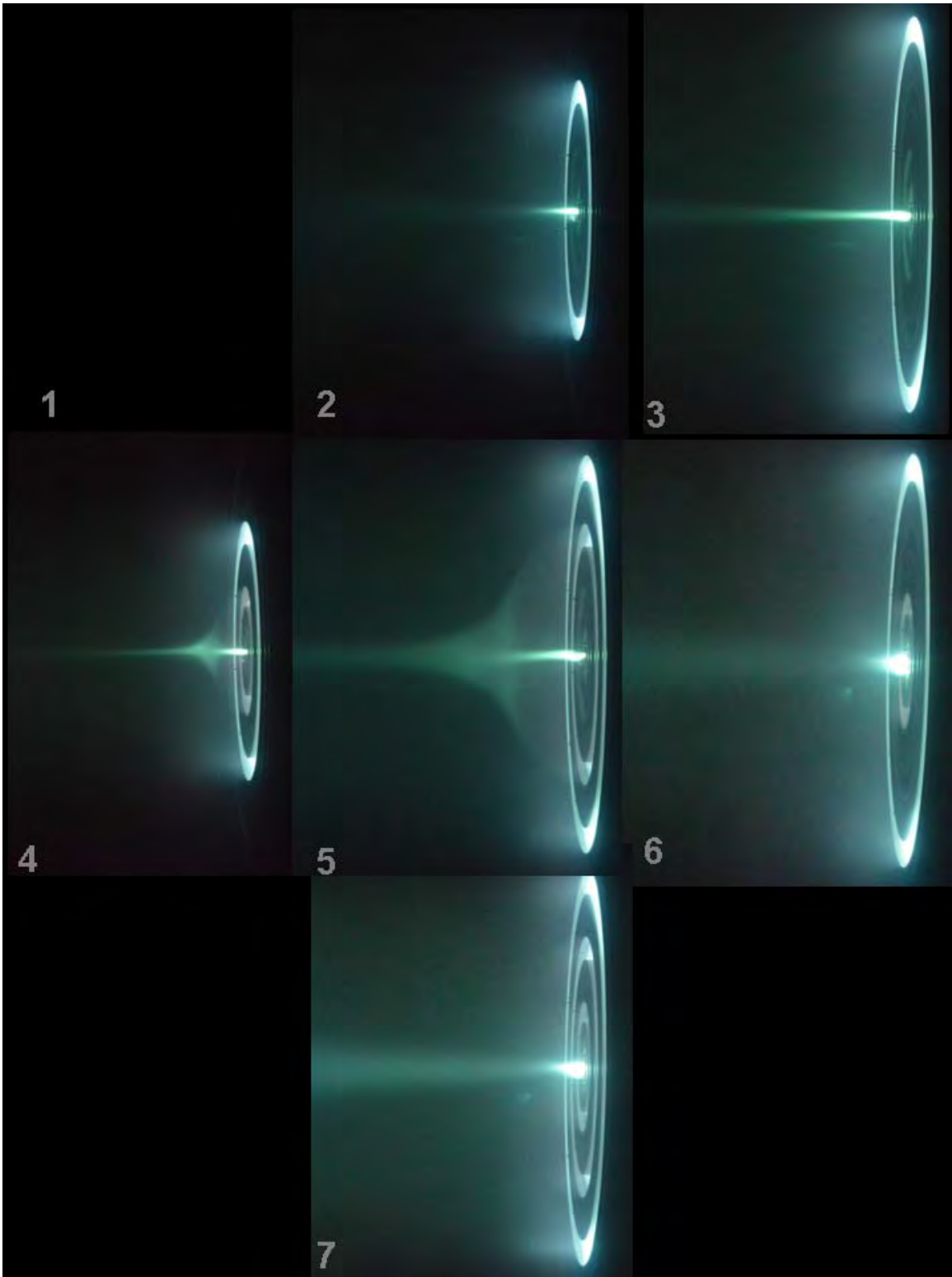
Figure 6.14. All operating modes of the X3 (side view, Camera 2). 300 V/200 A three-channel conditions. Operating points from top-left to bottom-right: (1) Inner (image corrupted, not shown) (Xe,8), (2) Middle (Xe,9), (3) Outer (Xe,10), (4) Inner+Middle (Xe,11), (5) Middle+Outer (Xe,12), (6) Inner+Outer (Xe,13), (7) Inner+Middle+Outer (Xe,14).
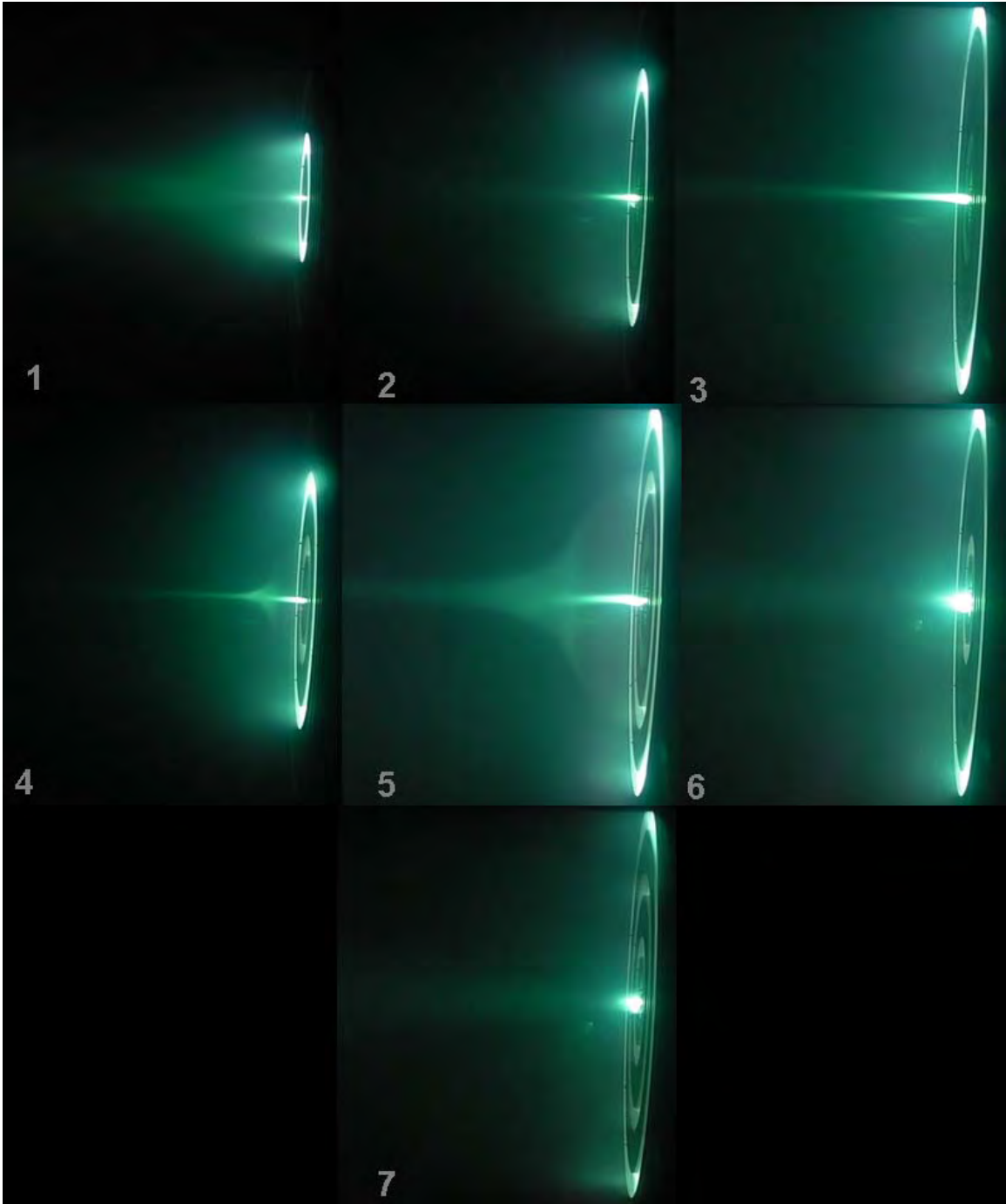
Figure 6.15. All operating modes of the X3 (side view, HDcam). 300 V/200 A three-channel conditions. Operating points from top-left to bottom-right: (1) Inner, (Xe,8), (2) Middle (Xe,9), (3) Outer (Xe,10), (4) Inner+Middle (Xe,11), (5) Middle+Outer (Xe,12), (6) Inner+Outer (Xe,13), (7) Inner+Middle+Outer (Xe,14).
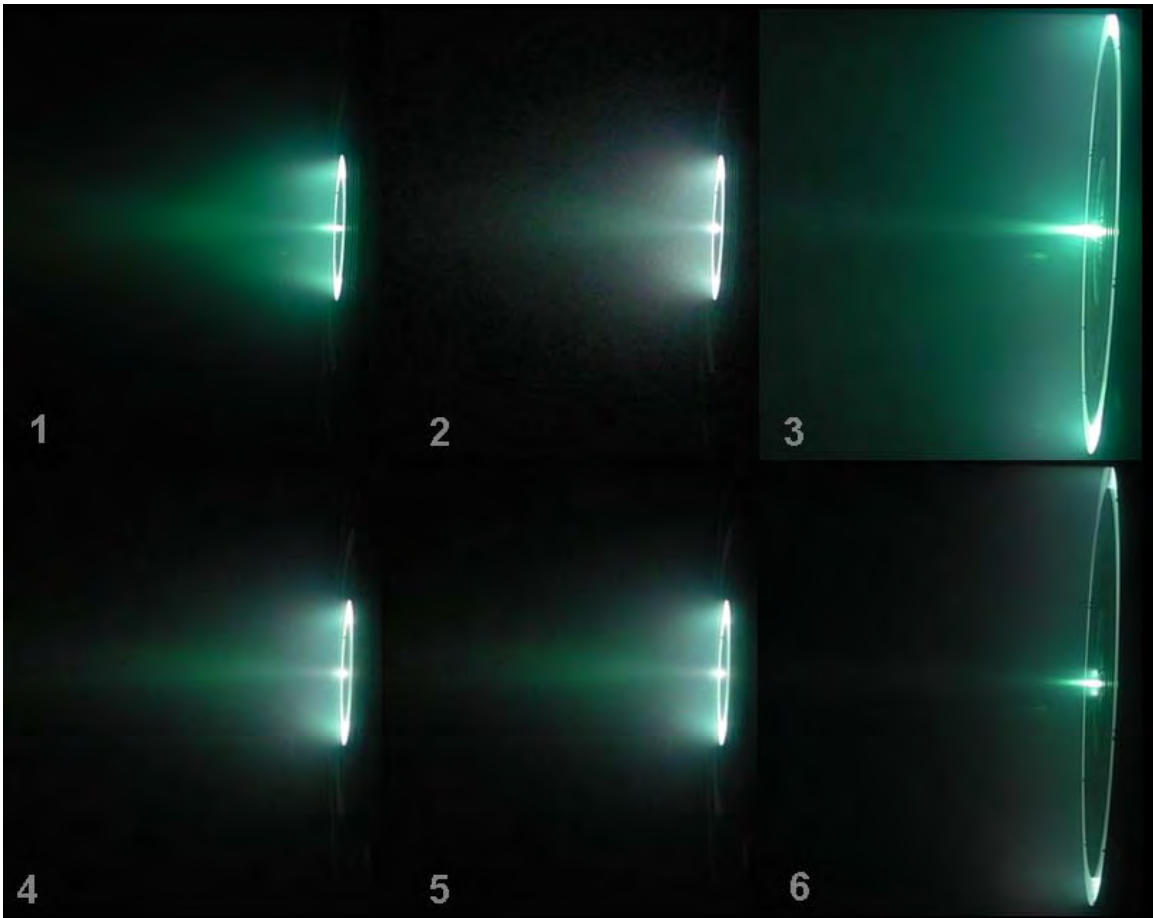
Figure 6.16. Extreme end of single-channel operation for the inner and outer channel (top) alongside the base lower current operation (bottom) (side view, HDcam). Top: (1) Inner, 300 V/38 A (Xe,15), (2) Inner, 550 V/13.1 A (Xe,16), (3) Outer, 300 V/122 A (Xe,17). Bottom: (4,5) Inner, 300 V/ 13.1 A (Xe,1), (6) Outer, 300 V/ 55.1 A (Xe,3).

The photographs contained herein show a measure of indication of uniform discharges. No hot-spots were observed during observation; while no head-on photographic data of xenon operation is presented in this document, the thruster was observed throughout operation to have an azimuthally uniform distribution of plasma throughout the discharge chamber. The pictures do identify possible points of investigation for diagnostic interrogation of the plume, with the most interesting being the "bell" or "saber" shape seen when multiple channels are on together (#4 and # 5 in both Figure 6.13 -Figure 6.15). This visible feature may likely be due to the seperatrix of the magnetic field of the X3. Unfortunately, a direct side-view of the thruster was not

obtained in this experimental setup and no figures containing overlays of magnetic field on top of plume photographs are able to be provided. This mimics operation of the X2 in dual channel mode and could very well have interesting plasma properties along its border.[9]

6.2.5. Brief thermal characterization

As previously noted, the X3 is outfitted with a large number of thermocouples that allow real-time monitoring of the temperature of key components of the thruster. As with the krypton data presented in Chapter V, only the data from the three-channel operating modes (Xe,7 and Xe, 14) are presented here (Figure 6.17 and Figure 6.18). In order to provide a comparison to simulation, temperature profiles at 30 kW and 60 kW are linearly extrapolated from the higher power operating conditions that were actually simulated. Only data for the magnets (zones z2-z7), the channel cups (zones z9,z10, and z11), and the outer radius of the thruster (zone z8) are available for the simulated cases.
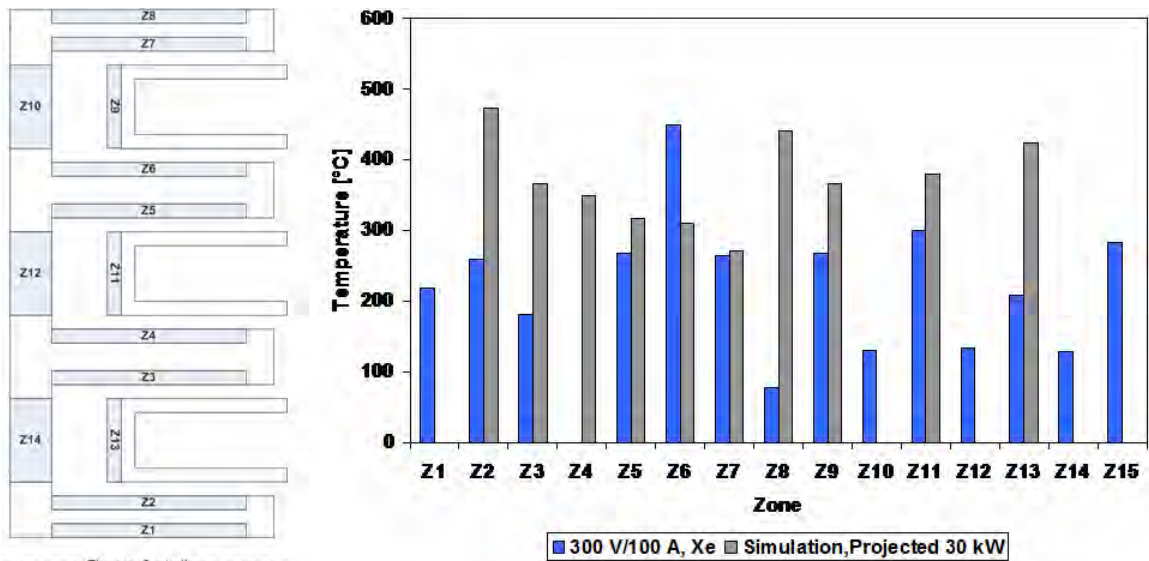
Figure 6.17. Thermal profile of the X3 with all three channels on, 300 V/100 A condition (Xe,7). (Left) Representative cross-section of the X3 with labeled zones where data were collected. (Right) Bar-graph containing absolute temperature values. Data for Z4 compromised by bad connections. Simulation values are linearly extrapolated from higher power results. Xenon propellant.
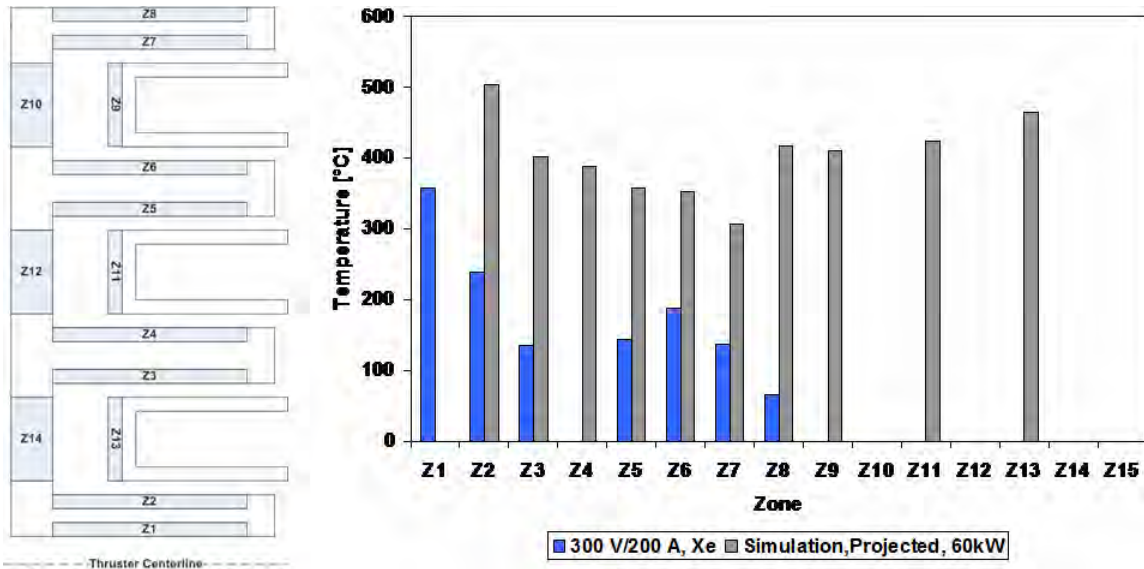
Figure 6.18.Thermal profile of the x3 with all three channels on, 300 V/200 A condition (Xe,14). (Left) Representative cross-section of the X3 with labeled zones where data were collected. (Right) Bar-graph containing absolute temperature values. Data for Z4 compromised by bad connections, file containing data for Z9-Z-15 corrupted. Xenon propellant

The primary question addressed by the data presented is: Will the thruster reach unacceptably high temperature during three-channel operation? The preliminary answer is a qualified no. Where comparison to simulation is possible, all measured temperatures are at or lower than simulated values. The only case where the measured temperature overshoots the simulated value is in zone z6 in Figure 6.17. It is more likely that this is due to some unknown source of error in the thermocouple data (e.g. a bad connection on that thermocouple wire during the test) than an actual physical process. There is nothing in the power consumption of the magnets across the two cases that suggests that the temperature should be that much higher than simulation. Further, the temperature does not follow the trend of the other five magnets.

Based upon the comparison to simulation seen in, we can tentatively project that the thruster will operate within acceptable temperature ranges at higher powers (e.g. 150 kW or 200 kW). We are able to say this because the simulations at those higher power levels show acceptable temperature ranges. The conclusion is tentative for two reasons. First, an

119

assumption is made that the temperatures will scale linearly with increasing power. Secondly, the temperature data presented here can not be considered truly steady state. Primarily due to the pumping capabilities of LVTF it is not possible to run the X3 at these discharge currents (100 A and 200 A) all the way to a complete thermal steady state. That said, both the 300 V/ 100 A (Xe,7) and the 300 V/ 200 A (Xe,14) occurred at the end of a full day of testing (>8-10 hours of thruster operation) where multiple other conditions were run with limited thruster off-time in between conditions. Here limited is meant to be much shorter than the thermal time constant.

A less quantitative result, though just as important, is that the thruster was far from melting during three-channel operation. This result is included simply because it answers the most common question posed to the design team "Will the X3 melt when you turn all three channels on?"

6.2.6. General conclusions

Preliminary thruster performance measurements indicate that the X3 is performing within an expected envelope when considered within the context of comparable thrusters operating at comparable fractions of their respective design discharge current densities. Based on the data (Figure 6.1-Figure 6.9), we cautiously project that the X3 will achieve expected performance at higher power levels. Further, comparison of thermocouple data to simulations allows us to preliminarily asses that the thruster is operating within acceptable temperature bounds. We make the tentative projection that the thruster will be able to operate successfully, in a thermal sense, at higher powers (e.g. 150 kW or 200 kW).

There is a distinct level of channel interaction as evidenced from the high-speed discharge current measurements. This seems to be a feature of NHTs as Liang[9] and McDonald's[99] work with the X2 both show increases in peak oscillation frequencies once moving into dual-channel mode. From the perspective of thruster performance, whether this interaction is good or bad remains to be seen. Further investigation in a facility with better pumping capacity than PEPL's LVTF is required.

CHAPTER VII

Future work

"E mo, bedgiuzzu, comu facimu?"

7.1. General commentary

Rarely is the doctoral work ever complete by the time the dissertation is submitted. In fact, it might be considered an important part of the process that one piece of work in forms the path for the next. Having come to the end of this document, one thing is certain: there is still a great deal more to discover about the X3. In an attempt to be as helpful as possible, this chapter is kept as succinct yet informative as possible.

7.2. Thruster burn-in

Beyond a doubt, the X3 ought to be burned in at discharge voltages greater than 550 V. To properly demonstrate the full performance throttling of this thruster, 800 V operation must be reached. To do this properly, the channels must first be burnt-in.

It is recommended that this testing take place with krypton at the same discharge currents presented in this work so that testing is not hampered by economic concerns. In order to minimize the impacts of possible pump run-away, testing must take place in a facility with higher pumping capacity than LVTF or upgrades to the system in place at PEPL must be undertaken. Such upgrades might include continued refinement of the extended beam dump, as well as installation of carbon shielding of the cryopumps to help protect them from the beam.

7.3. Performance testing

A test matrix that encompasses the full capabilities of the X3 with its seven operating modes and 200X power throttling ability is hundreds of data points large. To include such a matrix in this document is not useful. Instead, general recommendations are given.

First and foremost, completion of the xenon testing performed for this dissertation needs to be repeated in a chamber with higher pumping capacity. After burn in up to the 800-V operating conditions, the high end of the throttle range of the thruster should be explored (e.g. 800 V/ 250 A). Next, the krypton operating condition points presented herein should be explored, as well as krypton operation at 800 V. This later point is to demonstrate the upper reaches of the X3's Isp capabilities.

Not to be overlooked is a calibration of the modified thrust stand with thrusters that have established performance numbers. As they are readily available at PEPL, the H6 and the X2 are both recommended. The H6 is preferable at is better characterized and has been independently tested outside of PEPL.

7.4. Channel interaction via non-thrust stand diagnostics

The X3 should have its plume investigated for general plasma properties with an eye towards better understanding how the individual channel plumes interact with each other. The first test that would be useful to be performed is a radially swept Faraday probe in order to determine the beam current profile. Determining the beam divergence not only gives the designer a feel for how well the thruster meets specifications, but also it can help frame the argument for putting such a thruster in space by showing how/where the plume might interact with spacecraft surfaces. Moving into multi-channel operation, one

can utilize the Faraday probe at multiple axial locations downstream of the thruster to determine at what points the plume begins to merge.

A full suite of far-field diagnostics to include an EXB probe, Langmuir probe, and retarding potential analyzer are recommended to provide an alternate means of analyzing the performance of multiple channels. While a thrust-stand can show overall efficiency gains or losses, these diagnostics will allow the experimentalist to further pinpoint where these changes are occurring (e.g. voltage utilization).

7.5. Spacecraft interaction

As the ultimate goal is to launch an X3-like thruster into space, convincing mission planners that the thruster is safe to fly is critical. A short bullet-point list is presented below to help guide such an investigation:

- High-frequency fluctuations in ion and electron densities—position high speed Langmuir probes axially downstream, at 90 degrees to the thruster exit plane, and directly behind the thruster.

- EMI generation: install a pick-up antenna.

APPENDIX A

Table A. 1. Summary table of X3 telemetry for krypton operation including discharge properties mass flowrates. TC#= test condition, $V_{D,X}$ = discharge voltage of channel X, $I_{D,X}$ = discharge current of channel X, $P_{D,X}$ = discharge power of channel X, $P_{D,T}$ = total thruster discharge power, I=inner, M=middle, O=outer, $\dot{m}_{a,X}$ =anode mass flowrate of channel X, $\dot{m}_{a,T}$ =total anode mass flowrate, $\dot{m}_{c,i}$ =cathode internal mass flowrate, $\dot{m}_{c,e}$ =cathode external mass flowrate, $\dot{m}_{c,T}$ =total cathode mass flowrate.

| TC# | Discharge Properties | | | | | | | | | | mass flow rates [mg/s] | | | | | | |
	$V_{D,I}$ [V]	$I_{D,I}$ [A]	$P_{D,I}$ [kW]	$V_{D,M}$ [V]	$I_{D,M}$ [A]	$P_{D,M}$ [kW]	$V_{D,O}$ [V]	$I_{D,O}$ [A]	$P_{D,O}$ [kW]	$P_{D,T}$ [kW]	$\dot{m}_{a,I}$	$\dot{m}_{a,M}$	$\dot{m}_{a,O}$	$\dot{m}_{a,T}$	$\dot{m}_{c,i}$	$\dot{m}_{c,e}$	$\dot{m}_{c,T}$
Kr,1	300.5	13.0	3.9	-	-	-	-	-	-	3.9	8.3	-	-	8.3	0.83	-	0.83
Kr,2	-	-	-	299.8	32.0	9.6	-	-	-	9.6	-	19.3	-	19.3	1.93	-	1.93
Kr,3	-	-	-	-	-	-	299.6	55.1	16.5	16.5	-	-	32.8	32.8	1.95	1.33	3.28
Kr,4	300.2	13.3	4.0	300.2	31.3	9.4	-	-	-	13.4	6.6	15.6	-	22.2	1.95	0.27	2.22
Kr,5	-	-	-	299.4	31.9	9.5	299.3	55.2	16.5	26.1	-	13.8	30.1	43.9	1.95	2.52	4.47
Kr,6	300.7	13.2	4.0	-	-	-	300.4	57.1	17.2	21.1	7.2	-	29.9	37.1	1.95	1.67	3.62
Kr,7	300.5	13.1	3.9	299.4	31.8	9.5	299.3	55.2	16.5	30.0	5.7	14.1	29.4	49.3	1.95	2.69	4.64
Kr,8	550.7	13.1	7.2	-	-	-	-	-	-	7.2	9.1	-	-	9.1	0.91	-	0.91
Kr,9	-	-	-	449.3	32.1	14.4	-	-	-	14.4	-	19.8	-	19.8	1.95	-	1.95
Kr,10	-	-	-	-	-	-	549.6	51.6	28.4	28.4	-	-	26.4	26.4	1.95	0.69	2.64

Table A. 2. Summary table of X3 telemetry including discharge properties, magnet currents and cathode properties. TC#= test condition, $V_{D,X}$ = discharge voltage of channel X, $I_{D,X}$ = discharge current of channel X, $P_{D,X}$ = discharge power of channel X, $P_{D,T}$ = total thruster discharge power, I=inner, M=middle, O=outer, C#=coil # where coils are numbered moving radially outward from thruster centerline, V_{CG}=cathode-ground voltage, V_K=keeper voltage, I_K =keeper current.

TC#	Discharge Properties										Magnet currents [A]						Cathode Properties		
	$V_{D,I}$ [V]	$I_{D,I}$ [A]	$P_{D,I}$ [kW]	$V_{D,M}$ [V]	$I_{D,M}$ [A]	$P_{D,M}$ [kW]	$V_{D,O}$ [V]	$I_{D,O}$ [A]	$P_{D,O}$ [kW]	$P_{D,T}$ [kW]	C 1	C 2	C 3	C 4	C 5	C 6	V_{CG} [V]	V_K [V]	I_K [A]
Kr,1	300.5	13.0	3.9	-	-	-	-	-	-	3.9	7.48	5.88	7.55	6.63	7.23	7.36	-15.9	18.7	3.1
Kr,2	-	-	-	299.8	32.0	9.6	-	-	-	9.6	7.47	5.89	7.54	6.61	7.22	7.35	-17.1	-	-
Kr,3	-	-	-	-	-	-	299.6	55.1	16.5	16.5	7.48	5.85	7.55	6.63	7.22	7.36	-17.4	-	-
Kr,4	300.2	13.3	4.0	300.2	31.3	9.4	-	-	-	13.4	8.59	6.87	8.68	7.61	8.31	8.45	-16.7	-	-
Kr,5	-	-	-	299.4	31.9	9.5	299.3	55.2	16.5	26.1	9.19	7.33	9.44	8.28	9.03	9.17	-20.6	-	-
Kr,6	300.7	13.2	4.0	-	-	-	300.4	57.1	17.2	21.1	11.23	8.82	11.32	9.93	10.83	11.02	-29.2	4.7	1.6
Kr,7	300.5	13.1	3.9	299.4	31.8	9.5	299.3	55.2	16.5	30.0	11.21	8.84	11.31	9.92	10.83	11.02	-27.2	-	-
Kr,8	550.7	13.1	7.2	-	-	-	-	-	-	7.2	7.48	5.86	7.54	6.62	7.22	7.35	-18.2	18.9	3.0
Kr,9	-	-	-	449.3	32.1	14.4	-	-	-	14.4	7.48	5.88	7.53	6.62	7.22	7.36	-17.6	10.4	3.0
Kr,10	-	-	-	-	-	-	549.6	51.6	28.4	28.4	7.48	5.86	7.55	6.62	7.23	7.36	-18.4	7.7	3.0

APPENDIX B

Table B. 1. Summary table of X3 telemetry for xenon operation including discharge properties mass flowrates. TC#= test condition, $V_{D,X}$ = discharge voltage of channel X, $I_{D,X}$ = discharge current of channel X, $P_{D,X}$ = discharge power of channel X, $P_{D,T}$ = total thruster discharge power, I=inner, M=middle, O=outer, $\dot{m}_{a,X}$ =anode mass flowrate of channel X, $\dot{m}_{a,T}$ =total anode mass flowrate, $\dot{m}_{c,i}$ =cathode internal mass flowrate, $\dot{m}_{c,e}$ =cathode external mass flowrate, $\dot{m}_{c,T}$ =total cathode mass flowrate.

TC#	Discharge Properties										Mass Flowrates [mg/s]						
	$V_{D,I}$ [V]	$I_{D,I}$ [A]	$P_{D,I}$ [kW]	$V_{D,M}$ [V]	$I_{D,M}$ [A]	$P_{D,M}$ [kW]	$V_{D,O}$ [V]	$I_{D,O}$ [A]	$P_{D,O}$ [kW]	$P_{D,T}$ [kW]	$\dot{m}_{a,I}$	$\dot{m}_{a,M}$	$\dot{m}_{a,O}$	$\dot{m}_{a,T}$	$\dot{m}_{c,i}$	$\dot{m}_{c,e}$	$\dot{m}_{c,T}$
Xe,1	299.2	13.1	3.9	-	-	-	-	-	-	3.9	12.7	-	-	12.7	1.27	-	1.27
Xe,2	-	-	-	299.1	31.7	9.5	-	-	-	9.5	-	29.4	-	29.4	1.95	0.98	2.94
Xe,3	-	-	-	-	-	-	299.2	55.2	16.5	16.5	-	-	48.2	48.2	1.95	1.95	3.91
Xe,4	299.1	13.4	4.0	300.1	32.0	9.6	-	-	-	13.6	8.0	26.6	-	34.5	1.95	1.50	3.45
Xe,5	-	-	-	297.3	31.1	9.2	299.0	55.9	16.7	25.9	-	20.9	41.1	62.0	1.95	4.25	6.20
Xe,6	299.8	13.4	4.0	-	-	-	299.2	55.5	16.6	20.6	7.8	-	45.1	52.9	1.95	3.33	5.28
Xe,7	299.3	13.6	4.1	296.6	31.9	9.5	301.6	54.8	16.5	30.1	8.0	19.2	39.3	66.4	3.05	3.82	6.87
Xe,8	299.2	28.6	8.6	-	-	-	-	-	-	8.6	24.7	-	-	24.7	1.95	0.52	2.47
Xe,9	-	-	-	294.3	69.7	20.5	-	-	-	20.5	-	51.5	-	51.5	2.84	3.13	5.97
Xe,10	-	-	-	-	-	-	301.0	110.8	33.3	33.3	-	-	90.2	90.2	4.55	5.30	9.85
Xe,11	298.7	28.0	8.4	293.3	70.6	20.7	-	-	-	29.1	14.7	48.8	-	63.5	2.79	3.67	6.46
Xe,12	-	-	-	300.1	69.9	21.0	296.2	114.6	34.0	54.9	-	42.5	81.2	123.7	4.67	4.67	9.33
Xe,13	298.5	28.0	8.4	-	-	-	300.6	112.0	33.7	42.0	10.4	-	94.6	105.0	4.29	5.03	9.32
Xe,14	298.1	26.1	7.8	292.4	69.5	20.3	300.2	108.9	32.7	60.8	14.7	39.8	85.7	140.3	4.48	6.83	11.31
Xe,15	549.9	13.5	7.4	-	-	-	-	-	-	7.4	11.7	-	-	11.7	1.27	-	1.27
Xe,16	300.7	38.5	11.6	-	-	-	-	-	-	11.6	32.1	-	-	32.1	1.95	1.26	3.22
Xe,17	-	-	-	-	-	-	298.0	122.2	36.4	36.4	-	-	99.1	99.1	4.55	5.01	9.57

Table B. 2. Summary table of X3 telemetry including discharge properties, magnet currents and cathode properties. TC#= test condition, $V_{D,X}$ = discharge voltage of channel X, $I_{D,X}$ = discharge current of channel X, $P_{D,X}$ = discharge power of channel X, $P_{D,T}$ = total thruster discharge power, I=inner, M=middle, O=outer, C#=coil # where coils are numbered moving radially outward from thruster centerline, V_{CG}=cathode-ground voltage, V_K=keeper voltage, I_K =keeper current.

TC#	Discharge Properties										Magnet currents [A]						Cathode Properties		
	$V_{D,I}$ [V]	$I_{D,I}$ [A]	$P_{D,I}$ [kW]	$V_{D,M}$ [V]	$I_{D,M}$ [A]	$P_{D,M}$ [kW]	$V_{D,O}$ [V]	$I_{D,O}$ [A]	$P_{D,O}$ [kW]	$P_{D,T}$ [kW]	C 1	C 2	C 3	C 4	C 5	C 6	V_{CG} [V]	V_K [V]	I_K [A]
Xe,1	299.2	13.1	3.9	-	-	-	-	-	-	3.9	6.33	4.34	-	-	-	-	-16.2	17.0	3.6
Xe,2	-	-	-	299.1	31.7	9.5	-	-	-	9.5	-	-	7.55	7.69	-	-	-19.2	-	-
Xe,3	-	-	-	-	-	-	299.2	55.2	16.5	16.5	-	-	-	-	9.07	8.66	-17.0	-	-
Xe,4	299.1	13.4	4.0	300.1	32.0	9.6	-	-	-	13.6	7.85	7.97	8.71	7.88	4.47	-	-13.8	-	-
Xe,5	-	-	-	297.3	31.1	9.2	299.0	55.9	16.7	25.9	-	-	9.89	8.50	9.70	9.70	-11.2	-	-
Xe,6	299.8	13.4	4.0	-	-	-	299.2	55.5	16.6	20.6	8.49	8.19	-	-	7.30	7.39	-39.7	-	-
Xe,7	299.3	13.6	4.1	296.6	31.9	9.5	301.6	54.8	16.5	30.1	9.33	7.28	9.58	8.16	9.05	9.18	-14.2	-	-
Xe,8	299.2	28.6	8.6	-	-	-	-	-	-	8.6	5.44	4.44	-	-	-	-	-11.7	-	-
Xe,9	-	-	-	294.3	69.7	20.5	-	-	-	20.5	-	-	7.59	6.62	-	-	-13.1	-	-
Xe,10	-	-	-	-	-	-	301.0	110.8	33.3	33.3	-	-	-	-	7.68	7.28	-10.3	-	-
Xe,11	298.7	28.0	8.4	293.3	70.6	20.7	-	-	-	29.1	7.32	5.76	8.61	7.55	-	-	-7.7	-	-
Xe,12	-	-	-	300.1	69.9	21.0	296.2	114.6	34.0	54.9	-	-	8.62	6.89	9.09	9.17	-8.5	-	-
Xe,13	298.5	28.0	8.4	-	-	-	300.6	112.0	33.7	42.0	9.49	7.49	-	-	9.01	9.71	-34.9	4.6	3.6
Xe,14	298.1	26.1	7.8	292.4	69.5	20.3	300.2	108.9	32.7	60.8	11.39	8.83	11.42	9.91	10.82	11.04	-16.6	-	-
Xe,15	549.9	13.5	7.4	-	-	-	-	-	-	7.4	9.21	7.35	-	-	-	-	-17.8	17.2	3.6
Xe,16	300.7	38.5	11.6	-	-	-	-	-	-	11.6	5.33	5.02	-	-	-	-	-11.5	-	-
Xe,17	-	-	-	-	-	-	298.0	122.2	36.4	36.4	1.23	-	-	-	10.10	10.29	-14.3	-	-

Table B. 3. Summary table of X3 telemetry including discharge properties and performance parameters. TC#= test condition, $V_{D,X}$ = discharge voltage of channel X, $I_{D,X}$ = discharge current of channel X, $P_{D,X}$ = discharge power of channel X, $P_{D,T}$ = total thruster discharge power, I=inner, M=middle, O=outer, Isp_a=anode Isp, η_a=anode efficiency.

| TC# | Discharge Properties | | | | | | | | | | Performance | | |
	$V_{D,I}$ [V]	$I_{D,I}$ [A]	$P_{D,I}$ [kW]	$V_{D,M}$ [V]	$I_{D,M}$ [A]	$P_{D,M}$ [kW]	$V_{D,O}$ [V]	$I_{D,O}$ [A]	$P_{D,O}$ [kW]	$P_{D,T}$ [kW]	Thrust [N]	Isp_a [s]	η_a [%]
Xe,1	299.2	13.1	3.9	-	-	-	-	-	-	3.9	0.25	1955	60.4
Xe,2	-	-	-	299.1	31.7	9.5	-	-	-	9.5	0.50	1710	43.8
Xe,3	-	-	-	-	-	-	299.2	55.2	16.5	16.5	0.88	1850	48.4
Xe,4	299.1	13.4	4.0	300.1	32.0	9.6	-	-	-	13.6	0.78	2277	64.2
Xe,5	-	-	-	297.3	31.1	9.2	299.0	55.9	16.7	25.9	1.18	1919	42.6
Xe,6	299.8	13.4	4.0	-	-	-	299.2	55.5	16.6	20.6	1.16	2220	61.2
Xe,7	299.3	13.6	4.1	296.6	31.9	9.5	301.6	54.8	16.5	30.1	1.54	2347	59.0
Xe,8	299.2	28.6	8.6	-	-	-	-	-	-	8.6	-	-	-
Xe,9	-	-	-	294.3	69.7	20.5	-	-	-	20.5	-	-	-
Xe,10	-	-	-	-	-	-	301.0	110.8	33.3	33.3	-	-	-
Xe,11	298.7	28.0	8.4	293.3	70.6	20.7	-	-	-	29.1	-	-	-
Xe,12	-	-	-	300.1	69.9	21.0	296.2	114.6	34.0	54.9	-	-	-
Xe,13	298.5	28.0	8.4	-	-	-	300.6	112.0	33.7	42.0	-	-	-
Xe,14	298.1	26.1	7.8	292.4	69.5	20.3	300.2	108.9	32.7	60.8	-	-	-
Xe,15	549.9	13.5	7.4	-	-	-	-	-	-	7.4	-	-	-
Xe,16	300.7	38.5	11.6	-	-	-	-	-	-	11.6	0.63	1981	52.8
Xe,17	-	-	-	-	-	-	298.0	122.2	36.4	36.4	2.14	2181	62.8

BIBLIOGRAPHY

[1] Mukherjee, S., *The Emperor of All Maladies: A Biography of Cancer,* Scribner, August 2011.

[2] "NASA Spinoff." <spinoff.nasa.gov> November 2013.

[3] "Benefits of the NASA Space Program."

<https://www.sac.edu/AcademicProgs/ScienceMathHealth/Planetarium/Pages/Benefits-of-the-NASA-Space-Program.aspx.> November 2013.

[4] Foster, J.E., Personal communication. 2013.

[5] Artsimovich, L. A. and et al., "Development of the stationary plasma thruster (SPT) and its test on Meteor satellite," Kosmicheskie Issledovanija (in Russian), Vol. 7, No. 3, pp. 451-468, 1974.

[6] EP more fuel efficient than chemical, "Why Use Electric Propulsion?" European Space Agency-Science Programme. <http://sci.esa.int/science-e/www/object/index.cfm?fobjectid=34201> (8 Nov 2008)

[7] Tsiolkovsky, K. *The Exploration of Cosmic Space by Means of Reaction Devices.* Scientific Review (Russian) (5), 1903.

[8] Gallimore, A.D. Personal communication. 2010.

[9] Liang, R., "The Combination of Two Concentric Discharge Channels into a Nested Hall-Effect Thruster," Ph.D. Dissertation, University of Michigan, 2013.

[10] "Atlas V 401." <http://www.spaceflight101.com/atlas-v-401.html> November 2013.

[11] Aerojet Rocketdyne. "RL10 Engine." <http://www.rocket.com/rl10-engine-0> (November 2013)

[12] Moog. "Apogee/Upper Stage Thruster." <http://www.moog.com/products/thrusters/apogee-upper-stage-thrusters/> (November 2013)

[13] Ad-Astra Rocket Company. "VASIMR VX-200 reaches 200 kW power milestone." Press Release 011009, <www.adastrarocket.com/Release_200kW_01Oct2009Final.pdf> , September 2009.

[14] National Aeronautics and Space Administration, Glenn Research Center ""Solar Electric Propulsion System Demonstration Mission Concept Studies,"" Broad Agency Announcement, BAA NNC11ZMA017K, June 21, 2011.

[15] Strange, N., Landau, D., Polk, J., Brophy, J., and Mueller, J., ""Solar Electric Propulsion for a Flexible Path of Human Exploration."" 61st International Astronautical Congress, 2010.

[16] Patterson, M.J. and Benson, S.W., "NEXT Ion Propulsion System Development Status and Performance," *43rd AIAA/ASME/SAE/ASEE Joint Propulsion Conference and Exhibit*, AIAA Paper 2007-5199, Cincinnati, Ohio, July 2007.

[17] Brophy, J., Garner, C., Nakazono, B., Marcucci, M., Henry, M., and Noon, D., "The Ion Propulsion System for Dawn," *39th AIAA/ASME/SAE/ASEE Joint Propulsion Conference and Exhibit*, AIAA Paper 2003-4542, Huntsville, Alabama, July 2003.

[18] Polk, J., Kakuda, R., Anderson, J., Brophy, J., Rawlin, V., Patterson, M., et al., "Validation of the NSTAR ion propulsion system on the Deep Space One mission - Overview and initial results." *35th AIAA/ASME/SAE/ASEE Joint Propulsion Conference and Exhibit*, AIAA Paper 99-2274, Los Angeles, California, June 20-24 1999.

[19] Toki, K., Shimizu, Y., and Kuriki, K., "On-Orbit Demonstration of a Pulsed Self-Field Magnetoplasmadynamic Thruster System." Journal of Propulsion and Power. DOI: 10.2514/2.5655, Vol. 16, No. 5, September-October 2000, pp. 880-886.

[20] Slough, J., Kirtley, D., and Weber, T., "Pulsed Plasmoid Propulsion: The ELF Thruster," IEPC-2009-265, 31st International Electric Propulsion Conference, Ann Arbor, MI, September 20-24, 2009.

[21] Bober, A.S. and Maslennikov, " SPT in Russia-New Achievements," Proceedings of the 24th International Electric Propulsion Conference, Sept. 1995, pp. 54-60.

[22] Plenary session, International Electric Propuslion Conference, Wiesbaden, Germany, September 11 – 15, 2011.

[23] Aerojet Rocketdyne. "Aerojet Rocketdyne High-Power Solar electri Propulsion System: Providing Orbit Raising Propulsion for the Air Force Advanced Extremely High

Frequency SV-3 Satellite." Press Release. <http://www.rocket.com/article/aerojet-rocketdyne-high-power-solar-electric-propulsion-system-providing-orbit-raising> (7 October 2013).

[24] Jacobson, David T., and Jankovsky, Robert S., "Performance evaluation of a 50 kW Hall thruster." *AIAA-1999-457*, 37th Aerospace Sciences Meeting and Exhibit, Reno, NV, January 11, 1999.

[25] Jankovsky, R., Tverdokhlebov, S., and Manzella, D., "High power Hall thrusters." *AIAA-1999-2949*, 35th AIAA/ASME/SAE/ASEE Joint Propulsion Conference and Exhibit, Loss Angeles, CA, June 20, 1999.

[26] Florenz, R., Liu, T., Gallimore, A.D., Kamhawi, H., Brown, D.L., Hofer, R.R., and Polk, J.E., "Electric Propulsion of a Different Class: The Challenges of Testing for MegaWatt Missions," AIAA-2012-3942, 48th AIAA/ASME/SAE/ASEE Joint Propulsion Conference and Exhibit, Atlanta, GA, July 29 - August 1, 2012.

[27] Jacobson, D.T., John, J.W., Kamhawi, H., Manzella, D.H., and Peterson, P.Y., "An Overview of Hall Thruster Development at NASA's John H. Glenn Research Center." *41st Joint Propulsion Conference & Exhibit*. AIAA–2005–4242. July 2005.

[28] Florenz, R., Gallimore, A., and Peterson, P., "Developmental Status of a 100-kW Class Laboratory Nested Channel Hall Thruster," IEPC-2011-246, 32nd International Electric Propulsion Conference, Wiesbaden, Germany, September 11-15, 2011.

[29] "Newer U.S. Homes are 30% larger but consumer about as much energy as older homes."<http://www.eia.gov/todayinenergy/detail.cfm?id=9951&src=%E2%80%B9%20 Consumption%20%20%20%20%20%20Residential%20Energy%20Consumption%20Su rvey%20%28RECS%29-b3> February 12, 2013.

[30] "2014 Camarao Coupe." <http://www.chevrolet.com/camaro-sport-coupe.html>, November 2013.

[31] "2014 Ford Mustang V6." <http://www.ford.com/cars/mustang/trim/v6/>, November 2013.

[32] "Audi A-4." <http://www.audiusa.com/models/audi-a4>, November 2013.

[33] "Mini Hard top." <http://www.miniusa.com/content/miniusa/en/model/hardtop.html>, November 2013.

[34] "Sirius FM-6." http://sslmda.com/html/satexp/siriusfm6.html. 25 November 2013.

[35] Brophy, J. R., Gershman, R., Strange, N., Landau, D., Merrill, R.G., Kerslake, T., "300-kW Solar Electric Propulsion System Configuration for Human Exploration of Near Earth Asteroids." AIAA-2011-5514, 47th AIAA/ASME/SAE/ASEE Joint Propulsion Conference and Exhibit, San Diego, CA, July 31 - August 3, 2011.

[36] Planetary Resources—Mission statement. http://www.planetaryresources.com/mission/. 10 June 2013

[37] Hofer, R. R., and Randolph, T.M., "Mass and Cost Model for Selecting Thruster Size in Electric Propulsion Systems." *AIAA Paper 2011-5518*, July, 2011.

[38] Gilland, J. H., LaPointe, M. R., Oleson, S., Mercer, C., Pencil, E., and Mason, L., "MW-Class Electric Propulsion System Designs for Mars Cargo Transport." AIAA-2011-7253, AIAA SPACE 2011 Conference & Exposition, Long Beach, CA, September 27-29, 2011.

[39] Invited talk. 32nd International Electric Propulsion Conference, Wiesbaden, Germany, September 11-15, 2011.

[40] "Human Space Exploration Framework Summary", http://www.nasa.gov/exploration/new_space_enterprise/home/heft_summary.html, November 2013.

[41] Brown, D., Beal, B. and Haas, J., "Air Force Research Laboratory high power electric propulsion technology development," *IEEE Aerospace Conference*, 2010, pp. 1-9.

[42] Gulczinski, F. S., and Schilling, J. H. "Comparison of Orbit Transfer Vehicle Concepts Utilizing Mid-Term Power and Propulsion Options," *International Electric Propulsion Conference, IEPC-03-022*. Toulouse, France, 2003.

[43] Air Force DoD SBIR 11.2 solicitation AF112-177

[44] Defense Advanced Research Programs Agency, Tactical Technology Office, "Fast Access Spacecraft Testbed (FAST)," Broad Area Announcement, BAA 07-65, 2007.

[45] Brown, D.L. Personal communication. 2013.

[46] Donahue, B., "Solar Electric and Nuclear Thermal Propulsion Architectures for Human Mars Missions Beginning in 2033," Paper: AIAA 2010-6819, Jul. 2010.

[47] Klaus, K., Smith, D.B., Kapla, M.S., "Outer Planet Science Missions enabled by Solar Power," poster, Lunar and Planetary Science Conference (LPSC), Mar. 2010.

[48] Spence, B., White, S., Jones, A., Wachholz, J., Wilder, N., Cronin, P., Gregory, T., Barker, P., Allmandinger, T., Mardesich, N., Piszczor, M., Sharps, P., and Fatemi, N., "UltraFlex-175 Solar ArrayTechnology Maturation Achievements for NASA's New Millennium Program (NMP) Space Technology 8 (ST8)," IEEE Photovoltaic Energy Conversion Conference, Waikoloa, HI, May 2006..

[49] Mason, L.E., "Nuclear Power: An Enabling Technology for Space Science and Exploration." Seminar given at the University of Michigan, Ann Arbor, MI, December 8, 2011.

[50] Dawson, S.F., Stella, P., McAlpine, W., and Smith, B., "JUNO Photovoltaic Power at Jupiter." *AIAA-2012-3833*, 48th AIAA/ASME/SAE/ASEE Joint Propulsion Conference and Exhibit, Atlanta, GA, 1 August 2012.

[51] Randolph, T., Dougherty, R., Oleson, S., Fiehler, D., and Dipprey, N., "The Prometheus 1 Spacecraft Preliminary Electric Propulsion System Design." *AIAA-2005-3889*, 41st AIAA/ASME/SAE/ASEE Joint Propulsion Conference and Exhibit, Tucson, Arizona, July 10, 2005.

[52] Oh, David Y., "Evaluation of Solar Electric Propulsion Technologies for Discovery-Class Missions." Journal of Spacecraft and Rockets, DOI: 10.214/1.21613,Vol. 44, No. 2, March-April 2007, pp. 399-411.

[53] Piñero, L. R. "Development of Future High-Power PPUs for Electric Propulsion." Panel Presentation, 48th AIAA/ASME/SAE/ASEE Joint Propulsion Conference and Exhibit, Atlanta, GA, 1 August 2012.

[54] Piñero,L.R., "High Input Voltage Discharge Supply for High Power Hall Thrusters Using Silicon Carbide Devices", IEPC-2013-388, 33rd International Electric Propulsion Conference, Washington, D.C., October 6-10, 2013.

[55] Piñero,L.R, Kamhawi, H., Drummond, G., "Integration Testing of a Modular Discharge Supply for NASA's High Voltage Hall Accelerator Thruster." IEPC-2009-275, 31st International Electric Propulsion Conference, Ann Arbor, MI, September 20-24, 2009.

[56] Piñero,L.R., Hopson, M., Todd, P., Wong, B., "Perofrmance of the NEXT Engineering Model Power Processing Unit." AIAA-2007-5214, 43rd AIAA/ASME/SAE/ASEE Joint Propulsion Conference and Exhibit, Cincinnati, OH, July 8-11, 2007.

[57] Piñero,L.R. Personal communication. November 2013.

[58] Wei Liang; Glaser, J.; Rivas, J., "13.56 MHz high density dc-dc converter with PCB inductors," *Applied Power Electronics Conference and Exposition (APEC), 2013 Twenty-*

Eighth Annual IEEE , vol., no., pp.633,640, 17-21 March 2013 doi: 10.1109/APEC.2013.6520277

[59] Raymond, L., Wei Liang, Jungwon Choi, Rivas, J., "27.12 MHz large voltage gain resonant converter with low voltage stress," *Energy Conversion Congress and Exposition (ECCE), 2013 IEEE* , vol., no., pp.1814,1821, 15-19 Sept. 2013 doi: 10.1109/ECCE.2013.6646928

[60] Rivas, J. Personal communication. November 2013.

[61] Jahn, R.G., *Physics of Electric Propulsion.* Dover Publications. May 2006.

[62] Goebel, D.M., and Katz, I., *Fundamentals of Electric Propulsion: Ion and Hall Thrusters.* Wiley, November 2008.

[63] Hofer, R. R., "Development and Characterization of High-Efficiency, High-Specific Impulse Xenon Hall Thrusters," Ph.D. Dissertation, University of Michigan, 2004.

[64] Grishin, S. D. and Leskov, L. V., *Electric rocket engines for spacecraft*, Moscow,Machinostroenie, 1989.

[65] D-55 Nasa Jacobson, David T., and Jankovsky, Robert S., "Performance evaluation of a 50 kW Hall thruster." *AIAA-1999-457*, 37th Aerospace Sciences Meeting and Exhibit, Reno, NV, January 11, 1999.

[66] Lary, E. C., Meyerand, R. G., and Salz, F., "Ion acceleration in a gyro-dominatedneutral plasma - theory," *Bulletin of the American Physical Society, Sr. II*, Vol. 7, pp.441, 1962.

[67] Seikel, G. R. and Reshotko, E., "Hall current accelerator," *Bulletin of the AmericanPhysical Society, Sr. II*, Vol. 7, pp. 414, 1962.

[68] Bober, A. S. and Maslennikov, N. A., "SPT in Russia - new achievements," IEPC-95-06, 24th International Electric Propulsion Conference, Moscow, Russia, Sept. 19-23,1995.

[69] Arhipov, B. A., Vinogradov, V. N., Kozubsky, K. N., Kudriavtsev, S. S.*, et al.*, "Development and application of electric thrusters at EDB "Fakel"," IEPC-97-004, 25th International Electric Propulsion Conference, Cleveland, OH, Aug. 24-28, 1997.

[70] Morosov, A. I., "Stationary plasma thruster (SPT) development steps and future perspectives," IEPC-93-101, 23rd International Electric Propulsion Conference, Seattle, WA, Sept. 13-16, 1993.

[71]Garkusha, V. I., Lyapin, E. A., Semenkin, A. V., and Tverdokhlebov, S. O., "Anode layer thrusters, state-of-the-art and perspectives," IEPC-93-228, 23rd International Electric Propulsion Conference, Seattle, WA, Sept. 13-16, 1993.

[72] Tverdokhlebov, S. O., "Study of double-stage anode layer thruster using inert gases,"IEPC-93-232, 23rd International Electric Propulsion Conference, Seattle, WA, Sept. 13-16, 1993.

[73] McDonald, M., Gallimore, A., "Electron Trajectory Simulation in Experimental Hall Thruster Fields," IEPC-2011-243, 32nd International Electric Propulsion Conference, Wiesbaden, Germany, September 11-15, 2011.

[74] M. McDonald, M. Sekerak, A. Gallimore, and R. Hofer, "Plasma Oscillation Effects on Nested Hall Thruster Operation and Stability," IEEE-2013-2502, presented at the 34th IEEE Aerospace Conference, Big Sky, MT, March 2-9, 2013.

[75] "PEPL Thrusters: 6-kW HET." <http://pepl.engin.umich.edu/thrusters/6kW.html> (November 2013)

[76] Kamhawi, H., Haag, T.W., Jacobson, D.T., and Manzella, D.H., "Performance Evaluation of the NASA-300M 20 kW Hall Effect Thruster," AIAA-2011-5521, 47th AIAA/ASME/SAE/ASEE Joint Propulsion Conference and Exhibit, San Diego, CA, July 231 - August 3, 2011.

[77] Jacobson, D., Manzella, D., Hofer, R., and Peterson, P., ""NASA's 2004 Hall Thruster Program."" AIAA-2004-3600, 40th AIAA/ASME/SAE/ASEE Joint Propulsion Conference and Exhibit, Fort Lauderdale, Florida, July 11, 2004.

[78] Soulas, G.C., Haag, T.W., Herman, D.A., Huang, W., Kamhawi, H., and Shastry, R., "Performance Test Results of the NASA-457M v2 Hall Thruster," AIAA-2012-3940, 48th AIAA/ASME/SAE/ASEE Joint Propulsion Conference and Exhibit, Atlanta, GA, July 29 - August 1, 2012.

[79] Reid, B. M., "The Influence of Neutral Flow Rate in the Operation of Hall Thrusters," Ph.D. Dissertation, University of Michigan, 2009.

[80] Walker, M.L.R., and Gallimore, A.D., "Neutral density map of Hall thruster plume expansion in a vacuum chamber", Rev. Sci. Instrum., Art. No. 053509 , Volume 76, May 2005.

[81] Gallimore, A.D., Personal communication, October 1994.

[82] Liang, R. and Gallimore, A.D., "Constant-Power Performance and Plume Properties of a Nested-Channel Hall-Effect Thruster," IEPC-2011-049, 32nd International Electric Propulsion Conference, Wiesbaden, Germany, September 11-15, 2011.

[83] "Wire And Cable Derating Criteria". MIL-STD-975 Revision M NASA STANDARD ELECTRICAL, ELECTRONIC, AND ELECTROMECHANICAL (EEE) PARTS LIST. Retrieved   at: http://www.geocities.com/CapeCanaveral/Lab/9643/MIL_STD_975_wire.htm, January 2011.

[84] Gaston, D.M., "Selection of Wire and Circuit Protection Devices for STS Orbiter Vehicle Payload Electrical Circuits." NASA Technical Memorandum 102179. June 1991.

[85] "Cicoil Flexible Flat Cable," <http://www.cicoil.com/> 2013.

[86] Herman, D. A., Gallimore, A. D. "Discharge Chamber Plasma Structure of a 40-cm NEXT-type Ion Engine," AIAA-2005-4250, 41st Joint Propulsion Conference, Tucson, AZ, July 10-13, 2005.

[87] "Current Sensors-CDS Series." <http://fwbell.com/products/current-sensors-cds-series.aspx> 2013.

[88] Mesa Labs. "The Definer 220." http://www.mesalabs.com/bios-definer-220/ . 2013.

[89] Vestil Manufacturing. "Gantry Cranes & Jibs." <http://vestilmfg.com/products/mhequip/gantry-aha.htm> 2012.

[90] Haag, T. W., "Thrust stand for high-power electric propulsion devices," Review of Scientific Instruments, Vol. 62, No. 5, 1991, pp. 1186 – 1191, doi: 10.1063/1.1141998. 94

[91] Shabshelowitz, A., "Study of RF Plasma Technology Applied to Air-Breathing Electric Propulsion," Ph.D. Dissertation, University of Michigan, 2013.

[92] Jacobson, D., Manzella, D., Hofer, R., and Peterson, P., ""NASA's 2004 Hall Thruster Program."" AIAA-2004-3600, 40th AIAA/ASME/SAE/ASEE Joint Propulsion Conference and Exhibit, Fort Lauderdale, Florida, July 11, 2004.

[93] NASA GRC personnel, personal communication. November 2013.

[94] Brown, D. L., "Investigation of Low Discharge Voltage Hall Thruster Characteristics and Evaluation of Loss Mechanisms," Ph.D. Dissertation, University of Michigan, 2009.

[95] Randolph, T., Kim, V., Kaufman, H., Kozubsky, K., Zhurin, V. V., Day, M., Facility Effects on Stationary Plasma Thruster Testing, IEPC-93-093, 23rd International Electric Propulsion Conference, Seattle, WA, Sept. 13-16, 1993.

[96] Walker, M. L. R., "Effects of Facility Backpressure on the Performance and Plume of a Hall Thruster," Ph.D. Dissertation, University of Michigan, 2005.

[97] Kamhawi, H., Huang, W., and Haag, W., "Investigation of the Effects of Facility Background Pressure on the Performance and Voltage-Current Characteristics of the High Voltage Hall Accelerator", IEPC-2013-446, 33rd International Electric Propulsion Conference, Washington, D.C., October 6-10, 2013.

[98] Domonkos, M. T., "Evaluation of Low-Current Orificed Hollow Cathodes," Ph.D. Dissertation, University of Michigan, 1999.

[99] M. McDonald, M. Sekerak, A. Gallimore, and R. Hofer, "Plasma Oscillation Effects on Nested Hall Thruster Operation and Stability," IEEE-2013-2502, presented at the 34th IEEE Aerospace Conference, Big Sky, MT, March 2-9, 2013.